6-2018

Optimized Insulation and Filter Design of Rotating Machines Fed by Fast Front Pulses

Mohammed Khalil Hussain
Western Michigan University

Recommended Citation

Hussain, Mohammed Khalil, "Optimized Insulation and Filter Design of Rotating Machines Fed by Fast Front Pulses" (2018). *Dissertations*. 3290.
https://scholarworks.wmich.edu/dissertations/3290

OPTIMIZED INSULATION AND FILTER DESIGN OF ROTATING MACHINES FED BY FAST FRONT PULSES

by

Mohammed Khalil Hussain

A dissertation submitted to the Graduate College
in partial fulfillment of the requirements
for the degree of Doctor of Philosophy
Electrical and Computer Engineering
Western Michigan University
June 2018

Dissertation Committee:

Pablo Gomez, Ph.D., Chair
Johnson A. Asumadu, Ph.D.
Richard T. Meyer, Ph.D.

OPTIMIZED INSULATION AND FILTER DESIGN OF ROTATING MACHINES FED BY FAST FRONT PULSES

Mohammed Khalil Hussain, Ph.D.

Western Michigan University, 2018

AC rotating machines are exposed to fast front pulses when fed from inverters. This type of excitation produces dielectric stress in the machine's insulation system that can result in premature deterioration or even failure.

In this dissertation, a non-uniform transmission line model to predict the transient voltage distribution in a machine coil under steep-fronted surge conditions is described and implemented. This model is a function not only of frequency but also of space to represent the variation of electrical parameters in the overhang and slot regions of the coil. These parameters are computed using the finite element method. In order to increase the computational efficiency of the model, three strategies are proposed to represent the rest of the winding after the first coil as a function of frequency: Kron reduction, equivalent π circuit, and chain matrix. In addition, the amplifying effect of the feeder cable in the transient response of the machine winding is considered including such cable model in the transient simulations by means of a distributed parameter representation in the frequency domain.

Using the machine winding model, an optimization method to identify improvements in the insulation design of machine winding coils fed by fast front excitation is proposed. Different

optimization algorithms are applied to identify and evaluate geometrical and electrical modifications to the winding design aimed at minimizing the dielectric stress. Test cases considering different geometrical configurations show that the optimized designs considerably reduce the dielectric stress in the machine coils.

Furthermore, this dissertation proposes a method to reduce the effect of the feeder cable in an inverter-cable-motor setup by using an optimized RLC passive filter. The proposed method consists of finding the optimal tuning of the filter to mitigate the transient overvoltages and dielectric stress in the machine winding. Multi-objective optimization algorithms are used to find the optimal parameters of the filter that minimize the objective functions (rise time, setting time, peak time and overshoot) in the output voltage. The optimal parameter tuning of the proposed RLC filter circuit is compared with a conventional RLC filter when using original and optimized machine geometry, demonstrating a substantial reduction of transient overvoltages while avoiding overdamping and/or distortion of the output voltage.

Finally, the machine winding model is verified experimentally by measurements on a line-end stator coil. The effect of adding the feeder cable in the machine coil and the inclusion of RLC filters are also considered for a complete experimental validation of the modeling approach.

ACKNOWLEDGMENTS

First and foremost, I thank God for providing me with the strength and patience to reach this point of my life.

I would like to thank my supervisor and committee chair, Dr. Pablo Gomez, for his guidance, support, patience, and effort throughout my research. I would like also to thank my committee members, Dr. Johnson A. Asumadu and Dr. Richard T. Meyer for their time and valuable suggestions.

I would like to extend my warm thanks for my father since he passed away before seeing me reach this point, he was the major reason for my success in my life. Words cannot express how grateful I am to my mother for her support and prayer during my study. My sincere and great thanks go to my wife and daughters for their love and patience during this journey and through my whole life. My special thanks for my brother and sisters for their prayers.

I gratefully acknowledge the faculty and staff in the department of Electrical and Computer Engineering at Western Michigan University.

Finally, I would like to thank the Higher Committee for Education Development in Iraq (HCED) for the financial support to complete my study.

Mohammed Khalil Hussain

TABLE OF CONTENTS

CHAPTER

Table of Contents—Continued

CHAPTER

Table of Contents—Continued

CHAPTER

CHAPTER

Table of Contents—Continued

CHAPTER

LIST OF TABLES

List of Tables—Continued

LIST OF FIGURES

List of Figures—Continued

List of Figures—Continued

List of Figures—Continued

List of Figures—Continued

CHAPTER I

INTRODUCTION

1.1 Introduction

The early generation of AC adjustable-speed drives (ASDs), which appeared mainly in the 1980s, used pulse-width modulation (PWM) to provide adjustable-frequency to AC motor stators. The emergence of newer technologies in switching electronic devices used in converters, such as the insulated gate bipolar transistors (IGBT), triggered a growing use of machines for high power ASD applications [1]–[7]. Despite the many advantages of ASDs in terms of performance, size and efficiency, they also produce undesirable overvoltages and dielectric stresses in the rotating machines that result in a substantial reduction of their operating life [7]–[10].

Transient overvoltages due to switching operation is considered in the traditional insulation design of machine windings. These overvoltages may cause dielectric stresses leading to insulation failure. In recent decades, it has been found that the PWM-type excitation used in motors fed by inverters for speed and/or torque control produces additional stresses in the motors' insulation system [11]. In general, switching operations involved in the operation of inverters give rise to steep-fronted transient voltages which penetrate into the machine winding. Transient overvoltages are severe conditions for the winding insulation [11], [12].

In addition, in many industrial applications it is common to connect the motor and PWM inverter by means of a long cable [9], [13]. This cable further amplifies the undesired overvoltages in the motor windings. The magnitude of these overvoltages depends on the pulse rise time and on the characteristic impedance and length of the cable [14], [15].

Machines fed by voltage-source inverters have become increasingly common compared to conventional sinusoidal drives over the last decades. However, the insulation of this type of devices is subjected to additional electric and thermal stress due to the steep front voltage impulses involved [16]. Adequate insulation design of rotating machines to withstand transient overvoltages and dielectric stresses involves the accurate prediction of transient voltage distribution along of machine windings [17]. Since the 1980s, several computer-based modeling approaches have been proposed to predict the magnitude and distribution of transient overvoltages in machine windings under fast-front pulses [17]–[20].

Propagation of fast pulses along motor windings is one of the most important sources of dielectric stresses, which can result in premature deterioration or even failure of the motor. Thus, it is essential to consider such pulses for the correct design of winding insulation systems. Interturn insulation failure is caused by either flaw in the insulation system, owing to manufacturing irregularities, or by the incidence in service of a dielectric stress which is higher than the design intent. It is well known that high interturn stresses can be produced by steep-fronted surges impinging on stator coils, and that any increase in the severity or number of such surges will increase the probability of interturn insulation failure. Industrial surveys and other studies show that 30-40% of machine failures are due to stator winding insulation problems and 70% of these are due to turn and ground insulation failures [21].

Regarding design strategies to reduce dielectric stress, previous studies in underground cables, transformer bushings, insulator strings, and other power components, have shown that the electric field distribution in dielectric regions can be improved by an adequate selection of materials and modification of dielectric distances involved in the insulation system. Optimization techniques have been applied as a step forward to not just reduce, but actually minimize the dielectric stress of these devices [22]–[27].

In recent years, filters have been used to decrease the effect of feeder cable in machine windings. The filter topology can be either passive or active. Active filters are expensive because they require complex control algorithms and additional switches. Passive filters are less expensive, effective and robust, but defining their correct arrangements and parameters is a challenging task. Effective passive filters require the correct definition of parameters for the corresponding circuit. Furthermore, they should decrease the effects of transient overvoltages in machine windings and dielectric stress without or with very small delay in the rise time of the output voltage [28]–[31].

1.2 Significance and Motivation of the Research

Although some progress has been made to improve the design of ac rotating machines, the detrimental effects of transient overvoltages and dielectric stresses in the machine coils are still a big challenge, especially in high power adjustable speed applications. The resulting deterioration of the insulation system has a direct impact not only on the efficiency of the machine but also on its life cycle and related costs.

The present study proposes modifications in the insulation design of stator windings that can potentially increase the operating life of machines without the introduction of additional and/or high-performance insulating materials. In addition, this study proposes an improved RLC filter that can reduce the transient overvoltages produced by the feeder cable without affecting the correct operation of rotating machines fed by inverters.

1.3 Dissertation Goals

There are three main goals in this dissertation. The first goal is to implement an accurate and fast computer model of the form-wound stator winding from ac rotating machine in the frequency domain to predict the transient overvoltages along the coils. The second goal is to decrease the dielectric stress in the machine coils by optimizing their insulation design. The third goal is to decrease the effect of the feeder cable in terms of transient overvoltages and dielectric stresses by means of the definition of an optimized filtering technique.

1.4 Dissertation Organization

- Chapter one, Introduction: This chapter introduces the main concepts used in the next chapters, as well as the significance, motivation and goals of this dissertation.
- Chapter two, Pertinent Literature: This chapter contains the literature review of the machine winding model, optimization design of the machine, and filtering technique.
- Chapter three, Transmission Line Theory Applied to Machine Winding: This chapter contains a description of the machine winding and cable modeling approaches, as well as an explanation of three reduction strategies used in this dissertation to represent the rest of the winding when only a section of the winding is modeled in detail.
- Chapter four, Optimized Dielectric Design of Form-Wound Stator Coils from Rotating Machines: This chapter proposes a method to optimize the insulation design of the machine winding.
- Chapter five, Optimal Passive Filter applied to Inverter-Cable-Machine Setup: This chapter proposes a method to decrease the effect of the feeder cable by using an optimal RLC filter.

- Chapter six, Experimental Validation: This chapter presents the experimental verification of the machine winding model, the machine winding with feeder cable, and the conventional and proposed filters.
- Chapter seven, Conclusions and Future Work: This chapter contains conclusions of this dissertation and future work proposed.

CHAPTER II

PERTINENT LITERATURE

2.1 Introduction

The following is a partial list of relevant work related to the modeling of machine windings under fast front excitation, the use of optimization techniques to decrease the dielectric stress in the windings, and the application of filtering techniques to decrease the effect of the feeder cable on the generation of transient overvoltages.

2.2 Modeling of the Machine Winding

Although most studies of surge phenomena on power components have focused on overhead lines and transformers, it has been shown that the transient overvoltages propagating along the windings of rotating machines can result in deterioration or failure of the device [3], [4], [32]. These overvoltages are due to the injection of fast front pulses into the windings, which are generally related to switching conditions [33]. In recent years, this condition has also been associated with the use of inverters, which introduce fast and repetitive pulses into the windings [7]–[10], [13].

The representation of the coils and turns in each coil and the calculation of parameters of the machine windings are essential factors for an accurate prediction of the transient response under fast front excitation [11], [12], [34]. The feeder cable model is also important since it has been shown that it amplifies the transient overvoltages produced by the fast pulse propagation [14], [15].

Wright et al. [18] presented one of the first reports of the application of the theory of multiconductor transmission line (MTL) to study the surge propagation along a motor winding. This paper described the relationship between the series propagation of travelling waves in the machine coils in both regions (overhang and slot) with the various waves of parallel redistribution at the junctions between the overhang and slot regions. A single line-end coil (first coil ended with constant resistor) was used to represent the stator coil of a machine winding. The computation of parameters was based on the capacitive matrix and its relationship with the characteristic impedance and characteristic admittance of a lossless multiconductor transmission line.

Mclaren et al. [20] introduced the first attempt to calculate the inductance (L) and capacitance (C) matrices of a machine winding by means of a software package based on the finite element method. The self and mutual inductance matrices were calculated by using the flux density distribution in the region concerned. The capacitance matrix was calculated by using a curvilinear squares technique. The losses were added as a distributed effect using analytical expressions. A uniform multiconductor transmission line of the line-end coil was used to represent the machine winding model.

Guardado et al. [12] and [34] described two different ways to calculate the parameters of a machine winding model based on the geometry of the coil. Ref. [12] describes the use of a multiconductor transmission line end-coil model for predicting the voltage distribution along a machine winding. The capacitance matrix was calculated by using electrical field equations based on the equivalent capacitive network of the coil geometry. The inductance matrix was calculated based on the relationship between inductance, capacitance and wave velocity considering homogeneous insulation layers and assuming that the magnetic field does not penetrate the machine core at high frequencies. The conductance matrix losses were neglected, and the resistance matrix losses were calculated in a similar manner than the one used for overhead transmission lines. Ref. [34] describes the use of an equivalent circuit model of the machine winding. However, the flux penetration was included in the computation of parameters by means of the solution of the one-dimension diffusion equation in the slot of the machine. The coil electrical parameters were calculated considering both the magnetic flux in the iron and in the air.

Petrarca et al. [6] and Venegas et al. [11] applied finite element models to calculate the parameters of machine windings for transient overvoltage studies assuming a homogenous insulation layer in the stator coil. Ref. [6] describes the modeling of a machine winding under fast front excitation using four lossless multiconductor transmission lines in series connection with a shorted termination to represent a single stator coil in the slot and stator regions. The capacitance matrix was calculated by forced voltage and the inductance matrix was calculated by means of replacing the dielectric media with free space. In [11] the capacitance matrix of the machine winding was calculated by the electrostatic field energy equation. The resistance was calculated by using the power losses equation. The inductance matrix was calculated by using the stored magnetic energy over the region of analysis.

Oyegoke [35] introduced three approaches: multiconductor transmission line and scatter matrix concept (MTLSMC), Multiconductor transmission line and averaging techniques concept (MTLATC), and multiconductor transmission line concept for circuit simulator (MTLCCS) to represent the machine coil. In the MTLSMC approach, the line-end coil was divided into five parts defined by the cable and the slot junctions. The incident and reflected waves at a junction were connected by means of a scatter matrix. In the MTLATC approach, the computation of inter-turn voltages requires the solution with respect to voltage of the capacitance equivalent network. In the MTLCCS approach, using the same capacitance equivalent network from the previous method a capacitance matrix [C] was calculated using the indirect boundary equation method and the inductance matrix [L] was evaluated from a modified capacitance matrix assuming a homogeneous medium.

Mabrek et al. [36] used lumped mathematical models of the induction machine to predict the transient overvoltages in the machine winding based on experimental frequency response characteristics at standstill condition (SSFR). The parameter values were determined experimentally.

Krings et al. [5] described the use of an equivalent π-section lumped circuit model to investigate the voltage distribution in single-phase form-wound windings of large electrical machines due to fast transient voltage steps. The winding parameters were calculated using FEM.

Modeling of the feeder cable is important to study its magnifying effect on the transient overvoltages along the machine coil. Lupo et al. [1] and Petrarca et al. [2] used the MTL (multiconductor transmission line) model combined with a constant-parameter cable model to study the effect of the length of the feeder cable on the transient response of a machine coil considering the coil's end as short ended. The parameters of the machine winding were calculated using FEM and assuming homogeneous media for the stator coil. Time and frequency domain models were compared in [1]. FEM-based simulations were used to calculate the capacitance matrix and the inductance matrix was calculated by means of its relationship with the capacitance matrix in free space. The simulation results showed that the frequency domain model results in a better prediction of overvoltages at the motor terminals than the time domain model because the latter leads to an underestimation of the electrical stresses.

Von Jouanne et al. [13] presented the effect of long motor leads on AC motor drives considering different rise times of high frequency PWM inverter pulses. A lossless single-phase cable model based on the transmission theory was used to represent the motor lead. The parameters of the cable were calculated based on the geometrical configuration of the cable without including the frequency dependence. A lumped parameter circuit was used to represent the machine model.

Moreira et al. [14] studied the overvoltage problem along the machine winding fed by long cables at high frequencies. They proposed a high frequency model of the AC machine by means of a lumped parameter circuit that was validated only at a specific frequency range. The feeder cable was modeled by means of several lumped parameter segments.

De Paula et al. [10] described a time domain methodology for lumped parameter cable modeling. An “N-Branch” lumped circuit was proposed to represent the cable as a frequency independent element. Three different methods for cable parameter estimation were also studied and compared in order to be used as an effective tool in the analysis.

Basavaraja et al. [7] discussed the analysis of overvoltage phenomena in long cable PWM drives due to voltage wave reflection. This paper described the modeling of the system consisting of PWM inverter, cable, induction motor and their interaction. The cable and the induction motor were represented by lumped parameter models in MATLAB/Simulink.

Wang et al. [15] presented a novel modeling technique of long-cable-fed induction motor drives to study the overvoltage problem. An improved high-frequency lumped-parameter circuit was developed to represent the motor behavior for time and frequency-domain analyses. The feeder cable was represented by means of lumped π sections model whose parameters were obtained from measurements.

Previous studies provide different techniques available to date to calculate the parameters of the machine winding, represent the coils in the machine, and model the feeder cable. The parameters are either calculated by using FEM after assuming the different insulation layers as a single homogenous layer (one layer) or using measurements that are valid for specific cases. Current representation of the machine winding is done either using a uniform multiconductor transmission line model to represent the line-end coil or using an equivalent lumped circuit. Finally, the feeder cable model commonly used is an equivalent lumped parameter model considering a particular geometry and length.

2.3 Optimized Design of Machine

Several researchers have studied the effects of machine design on the transient overvoltages and insulation stress produced by fast front transients by means of experimental and computational techniques.

Wright et al. [19] presented one of the first reports that dealt with the effects of coil and surge excitation shapes on transient overvoltage along machine windings. This paper provides guidelines to study the effects of the surge rise time, coil shape, and coil size on transient voltage distribution along the coils. It concluded that the coil size and the number of turns in each coil has little effect on the maximum interturn voltage related to fast transient response.

Guardado et al. [37] studied the effect of design coil parameters on the winding subject by steep front excitation. This study proposed guidelines of coil parameters design that increase or decrease the interturn voltages based on percentage change in the insulation thickness, insulation permittivity, turn geometry, coil length, and number of turns in each coil. This work showed that the dominating factors for interturn voltage are the coil turns and waveform duration and secondary factors are the insulation thickness, insulation permittivity, and conductor dimension.

Palko et al. [38] presented the geometrical optimization of a squirrel cage induction motor by using genetic algorithms. The geometry of the motor is modeled by using two-dimensional finite element method. The optimized design of the motor includes the slot shapes, slot openings, slot numbers and the air gap length. The objective function of the optimization algorithm is to minimize the electromagnetic losses of the motor.

Feyzi et al. [39] and [40] presented the optimization of the slot shape of an induction motor. In [39] the authors describe the combination of the finite element method and an iterative method. The design variables are based on the shape of the slot geometry. The objective function of the optimization procedure is to minimize the installation and operation costs. Ref. [40] describes the optimization of the slot shape of an induction motor by means of the finite element method and three optimization algorithms (random search method, direct search method, and indirect search method). The slot depth is the design variable, while the objective function includes the motor lifetime, installation costs, load factor, material volumes, losses, etc.

Guidelines based on simulation and experimental procedures have been used to specify design improvements in machine windings. Furthermore, the shapes of stator or rotor slots have been optimized to increase some factors related to improving the efficiency of rotating machines. There are no proposals to date related to the optimization of the design of insulation layers inside the coil in terms of the minimization of dielectric stress.

2.4 Filter Techniques Applied in Machine

Passive filters are used to decrease the effects of feeder cable in machine winding in terms of transient overvoltages and potential difference between turns. The effectiveness of the filters is defined by their ability to reduce the transient overvoltages without or with very small delay on the output voltage waveform. However, an effective filter requires the correct definition of RLC parameters for the corresponding circuit.

Jouanne et al. [28] presented filtering techniques to reduce the transient overvoltages in machine windings fed by inverters through long cables. The proposed RLC filter was connected at the motor terminals. The parameters of the filter were selected to overdamp the output voltages. The machine and cable models were represented by means of lumped parameter equivalent circuits.

Rendusara et al. [29] proposed a new inverter output filter configuration to reduce both the differential mode and the common mode dv/dt at the motor terminals. In this configuration, the star point of the RLC filter is connected to the dc link midpoint. To neglect the effect of the cable, the parameters of the RLC filter were selected so that the input voltage of the filter was equal to the input voltage at the motor terminals.

Moreira et al. [31] concluded that the RLC filter is the most interesting solution to mitigate the overvoltage problem in motors fed by adjustable speed drives. In their proposed filter, the value of R was selected to be equal to the feeding cable characteristic impedance and the values of L and C were selected to define an overdamped circuit. The cable and machine winding models were represented by means of lumped equivalent circuits.

Castelli-Dezza et al. [41] used an RC passive filter in a universal motor model to reduce the output overvoltage. The cable and the universal motor models were represented by means of lumped equivalent circuits. The R value was defined as equal to the surge impedance of the cable and the C value was obtained from the charge equation considering the capacitor voltage as equal to 10% of the dc voltage.

Anirudh Acharya et al. [42] proposed a new procedure for designing an LC clamp filter to reduce the output overvoltage from motor drives and increase the rise time. Also, they proposed the addition of another LCL filter at the output terminal of the inverter to decrease the effect of the feeder cable. The parameters of the LC clamp filter were calculated based on the resonant frequency of the system. The parameters of the LCL filter were calculated based on the limitation of resonant current between 0.1 and 0.5 p.u.

Different circuits of passive filter have been used to date in machine applications to decrease the transient overvoltages related to the use of inverters. The filter parameters are either calculated based of specific frequencies or selected based on trial-and-error to overdamp the overvoltages in the machines.

2.5 Contributions

Based on the literature review described in the previous sections, much work has been done in modeling of machine coils, optimized design of machines, and filtering techniques to decrease the effect of the feeder cable.

In this dissertation, in order to have an accurate computer model of the machine coils, a non-uniform transmission line model based on cascaded connection of chain matrices is applied. This model allows taking into account the variation of electrical parameters in the slot and overhang regions. The electrical parameters are computed separately based on geometry of machine coil by using FEM-based simulation program COMSOL Multiphysics for non-homogeneous media. The cable is included by means of a distributed parameter model defined in the frequency domain. In order to achieve a computationally efficient model of the machine coils without any loss of accuracy, three strategies to represent the rest of the winding after the first coil as a function of frequency are proposed and compared: Kron reduction, equivalent π circuit, and chain matrix.

In addition, a method is proposed to improve the insulation design of rotating machines fed by frequency converters by means of the application of optimization techniques aimed at minimizing the dielectric stress in the windings.

Finally, a method is proposed to find the optimal tuning of an RLC passive filter using multi-objective optimization algorithms to minimize the effect of feeder cable in terms of transient overvoltages and dielectric stress in the machine winding.

CHAPTER III

TRANSMISSION LINE THEORY APPLIED TO MACHINE WINDING

3.1 Introduction

In this chapter, a non-uniform transmission line model is described and applied to predict the transient voltage distribution in a machine coil under steep-fronted surge conditions. The non-uniform transmission line model is a function not only of frequency, but also of space to represent the variation of electrical parameters in the overhang and slot regions of the coil. These parameters are computed using the finite element method. The model allows the computation of transient overvoltages in a turn-by-turn basis. The first coil in the machine winding is usually the one affected by the maximum values of inter-turn voltage. Three strategies to represent the rest of the winding after the first coil as a function of frequency are proposed: Kron reduction, equivalent π circuit, and chain matrix. The feeder cable is included in the simulation of the transient response of the machine winding by means of a frequency-domain distributed parameter model. The modeling approach described in this chapter is validated experimentally in Chapter VI of this dissertation.

3.2 Modeling Approach of Machine Winding

The coils of typical electrical machines are distributed around the stator. Such coils are connected outside the stator forming a winding or phase. Figure 3-1 shows a typical stator coil arrangement. It can be noticed that the coil occupies two regions: the slot and the overhang. The closed loop of the stator coils is formed via an alternating series connection of both regions [3], [4], [43]–[45].

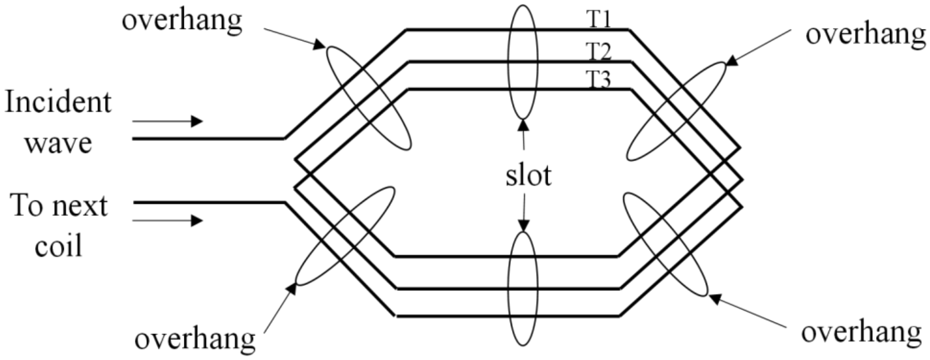

Figure 3-1: Coil sections in the stator frame (3 turns are considered for the purpose of illustration)

In this dissertation, a non-uniform transmission line model based on cascaded connection of chain matrices is implemented. This model allows taking into account the variation of electrical parameters in the slot and overhang regions of the coil.

3.2.1 Non-uniform Multiconductor Transmission Line Model

The distribution of electric and magnetic fields is different in the slot and overhang regions, resulting in different electrical parameters for each region. In order to take this into account, a non-uniform multiconductor transmission line model in the frequency domain is applied. This model is based on the cascaded connection of chain matrices of uniform line segments. Voltage and current waves' propagation along a non-uniform multiconductor transmission line are described by the following Telegrapher equations in the frequency domain [32], [46]–[49]:

$$\frac{d}{dx}\begin{bmatrix}\mathbf{V}(x,s)\\ \mathbf{I}(x,s)\end{bmatrix}=\begin{bmatrix}0 & -\mathbf{Z}(x,s)\\ -\mathbf{Y}(x,s) & 0\end{bmatrix}\begin{bmatrix}\mathbf{V}(x,s)\\ \mathbf{I}(x,s)\end{bmatrix} \tag{3.1}$$

where $\mathbf{V}(x,s)$ and $\mathbf{I}(x,s)$ are the voltage and current vectors in the Laplace domain (s) at any point x, $\mathbf{Z}(x,s)$ and $\mathbf{Y}(x,s)$ are the longitudinal impedance and transversal admittance matrices per-unit length, defined as

$$\mathbf{Z}(x,s) = \mathbf{R}(x,s) + s\mathbf{L}(x,s) \tag{3.2}$$

$$\mathbf{Y}(x,s) = \mathbf{G}(x,s) + s\mathbf{C}(x,s) \tag{3.3}$$

where $\mathbf{R}(x,s)$, $\mathbf{L}(x,s)$, $\mathbf{C}(x,s)$ and $\mathbf{G}(x,s)$ are the resistance, inductance, capacitance, and conductance matrices per unit length, respectively. Section 3.3 describes in detail the computation of these parameters.

As seen in (3.1) , the electrical parameters of the line are in general frequency and space dependent. Assuming that the parameters are constant over a line segment Δx and applying boundary conditions at x and $x+\Delta x$, the following relation between voltages and currents on both sides of the segment is obtained in terms of the chain matrix [50], [51]:

$$\begin{bmatrix} \mathbf{V}(x+\Delta x,s) \\ \mathbf{I}(x+\Delta x,s) \end{bmatrix} = \boldsymbol{\phi}(\Delta x,s) \begin{bmatrix} \mathbf{V}(x,s) \\ \mathbf{I}(x,s) \end{bmatrix} \tag{3.4}$$

The chain matrix of the segment is given by

$$\boldsymbol{\phi}(\Delta x,s) = \begin{bmatrix} \cosh(\boldsymbol{\psi}\Delta x) & -\mathbf{Y}_0^{-1}\sinh(\boldsymbol{\psi}\Delta x) \\ -\mathbf{Y}_0\sinh(\boldsymbol{\psi}\,\Delta x) & \mathbf{Y}_0\cosh(\boldsymbol{\psi}\Delta x)\mathbf{Y}_0^{-1} \end{bmatrix} \tag{3.5}$$

where $\boldsymbol{\psi}$ is the propagation constant matrix, computed as

$$\boldsymbol{\psi} = \mathbf{M}\sqrt{\boldsymbol{\lambda}}\,\mathbf{M}^{-1} \tag{3.6}$$

$\mathbf{M}$ and $\boldsymbol{\lambda}$ are the eigenvalue and eigenvector matrices of the $\mathbf{Z}(x,s)\mathbf{Y}(x,s)$ product, respectively; $\mathbf{Y}_0$ is the characteristic admittance matrix of the line segment computed as

$$\mathbf{Y}_0 = \mathbf{Z}(x,s)^{-1}\boldsymbol{\psi} \tag{3.7}$$

3.2.2 Cascaded Connection of Chain Matrices

The two-port line representation given by (3.4) is the basis of the non-uniform line approach used for modeling a winding coil [46]. The following procedure is applied:

- The line representing the coil is divided in 5 segments, as shown in Figure 3-2.
- The chain matrix from each segment is computed according to (3.5). It can be noticed that such matrix is a function of the parameters **Z** and **Y**, which are different in the overhang and slot regions.
- Cascaded connection is applied (product of chain matrices) to obtain the chain matrix of the complete coil, as shown in Figure 3-3.

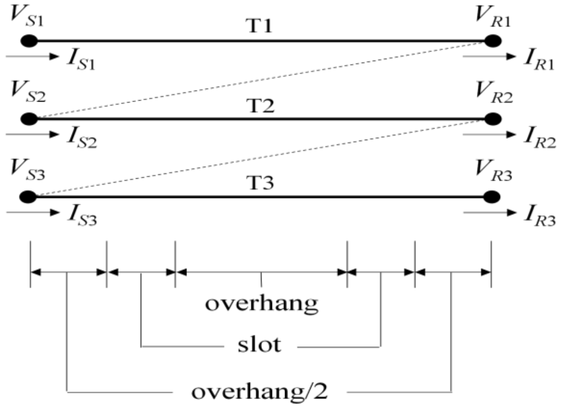

Figure 3-2: Multiconductor transmission line model of the coil with zig-zag connection

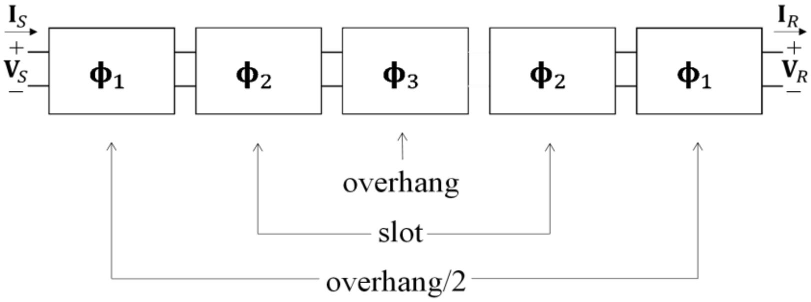

Figure 3-3: Cascaded connection of chain matrices to model all regions of the coil

The relationship between voltages and currents at the beginning (node S) and end (node R) of the complete coil is obtained as

$$\begin{bmatrix}\mathbf{V}_R\\ \mathbf{I}_R\end{bmatrix} = \boldsymbol{\Phi}_1\boldsymbol{\Phi}_2\boldsymbol{\Phi}_3\boldsymbol{\Phi}_2\boldsymbol{\Phi}_1\begin{bmatrix}\mathbf{V}_S\\ \mathbf{I}_S\end{bmatrix} = \begin{bmatrix}\boldsymbol{\Phi}_{11} & \boldsymbol{\Phi}_{12}\\ \boldsymbol{\Phi}_{21} & \boldsymbol{\Phi}_{22}\end{bmatrix}\begin{bmatrix}\mathbf{V}_S\\ \mathbf{I}_S\end{bmatrix} \tag{3.8}$$

where $\boldsymbol{\Phi}_{11}$, $\boldsymbol{\Phi}_{12}$, $\boldsymbol{\Phi}_{21}$ and $\boldsymbol{\Phi}_{22}$ are the elements (submatrices) of the chain matrix of the complete coil. This chain matrix model is transformed into an equivalent nodal form in order to introduce the zig-zag connection required to preserve continuity as the pulse propagates along the turns [51], [52]. This yield:

$$\begin{bmatrix}\mathbf{V}_S\\ \mathbf{V}_R\end{bmatrix} = \begin{bmatrix}\mathbf{Y}_{SS}+\mathbf{Y}_{con11} & -(\mathbf{Y}_{SR}+\mathbf{Y}_{con12})\\ -(\mathbf{Y}_{SR}+\mathbf{Y}_{con21}) & \mathbf{Y}_{RR}+\mathbf{Y}_{con22}\end{bmatrix}^{-1}\begin{bmatrix}\mathbf{I}_S\\ \mathbf{I}_R\end{bmatrix} \tag{3.9}$$

where

$$\mathbf{Y}_{SS} = -\boldsymbol{\Phi}_{12}^{-1}\boldsymbol{\Phi}_{11} \tag{3.10}$$

$$\mathbf{Y}_{SR} = -\boldsymbol{\Phi}_{12}^{-1} = -\boldsymbol{\Phi}_{22}\boldsymbol{\Phi}_{12}^{-1}\boldsymbol{\Phi}_{11} + \boldsymbol{\Phi}_{21} \tag{3.11}$$

$$\mathbf{Y}_{RR} = -\boldsymbol{\Phi}_{22}\boldsymbol{\Phi}_{12}^{-1} \tag{3.12}$$

$$\boldsymbol{Y}_{con11} = \begin{bmatrix} Y_S & 0 & \dots & \dots & 0\\ 0 & Y_{con} & 0 & 0 & \vdots\\ \vdots & 0 & \ddots & 0 & \vdots\\ \vdots & \vdots & 0 & \ddots & 0\\ 0 & 0 & 0 & 0 & Y_{con}\end{bmatrix} \tag{3.13}$$

$$\boldsymbol{Y}_{con12} = \begin{bmatrix} 0 & \dots & \dots & \dots & 0\\ Y_{con} & 0 & \dots & \dots & \vdots\\ 0 & \ddots & \ddots & \dots & \vdots\\ \vdots & 0 & \ddots & \ddots & \vdots\\ 0 & 0 & 0 & Y_{con} & 0\end{bmatrix} \tag{3.14}$$

$$\boldsymbol{Y}_{con21} = \begin{bmatrix} 0 & Y_{con} & 0 & \dots & 0 \\ \vdots & 0 & \ddots & \ddots & \vdots \\ \vdots & \vdots & 0 & \ddots & 0 \\ \vdots & \vdots & \vdots & 0 & Y_{con} \\ 0 & 0 & 0 & 0 & 0 \end{bmatrix} \tag{3.15}$$

$$\boldsymbol{Y}_{con22} = \begin{bmatrix} Y_{con} & 0 & \dots & \dots & 0 \\ 0 & \ddots & 0 & \dots & \vdots \\ \vdots & 0 & \ddots & 0 & \vdots \\ \vdots & \vdots & 0 & Y_{con} & 0 \\ 0 & 0 & 0 & 0 & Y_L \end{bmatrix} \tag{3.16}$$

In (3.13)-(3.16), Y_{con} is a large admittance introduced for the zigzag connection, Y_S is the source admittance, and Y_L is the admittance corresponding to the rest of the winding. Finally, the frequency domain nodal voltages obtained from (3.9) are transformed into the time domain by means of the numerical Laplace transform [53].

3.3 Parameter Computation

The elements of the capacitance, inductance, and dielectric losses matrices in the overhang and slot regions are calculated using FEM-based simulation program COMSOL Multiphysics [54]. The series losses are computed from the concept of complex penetration depth [33], [55]. For the computation of inductive elements, it is considered that, at high frequencies such as those related to the pulses produced by frequency converters, the slot walls behave as magnetic field insulation due to eddy currents [56].

3.3.1 Capacitance

The capacitance matrix **C** is calculated using the forced voltage method in the electrostatics module of COMSOL, according to [33], [54]

$$\begin{bmatrix} Q_1 \\ \vdots \\ Q_n \end{bmatrix} = \begin{bmatrix} C_{11} & \cdots & C_{1n} \\ \vdots & \ddots & \vdots \\ C_{n1} & \cdots & C_{nn} \end{bmatrix} \begin{bmatrix} V_1 \\ \vdots \\ V_n \end{bmatrix} \tag{3.17}$$

When element *i* is excited, COMSOL computes the charge (from charge density) in the n elements due to such excitation, and the *i*-th column of the capacitive matrix is obtained. Thus, the complete matrix is obtained after n simulations.

3.3.2 Inductance

The inductance matrix **L** is calculated using the magnetic energy method [33], [54]. When using this method, the current is nonzero on one or two terminals at a time and the energy density integrated over the whole geometry is computed. Self-inductance L_{ii} is calculated from the magnetic energy $W_{m,i}$ obtained when applying current I_i to turn *i*:

$$L_{ii} = \frac{2W_{m,i}}{I_i^2} \tag{3.18}$$

Mutual inductance L_{ij} is calculated from the magnetic energy $W_{m,ij}$ obtained when applying current to turns *i* and *j* simultaneously:

$$L_{ij} = \frac{W_{m,ij}}{I_i \, I_j} - \frac{1}{2}\left(\frac{I_i}{I_j} L_{ii} + \frac{I_j}{I_i} L_{jj}\right) \tag{3.19}$$

All self-elements are computed first and then used in the computation of mutual elements.

3.3.3 Losses

The series losses in the coil (**R**) are computed from the concept of complex penetration depth [33], [55]. These losses are calculated by using the impedance of the conductor (Z_c) per unit length taking into account the effect of dc losses and skin effect at high frequency:

$$Z_c = \sqrt{R_{dc}^2 + Z_{hf}^2} \tag{3.20}$$

Where

$$R_{dc} = \frac{\rho_c}{A} \tag{3.21}$$

$$Z_{hf} = \frac{\rho_c}{2P(W + H)} \tag{3.22}$$

$$P = \sqrt{\frac{\rho_c}{s\mu_0}} \tag{3.23}$$

Where ρ_c is the resistivity of the conductor, A is the cross-sectional area of the conductor, W is the conductor's width, H is the conductor's height, μ_0 is the permeability of conductor and P is the penetration depth [33], [55].

The dielectric losses matrix (**G**) is computed using the "electric currents" module in COMSOL [53]. Terminal voltage is applied to each conductor to calculate the elements of **G** (the procedure is similar to the calculation of the capacitance matrix) [54]. The permittivity and conductivity of each insulation layer are required. Finally, the series impedance and shunt admittance matrices required by the model are computed as **Z** = **R** + s**L** and **Y** = **G**+s**C**.

3.4 Equivalent Components in Machine Windings

In practice, the complete machine winding is assembled connecting the end of the first coil to the beginning of the next coil and so forth, until the winding is complete as, shown in Figure 3-4 [43]–[45]. The first coil usually presents higher transient overvoltages and dielectric stresses than the remaining coils [12]. Therefore, for the purpose of simplification of the transient study, only the first coil is modeled and analyzed in detail in this dissertation. This leaves the question of the type of terminal impedance/admittance to connect at the end of the coil to represent the remaining coils of the winding accurately. A common practice is to approximate this terminal impedance by means of a constant resistive value. However, the transient response of the coil is evidently non-purely resistive, and the parameters are also frequency dependent. It is also common to analyze the transient response of the coil considering it as open ended or shorted. None of these connections resemble the practical condition in which the coil is part of a complete winding.

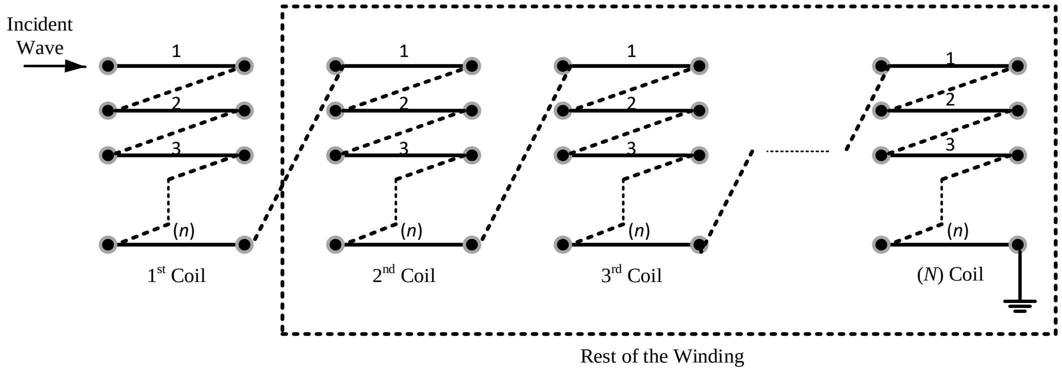

Figure 3-4: Representation of machine winding

A complete model can be achieved by defining the admittance matrix of each coil and connecting them together to find a total admittance of the machine winding. The matrix size depends on the number of coils and the number of turns per coil. If a coil has *n* turns, the size of the coil's admittance matrix is $2n \times 2n$. If the machine has *n* coils, the matrix size of the complete winding will be $(2Nn\text{-}(N\text{-}1)) \times (2Nn\text{-}(N\text{-}1))$. Although this modeling approach allows measuring at any turn from any coil, it also results in a very large system. Besides, the information from all turns is usually not required.

In this dissertation, three strategies: Kron reduction, equivalent π circuit, and chain matrix, are considered and compared for a detailed inclusion of the rest of the coils in the winding as a function of the frequency. The first coil is modeled and analyzed in detail and reduction strategies are applied to condense the rest of the winding as shown in Figure 3-5.

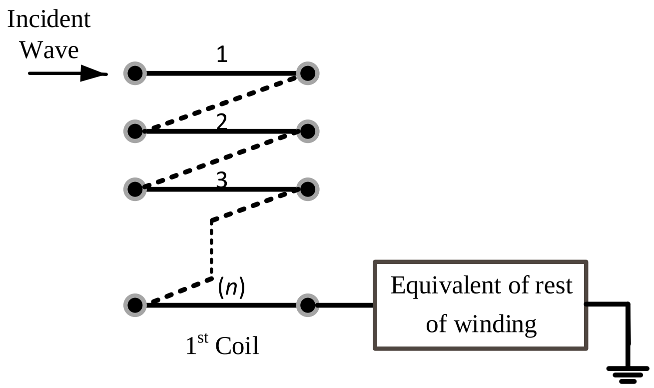

Figure 3-5: Equivalent representation of machine winding model

3.4.1 Kron Reduction

This well-known technique can be used to reduce the nodes from all coils except for the ones under analysis. To eliminate node P from the machine winding model, (3.24) is used for elimination [57].

$$Y_{ij(new)} = Y_{ij(old)} - \frac{Y_{iP}Y_{Pj}}{Y_{PP}} \tag{3.24}$$

This reduction can be applied to:

a) Keep the terminal nodes from each coil of the rest of the winding. The total admittance matrix size would be (2n+N-1)×(2n+N-1). This approach will be called Kron reduction 1 in the remaining of this text.

b) Reduce the system even further to keep only a two-port model corresponding to the rest of the winding (size 2×2). The total admittance matrix size would be

(2n+1)×(2n+1). This option will be called Kron reduction 2 in the remaining of this text.

3.4.2 Equivalent π Circuit

A two-port model can be used to represent each coil of the winding by means of its admittance matrix [33]:

$$\boldsymbol{Y}_{Bus} = \begin{bmatrix} \boldsymbol{Y}_{SS} & -\boldsymbol{Y}_{SR} \\ -\boldsymbol{Y}_{SR} & \boldsymbol{Y}_{RR} \end{bmatrix} \tag{3.25}$$

The corresponding π circuit is shown in Figure 3-6. An equivalent π circuit can be obtained from the series connection of the π-circuits from coils 2 to *N*, as shown in Figure 3-7. In this case Kron's technique is first applied as described in step 3.4.1a. The series connection of the *N*-1 π-circuits results in the equivalent circuit shown in Figure 3-8. Finally, the admittance matrix of this circuit is calculated (size 2×2). The size of the complete admittance matrix, including the first coil modeled turn by turn, is (2*n*+1)×(2*n*+1).

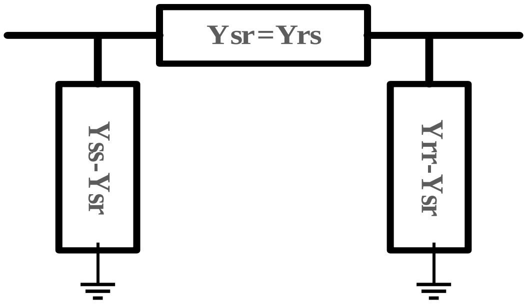

Figure 3-6: Equivalent Ybus component

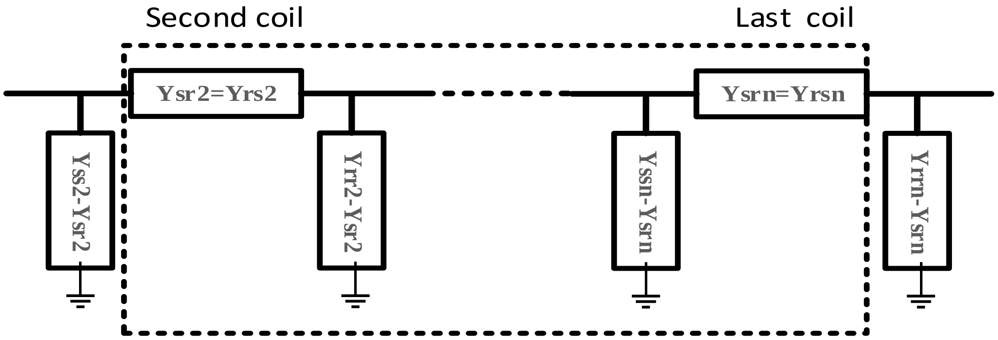

Figure 3-7: Series connection of π circuits from coils 2 to *N*

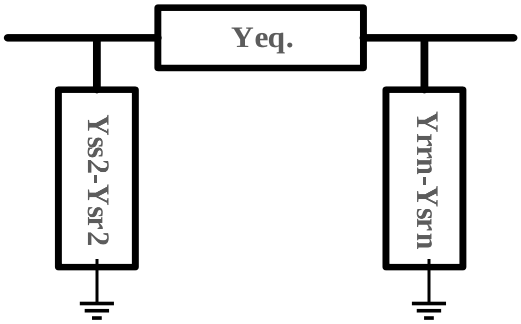

Figure 3-8: Equivalent π circuit for the rest of the winding

3.4.3 Equivalent Chain Matrix

In this case Kron's technique is also applied first as described in step 3.4.1a. Then, the admittance model for each coil is transformed into the chain matrix model given by

$$\begin{bmatrix} \mathbf{V}_L \\ \mathbf{I}_L \end{bmatrix} = \begin{bmatrix} \mathbf{\Phi}_{11} & \mathbf{\Phi}_{12} \\ \mathbf{\Phi}_{21} & \mathbf{\Phi}_{22} \end{bmatrix} \begin{bmatrix} \mathbf{V}_0 \\ \mathbf{I}_0 \end{bmatrix} \tag{3.26}$$

where

$$\mathbf{\Phi}_{11} = \mathbf{Y}_{SR}^{-1}\mathbf{Y}_{SS} \tag{3.27}$$

$$\mathbf{\Phi}_{12} = -\mathbf{Y}_{SR}^{-1} \tag{3.28}$$

$$\mathbf{\Phi}_{21} = \mathbf{Y}_{SR} - \mathbf{Y}_{RR}\mathbf{Y}_{SR}^{-1}\mathbf{Y}_{SS} \tag{3.29}$$

$$\mathbf{\Phi}_{22} = \mathbf{Y}_{RR}\mathbf{Y}_{SR}^{-1} \tag{3.30}$$

The equivalent chain matrix of the complete set of coils (2 to *N*) is obtained simply as

$$\mathbf{\Phi}_{total} = \mathbf{\Phi}_{coil}^{N-1} \tag{3.31}$$

This matrix is then transformed back into an admittance matrix of size (2×2) using equations (3.10)-(3.12). The size of the complete admittance matrix including the first coil is $(2n+1)\times(2n+1)$.

3.5 Distributed Parameter Cable Model

Accurate modeling of the feeder cable in the inverter-cable-coil setup is very important for a correct prediction of the winding's transient response. Figure 3-9 shows the model used in this dissertation, which corresponds to an equivalent circuit in the frequency domain obtained from short and open circuit measurements using an LCR meter (Agilent E4980) [14]. The parameters of the cable model are calculated from the short circuit impedance Z_{sc} and open circuit impedance Z_{oc} measured at low and high frequencies (f_{low} and f_{high}, respectively).

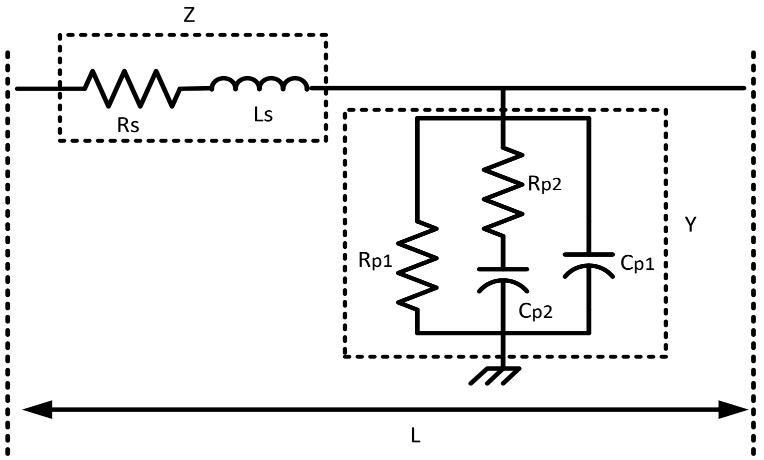

Figure 3-9: Equivalent circuit per unit length of the cable

The cable parameters are obtained as follows:

$$R_s = \frac{2}{3}\ \mathrm{Re}\{Z_{sc}\}_{flow} \tag{3.32}$$

$$L_s = \frac{2}{3}\frac{1}{2\,\pi\, f_{high}}\ \mathrm{Im}\{Z_{sc}\}_{fhigh} \tag{3.33}$$

$$R_{p1} = 2\ (Real\ \{Z_{oc}\}_{flow})\left[\left(\frac{\mathrm{Im}\{Z_{oc}\}_{flow}}{\mathrm{Re}\{Z_{oc}\}_{flow}}\right)^2 + 1\right] \tag{3.34}$$

$$R_{p2} = 2\ (Real\ \{Z_{oc}\}_{fhigh})\left[\left(\frac{\mathrm{Im}\{Z_{oc}\}_{fhigh}}{\mathrm{Re}\{Z_{oc}\}_{fhigh}}\right)^2 + 1\right] \tag{3.35}$$

$$C_{p2} = \left[\left(2\pi\ f_{high}\right)\left(\frac{\mathrm{Re}\{Z_{oc}\}_{fhigh}}{\mathrm{Im}\{Z_{oc}\}_{fhigh}}\right)R_{p2}\right]^{-1} \tag{3.36}$$

$$C_{p1} = \left[(2\pi\ f_{low})\left(\frac{\mathrm{Re}\{Z_{oc}\}_{flow}}{\mathrm{Im}\{Z_{oc}\}_{flow}}\right)\left[R_{p2}\right]\right]^{-1} - C_{p2} \tag{3.37}$$

The series impedance and shunt admittance per unit length of the cable are defined as

$$Z = R_s + sL_s \tag{3.38}$$

$$Y = \frac{1}{R_{P1}} + \frac{1}{R_{p2} + \frac{1}{sC_{p2}}} + sC_{p1} \tag{3.39}$$

These parameters are introduced into the distributed parameter admittance model of the cable as follows:

$$\begin{bmatrix} I_S \\ I_R \end{bmatrix} = \begin{bmatrix} Y_{SS} & Y_{SR} \\ Y_{RS} & Y_{RR} \end{bmatrix}\begin{bmatrix} V_S \\ V_R \end{bmatrix} \tag{3.40}$$

where V_S, I_S and V_R, I_R are the voltages and currents and the sending and receiving ends of the cable, respectively. The elements of the admittance matrix are defined as

$$Y_{SS} = Y_{RR} = Y_0\ coth(\gamma L) \tag{3.41}$$

$$Y_{SR} = Y_{RS} = -Y_0\ \text{csch}(\gamma L) \tag{3.42}$$

where L is the length of the cable, γ is the propagation constant and Y_0 is the is the characteristic admittance of the cable defined as:

$$\gamma = \sqrt{ZY} \tag{3.43}$$

$$Y_o = \sqrt{\frac{Y}{Z}} \tag{3.44}$$

3.6 Applications

The modeling approach of the machine winding described in the previous sections of this chapter is applied to two different geometries of form-wound stator coils. The computation of parameters, simulation of voltage transient response, and winding reduction strategies are presented below for both geometries. The effect of including the feeder cable in the transient analysis is also studied.

3.6.1 Geometrical Configuration

In the machine winding, the stator bar contains conductors and dielectric layers with different relative permittivities. In this dissertation, two different coil cross-sections are considered, as shown in Figures 3-10 and 3-11. The first configuration has ten conductors per slot from a single coil with two layers of insulation: interturn insulation and ground wall insulation [20], [58], [59]. The second configuration also has ten conductors per slot but it includes three layers of insulation: interturn insulation, main insulation and ground wall insulation [1], [2]. In both cases the winding under analysis corresponds to a form-wound stator with 36 coils containing

10 turns each. The main geometrical parameters of both configurations are summarized in Tables 3-1 and 3-2.

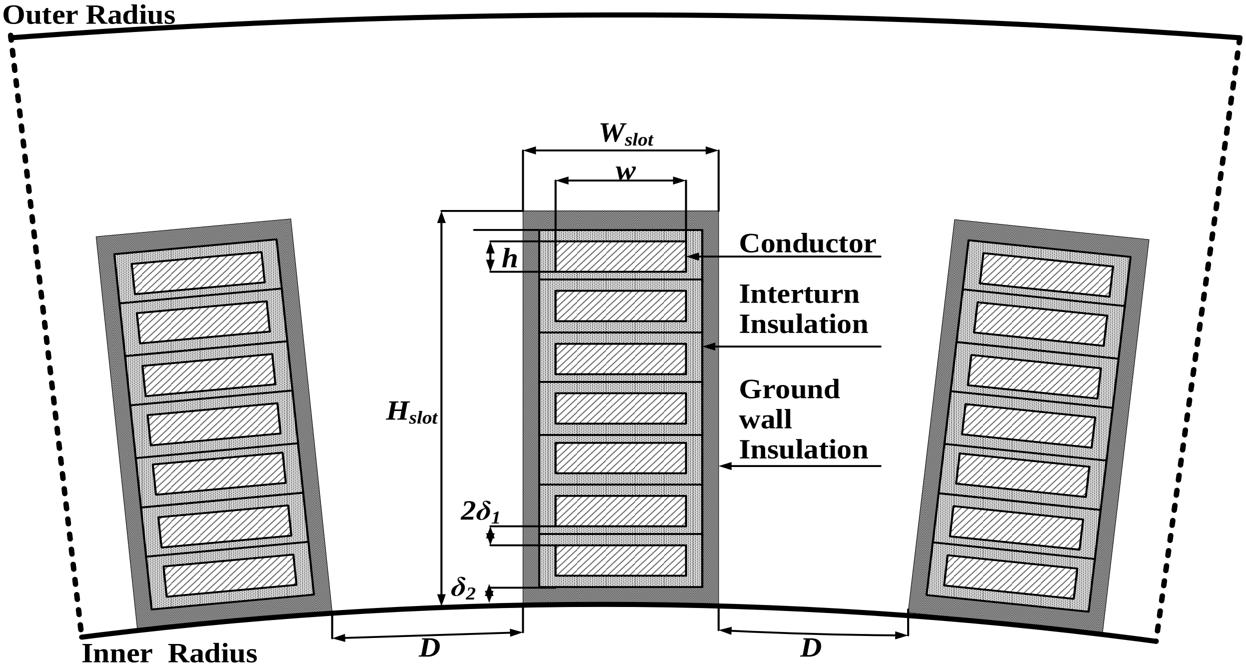

Figure 3-10: 2-layer geometry

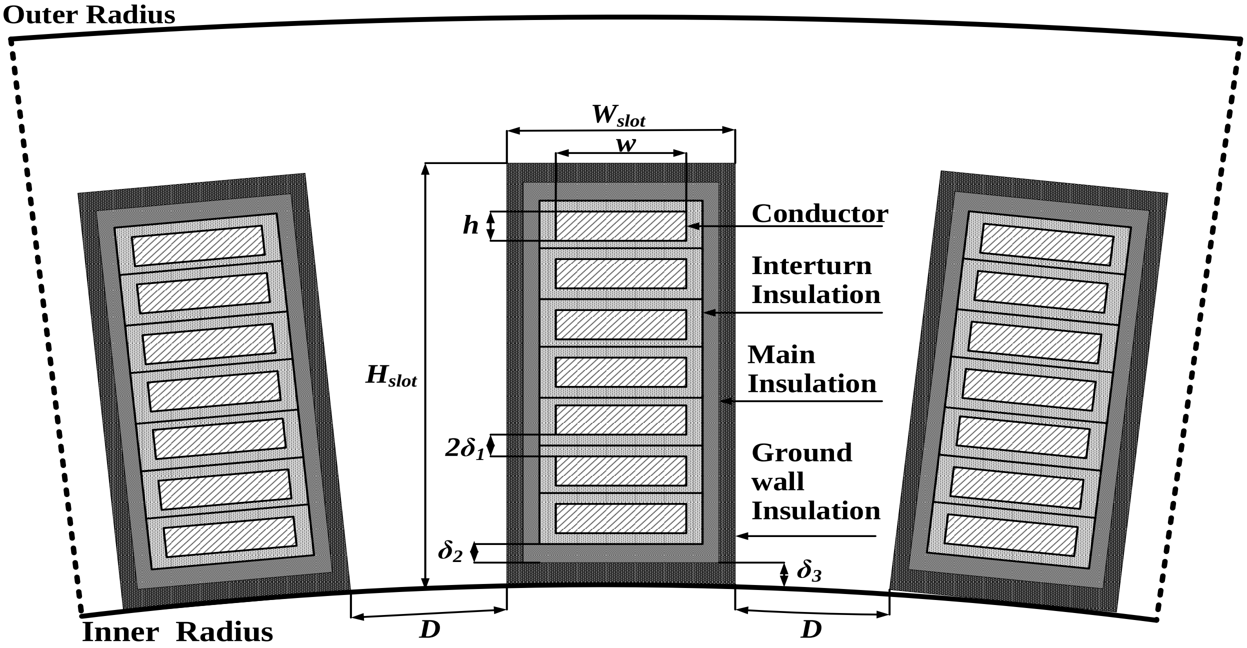

Figure 3-11: 3-layer geometry

Table 3-1: Main parameters for the 2-layer geometry

Parameter	Value
Turns per stator coil	10
Length of overhang region	0.2 m
Conductor width (w)	8 mm
Conductor height (h)	2.24 mm
Resistivity of stator bar conductor	1.7×10^{-8} Ω·m
Thickness of interturn insulation ($2\delta_1$)	0.62 mm
Thickness of ground wall insulation (δ_2)	1.02 mm
Relative permittivity of the interturn insulation (A)	2.6
Relative permittivity of the ground wall insulation (B)	4.2
Outer radius	235 mm
Inner radius	180 mm
Distance between slots (D)	5 mm
Slot width (W_{slot})	10.66 mm
Slot Height (H_{slot})	30.64 mm
Slot length	0.38m

Table 3-2: Main parameters for the 3-layer geometry

Parameter	Value
Turns per stator coil	10
Length of overhang region	0.2 m
Conductor width (w)	6.08 mm
Conductor height (h)	1.59 mm
Resistivity of stator bar conductor	1.7×10^{-8} Ω·m
Thickness of interturn insulation ($2\delta_1$)	0.22 mm
Thickness of main insulation (δ_2)	0.96 mm
Thickness of ground wall insulation (δ_3)	0.33 mm
Relative permittivity of the interturn insulation (A)	2.5
Relative permittivity of the main insulation (B)	2
Relative permittivity of the ground wall insulation (C)	4
Outer radius	195 mm
Inner radius	150 mm
Distance between slots (D)	4.2 mm
Slot width (W_{slot})	8.9 mm
Slot Height (H_{slot})	20.7 mm
Slot length	0.38 m

3.6.2 Parameter Computation

Figure 3-12 shows examples of FEM simulations for the computation of capacitive and inductive elements in the slot region. The slot boundaries are removed for the overhang region, resulting in different sets of parameters.

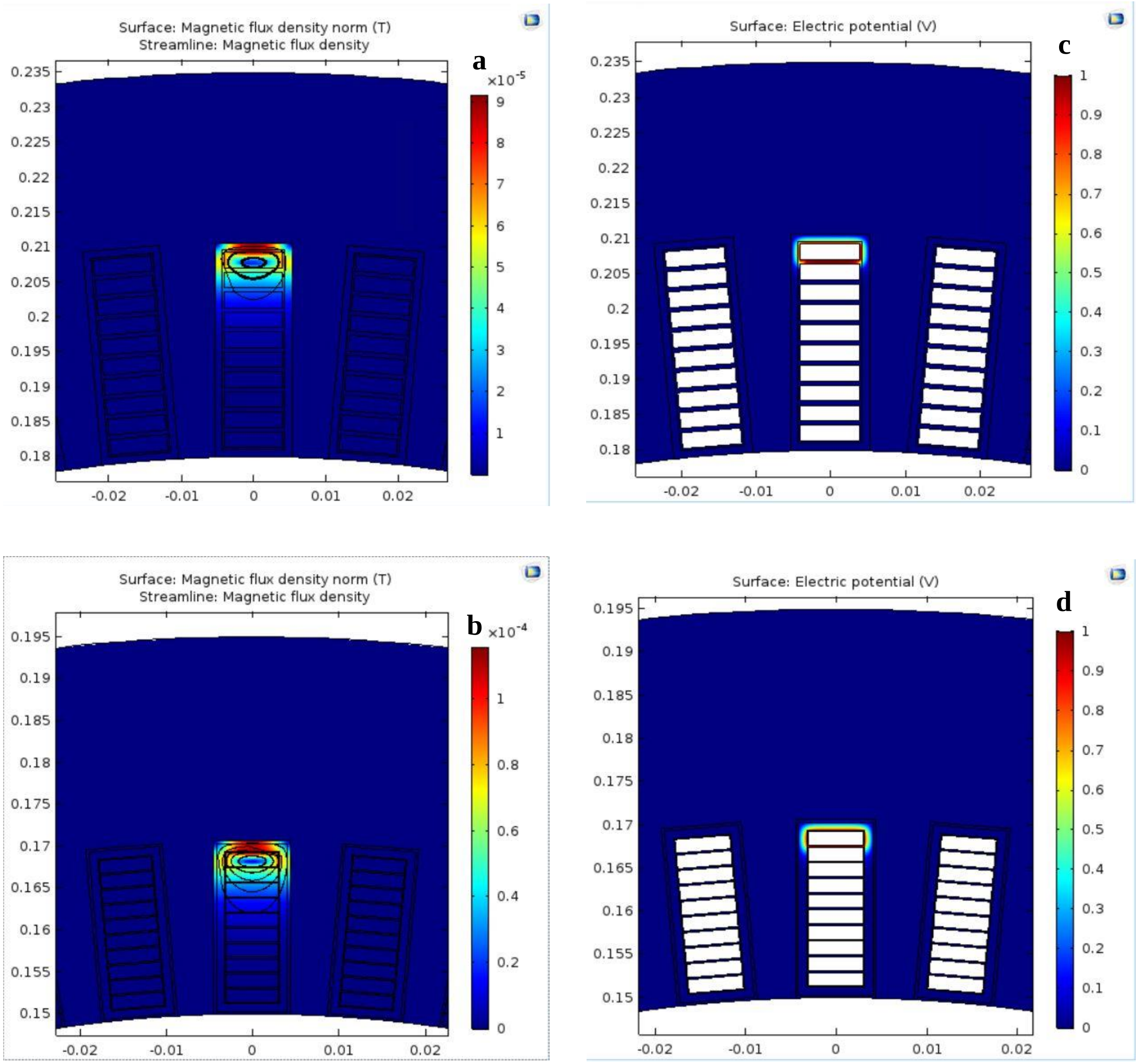

Figure 3-12: Inductance calculation using magnetic energy method in FEM: (**a**) 2-layer geometry, (**b**) 3-layer geometry; Capacitance calculation using forced voltage method in FEM: (**c**) 2-layer geometry, (**d**) 3-layer geometry

3.6.3 Transient Overvoltages in Machine Winding Model

The waveforms in Figures 3-13 and 3-14 show the distribution of transient voltages along the 2-layer and 3-layer coils respectively in the first coil for all turns (1-10 turns). In order to represent a pulse from a PWM inverter, a step voltage waveform excitation with magnitude of 1750 V is applied; two different rise times are considered and compared: 25 ns and 100 ns. This voltage source is injected directly to the beginning of the machine winding. Table 3-3 shows the maximum transient voltages for the two geometries under consideration.

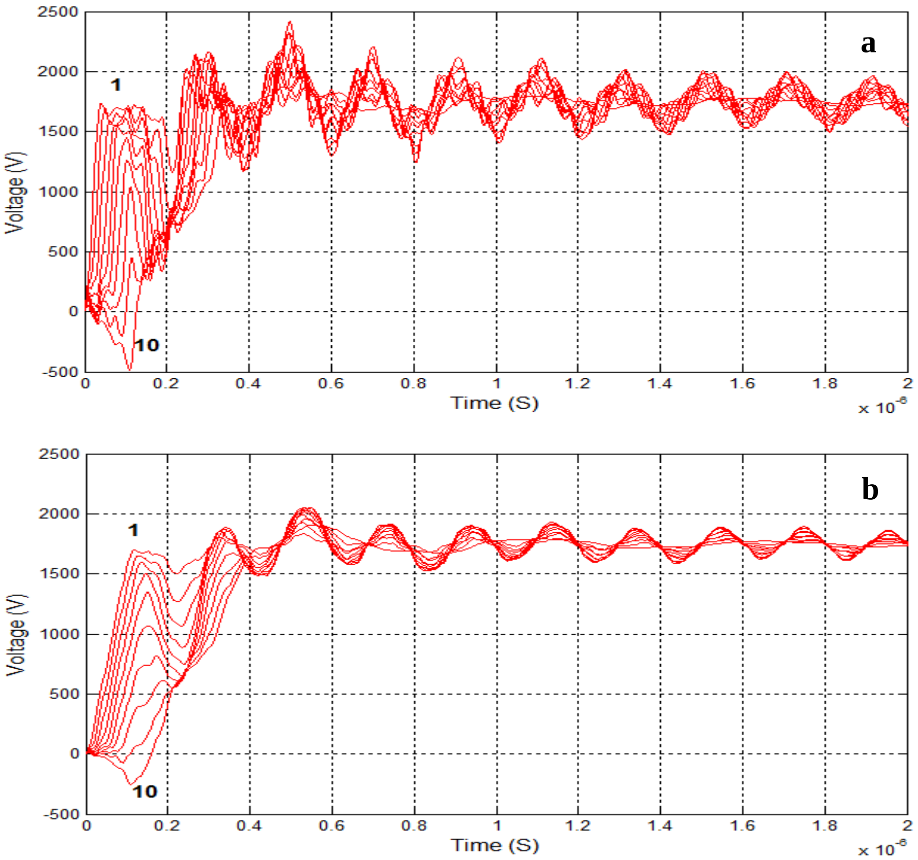

Figure 3-13: Transient overvoltage at all turns of the coil in 2-layer geometry for an excitation with: (**a**) 25 ns of rise time and (**b**) 100 ns of rise time

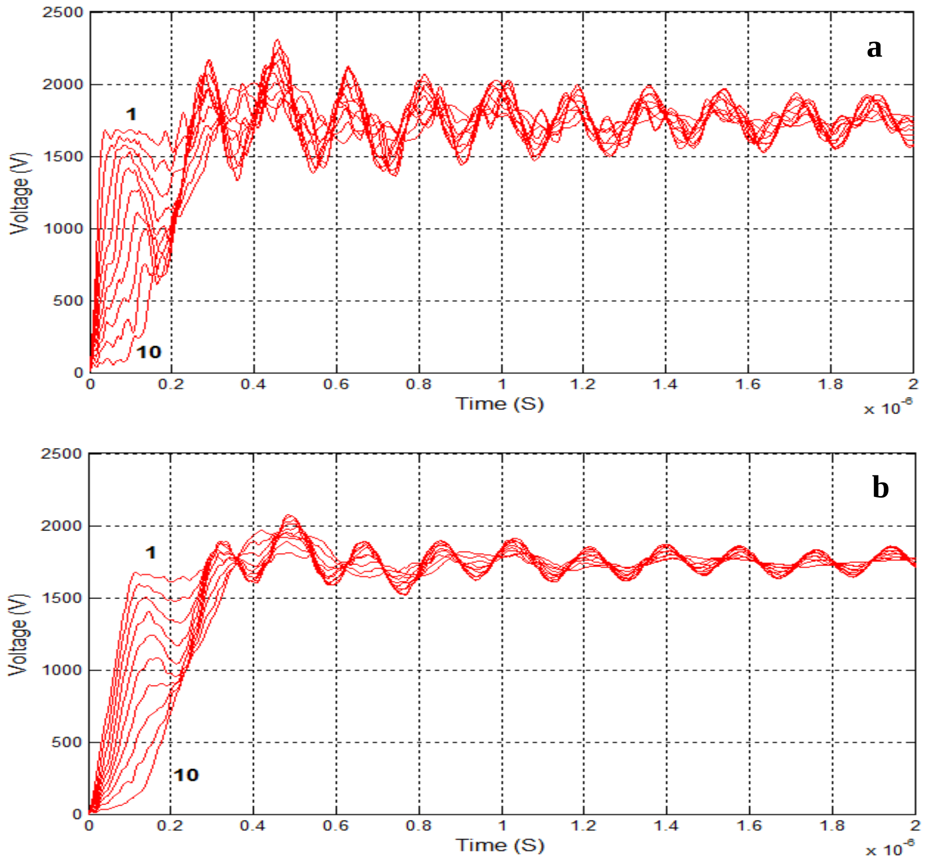

Figure 3-14: Transient overvoltage at all turns of the coil in 3-layer geometry for an excitation with: (**a**) 25 ns of rise time and (**b**) 100 ns of rise time

Table 3-3: Max. transient overvoltage for an excitation with rise time of 25ns and 100ns in 2-layer and 3-layer geometries

Geometry	Max. overvoltage, 25 ns [V]	Max. overvoltage, 100 ns [V]
2-layer	2414.57	2059.09
3-layer	2309.36	2078.56

3.6.4 Potential Difference Between Turns in Machine Winding Model

In this section, the maximum potential difference between adjacent turns is computed for the complete stator windings, which in both cases under consideration consists of 36 coils containing 10 turns each. This potential difference is directly related to the dielectric stress between turns produced by the fast front excitation. Figures 3-15 and 3-16 show the potential difference for the excitations with 25 ns and 100 ns of rise time, respectively. It can be noticed that the largest potential differences occur in each geometry at the first coil, and that these values are reduced as the rise time increases. Table 3-4 shows the maximum potential difference for the two geometries considered and for the 2 rise times applied to the winding.

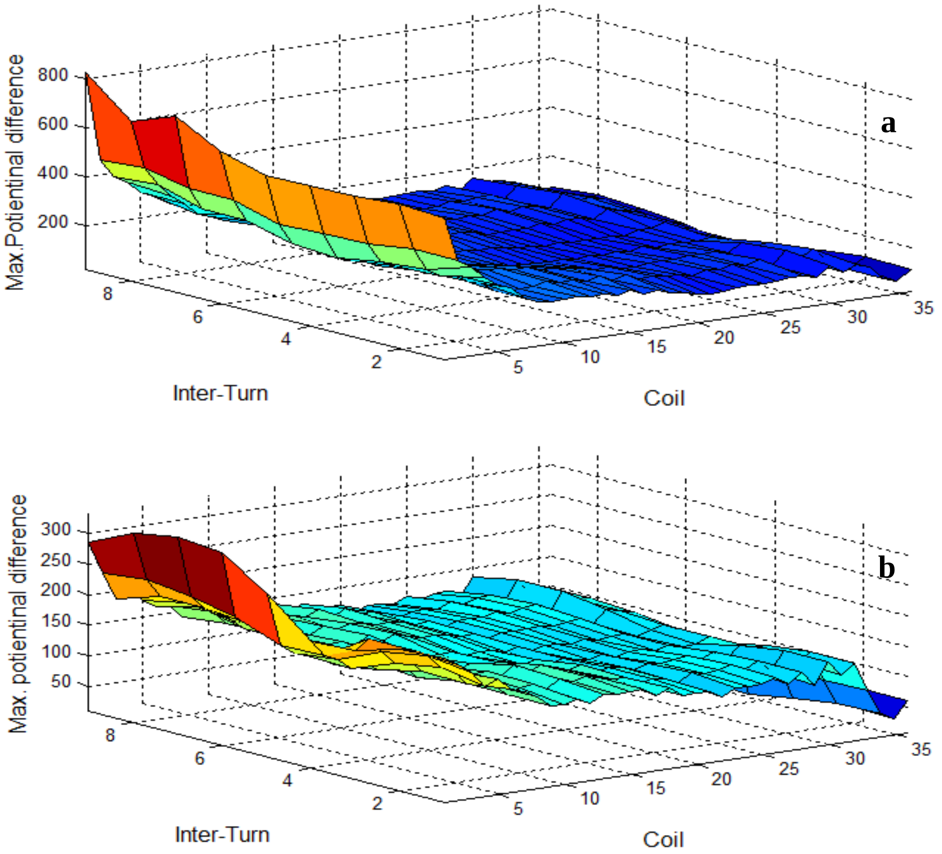

Figure 3-15: Distribution of maximum potential difference along the machine winding in 2-layer geometry: (**a**) 25 ns rise time, (**b**) 100 ns rise time

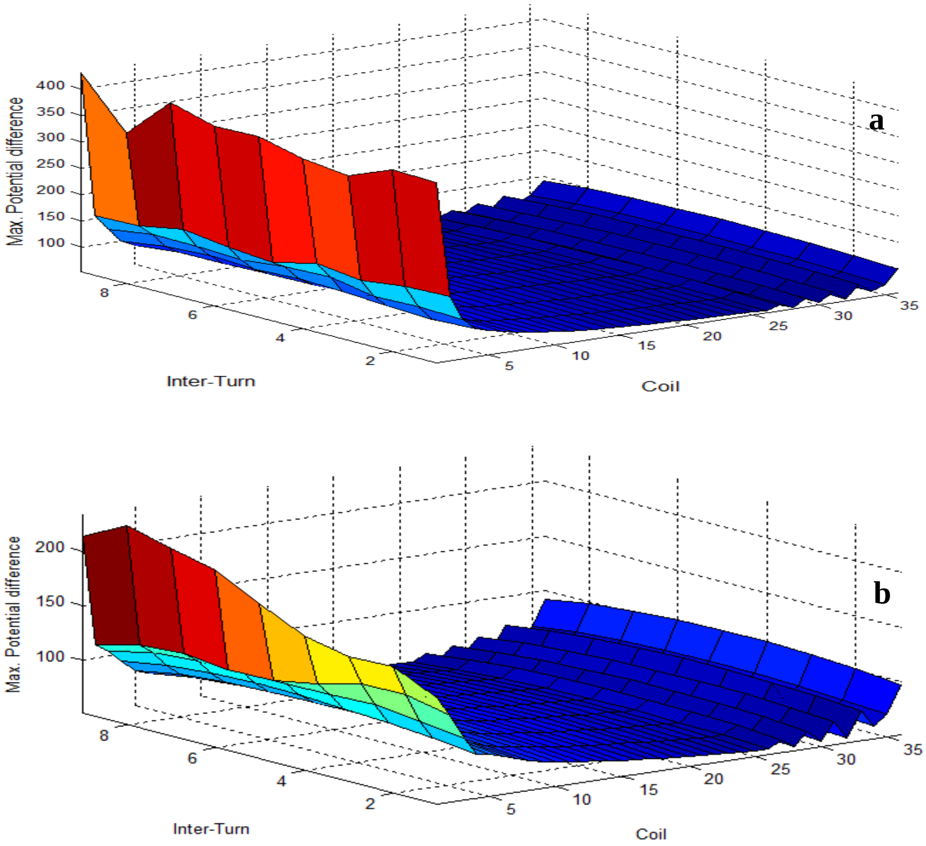

Figure 3-16: Distribution of maximum potential difference along the machine winding in 3-layer geometry: (**a**) 25 ns rise time, (**b**) 100 ns rise time

Table 3-4: Max. potential difference for an excitation with rise time of 25 ns with rise time of 25ns and 100ns in 2-layer and 3-layer geometries

Geometry	Max. potential difference, 25 ns [V]	Max. potential difference, 100 ns [V]
2-layer	824.17	332.12
3-layer	431.67	233.34

3.6.5 Equivalent of the Rest of the Winding

The transient voltage response of the first coil of the winding is simulated in this section, representing the remaining coils by means of an equivalent network calculated using the strategies described in Section 3.4. The sending node of the first coil is excited by means of a step voltage with a magnitude of 1750 V. Similarly, to the previous sections, rise times of 25 and 100 ns are considered for the excitation. Figures 3-17 and 3-18 show the transient overvoltages in the 2-layer and 3-layer geometries for all turns of the first coil. The results from all 3 strategies for equivalent representation of the rest of the winding are indistinguishable (only one of them is shown for simplicity). From these figures, it can be noticed that the transient overvoltages obtained with the complete winding are identical to those obtained with the reduction methods applied.

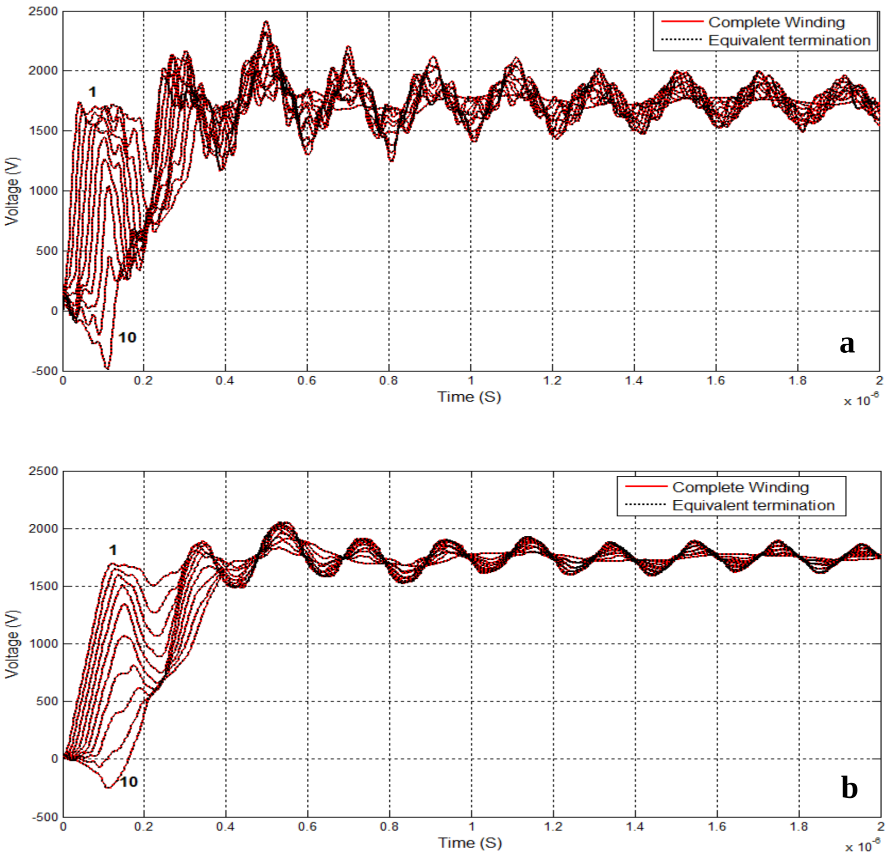

Figure 3-17: Transient overvoltage at all turns of the coil in 2-layer geometry for an excitation with: (**a**) 25 ns of rise time and (**b**) 100 ns of rise time

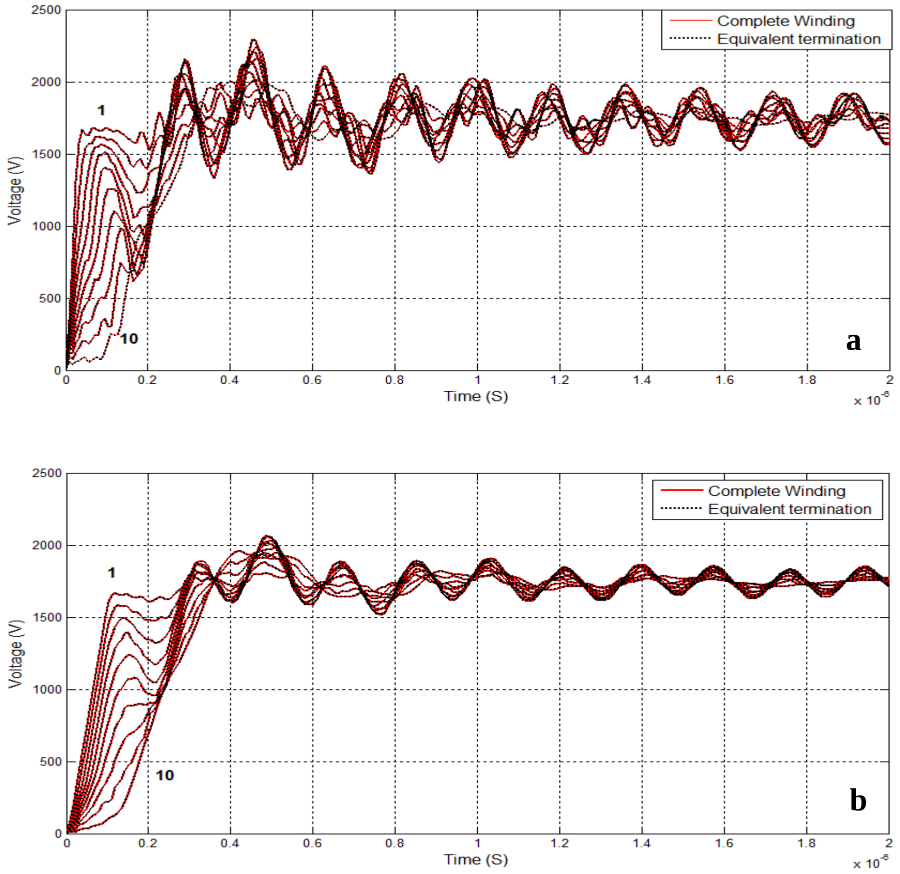

Figure 3-18: Transient overvoltage at all turns of the coil in 3-layer geometry for an excitation with: (**a**) 25 ns of rise time and (**b**) 100 ns of rise time

Table 3-5: Size of admittance matrix Y_{bus} of the complete system vs reduced system

Strategies	Size of admittance matrix		
	Complete systems	Reduced system	% Reduced
Kron reduction (1)	685x685	55 x 55	91.97
Kron reduction (2)		21 x 21	96.93
Equivalent π circuit		21 x 21	96.93
Equivalent chain matrix		21 x 21	96.93

Table 3-5 shows a comparison of the size of admittance matrix Y_{bus} for the complete and the reduced system for all reduction strategies under analysis when the number of turns (n) is 10 and the number of coils (N) is 36. Tables 3-6 and 3-7 show a comparison of the computer time required by all reduction strategies under analysis for the 2 and 3-layer geometries. The number of time samples required for all simulations is 2048 and the rise time in all cases is 25 ns. As shown in these tables, all strategies result in a substantial decrease in computer time when compared to the simulation of the complete winding (without reduction).

Table 3-6: Computer time for the solution of the complete system vs reduced system in 2-layer geometry

Strategies	Simulation time (seconds)		
	Complete system	Reduced system	Times faster
Kron reduction (1)	211.283	8.266046	25.5603
Kron reduction (2)		7.112430	29.7062
Equivalent π circuit		6.525812	32.3765
Equivalent chain matrix		6.232352	33.9010

Table 3-7: Computer time for the solution of the complete system vs reduced system in 3-layer geometry

Strategies	Simulation time (seconds)		
	Complete system	Reduced system	Times faster
Kron reduction (1)	211.789	8.485226	24.9597
Kron reduction (2)		6.956994	30.4426
Equivalent π circuit		6.492864	32.6187
Equivalent chain matrix		6.380827	33.1915

3.7 Transient Overvoltages in Machine Winding Model Including Feeder Cable

This section demonstrates the amplifying effect of the feeder cable on the transient overvoltages. As shown in Figures 3-19 and 3-20, when connecting the source input to the machine winding models (2 and 3-layer geometries) through different lengths of feeder cable (1, 3 and 5 m), the overvoltages substantially increase as the length of the cable increases. Tables 3-8 and 3-9 show the maximum transient voltages for the 2 and 3-layer geometries with different lengths of the feeder cable.

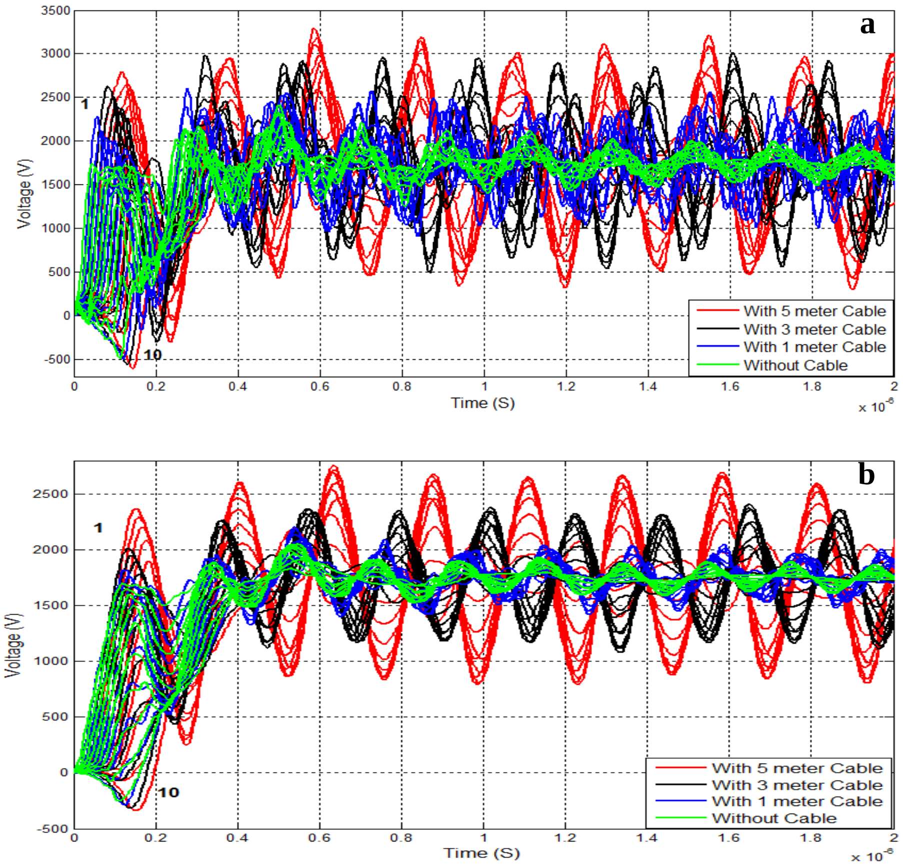

Figure 3-19: Transient overvoltage at all turns of the coil in 2-layer geometry with different length of cable for an excitation with: (**a**) 25 ns of rise time and (**b**) 100 ns of rise time

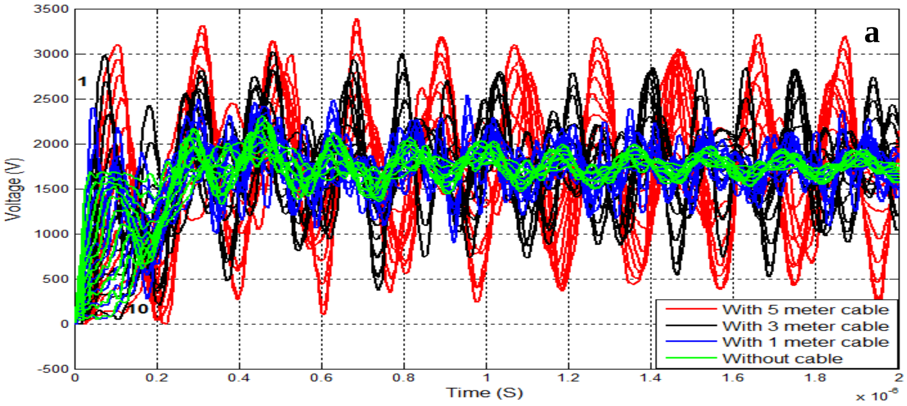

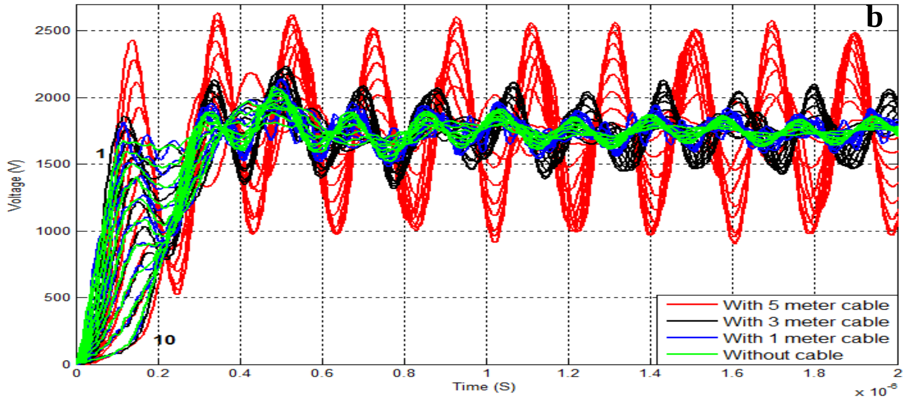

Figure 3-20: Transient overvoltage at all turns of the coil in 3-layer geometry with different lengths of cable for an excitation with: (**a**) 25 ns of rise time and (**b**) 100 ns of rise time

Table 3-8: Max. transient overvoltage for an excitation with rise time of 25 ns and 100 ns in 2-layer geometry with different lengths of cable

Length of cable for 2-layer geometry [m]	Max. overvoltage, 25 ns [V]	Max. overvoltage, 100 ns [V]
1	2599.56	2207.51
3	3016.06	2407.93
5	3288.22	2753.07

Table 3-9: Max. transient overvoltage for an excitation with rise time of 25 ns and 100 ns in 3-layer geometry with different lengths of cable

Length of cable for 3-layer geometry [m]	Max. overvoltage, 25 ns [V]	Max. overvoltage, 100 ns [V]
1	2539.58	2140.76
3	3015.32	2230.93
5	3389.63	2633.84

3.7.1 Potential Difference Between Turns in Machine Winding Model Including Feeder Cable

The effect of the length of the connection cable on the potential difference between turns for both cases under consideration (2-layer and 3-layer coils) is analyzed in Figures 3-21 to 3-26 , as well as in Tables 3-10 and 3-11. According to these results, the maximum potential difference is directly proportional to the length of the feeder cable.

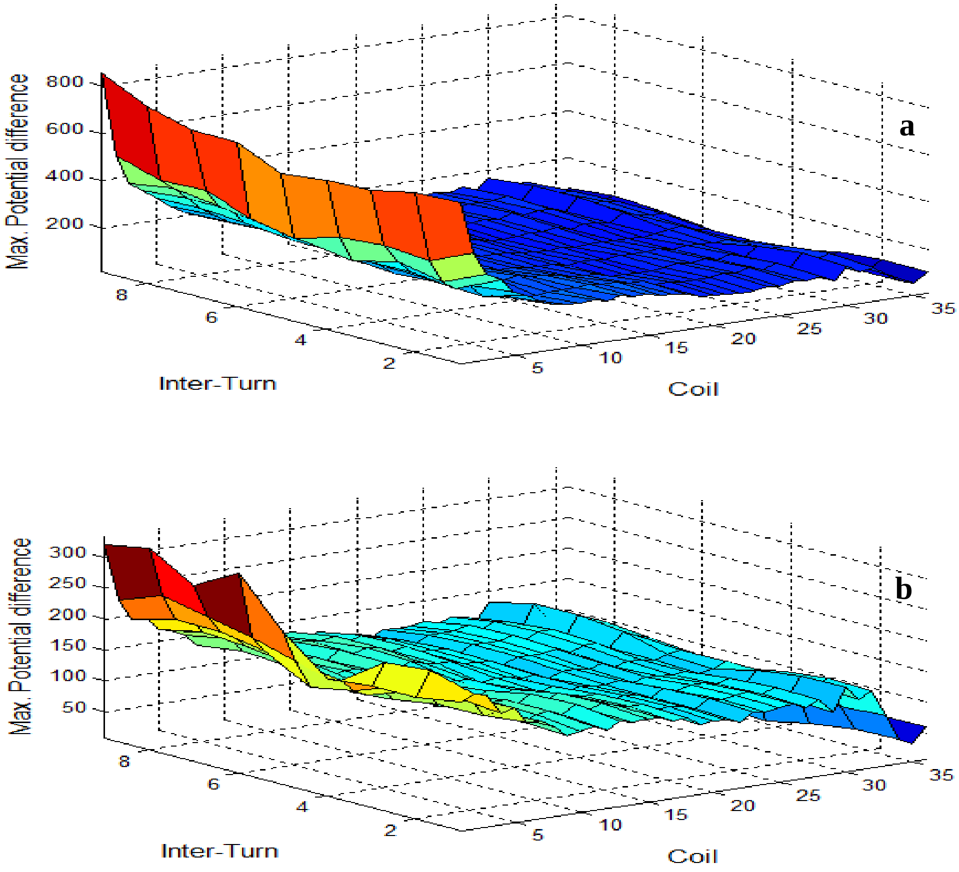

Figure 3-21: Distribution of maximum potential difference along the machine winding in 2-layer geometry with 1-meter cable: (**a**) 25 ns rise time, (**b**) 100 ns rise time

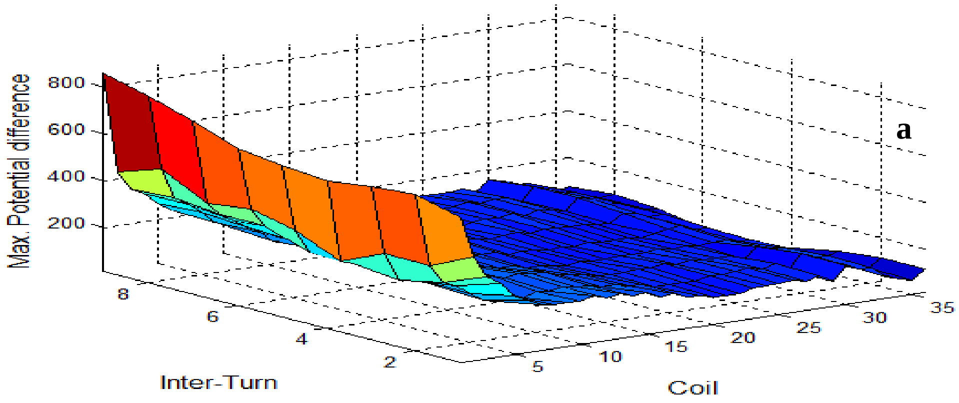

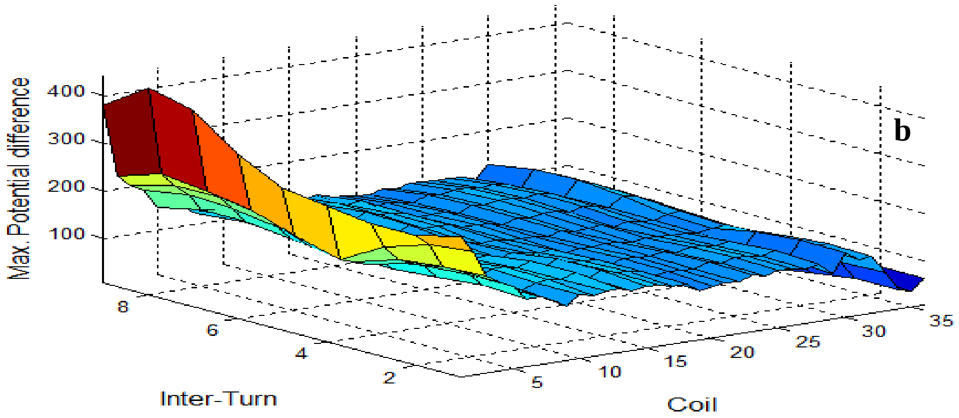

Figure 3-22: Distribution of maximum potential difference along the machine winding in 2-layer geometry with 3-meter cable: (**a**) 25 ns rise time, (**b**) 100 ns rise time

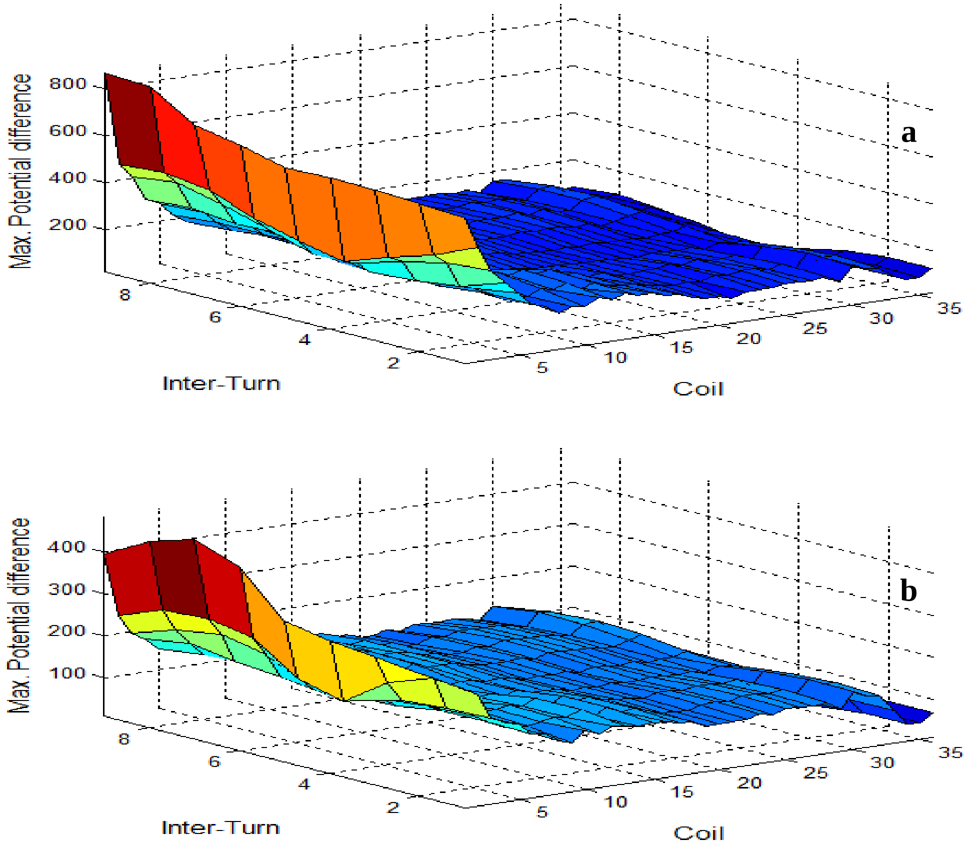

Figure 3-23: Distribution of maximum potential difference along the machine winding in 2-layer geometry with 5-meter cable: (**a**) 25 ns rise time, (**b**) 100 ns rise time

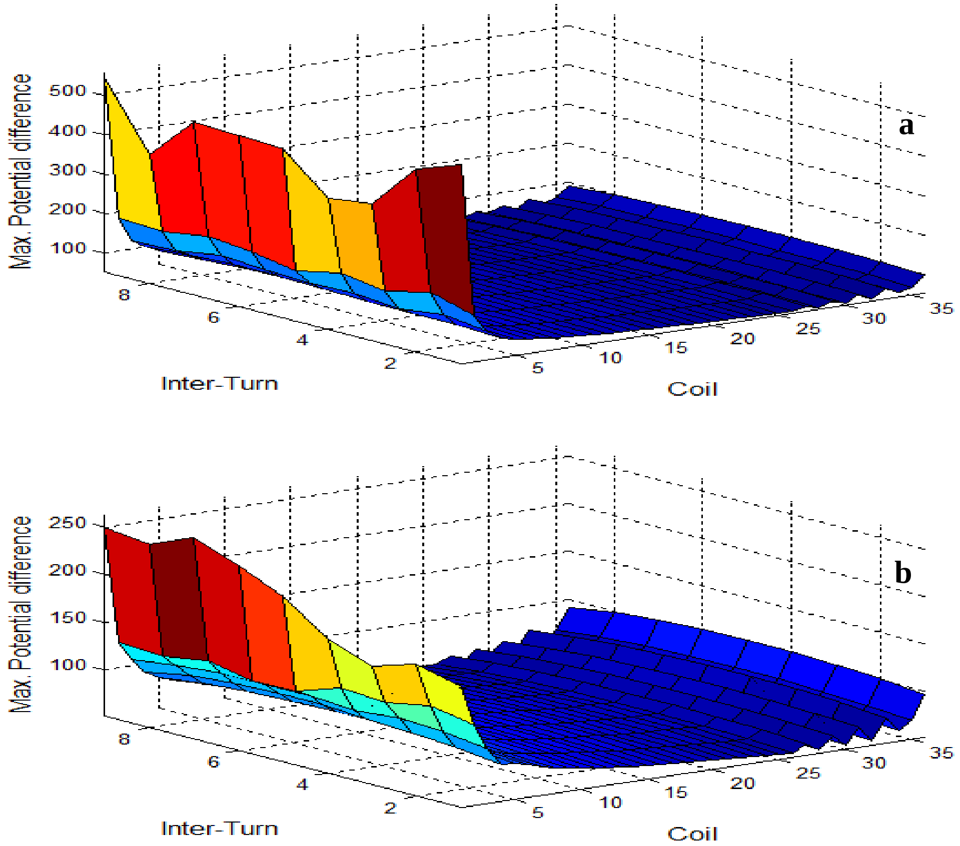

Figure 3-24: Distribution of maximum potential difference along the machine winding in 3-layer geometry with 1-meter cable: (**a**) 25 ns rise time, (**b**) 100 ns rise time

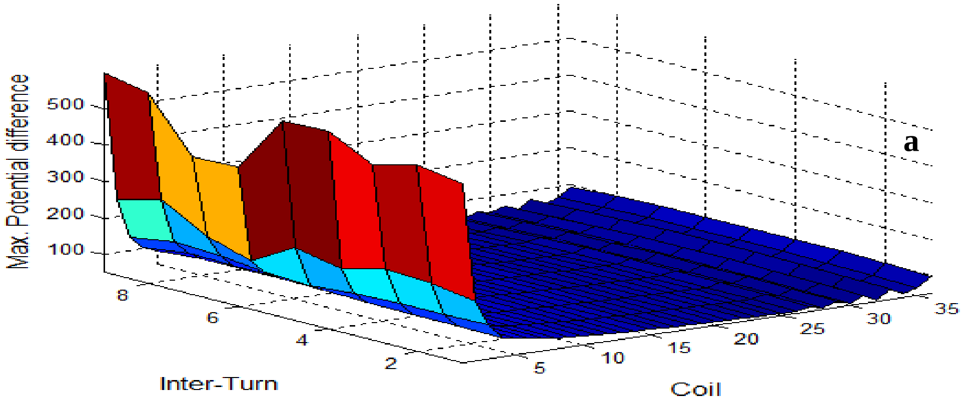

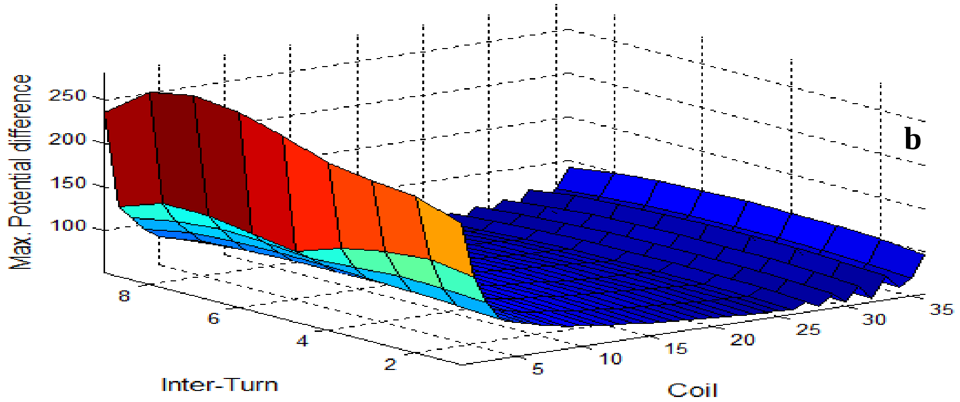

Figure 3-25: Distribution of maximum potential difference along the machine winding in 3-layer geometry with 3-meter cable: (**a**) 25 ns rise time, (**b**) 100 ns rise time

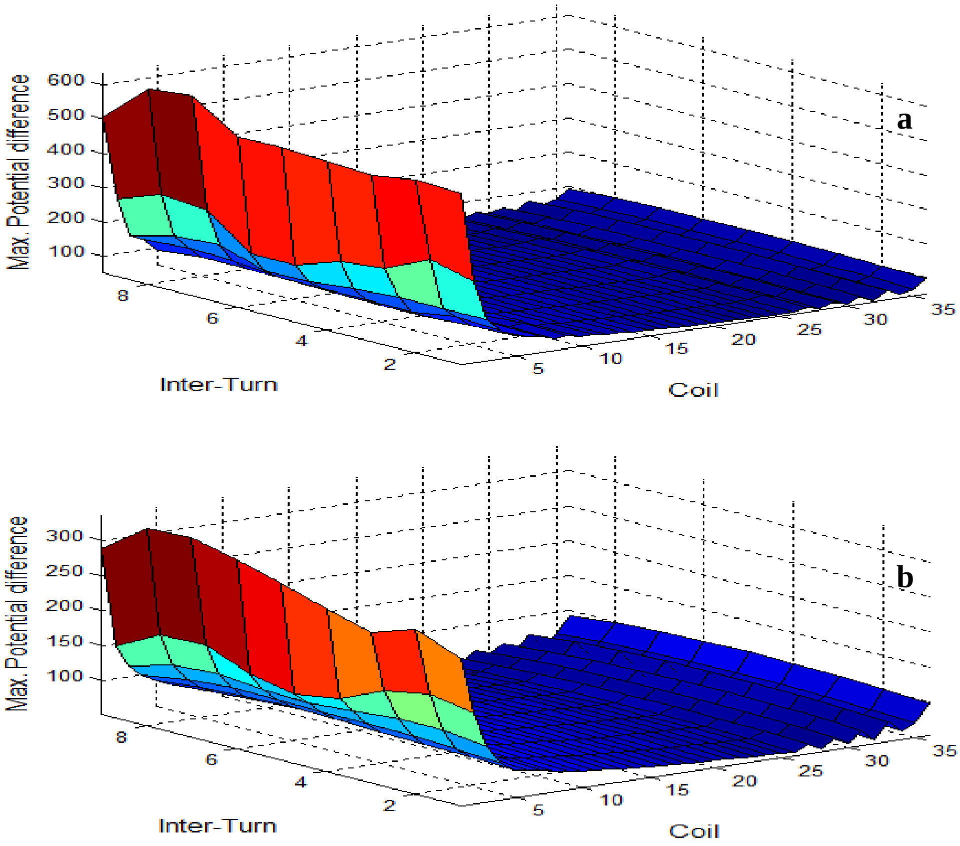

Figure 3-26: Distribution of maximum potential difference along the machine winding in 3-layer geometry with 5-meter cable: (**a**) 25 ns rise time, (**b**) 100 ns rise time

Table 3-10: Max. potential difference for an excitation with rise time of 25 ns and 100 ns in 2-layer geometry with different length of cable

Length of cable for 2-layer geometry [m]	Max. potential difference, 25 ns [V]	Max. potential difference, 100 ns [V]
1	854.222	335.991
3	860.457	440.527
5	868.089	483.304

Table 3-11: Max. potential difference for an excitation with rise time of 25 ns and 100 ns in 3-layer geometry with different length of cable

Length of cable for 3-layer geometry [m]	Max. potential difference, 25 ns [V]	Max. potential difference, 100 ns [V]
1	557.677	262.834
3	596.407	280.821
5	633.488	336.588

3.8 Summary

A frequency domain non-uniform multiconductor transmission line approach has been used to study the fast-front transient response of a machine winding coil under fast front excitation. The parameters of the coil were calculated using the finite element method. The results when applying a fast front excitation to the coil show that the rise time of the source has an important effect on the transient overvoltages produced at different turns of the coil, as well as in the potential difference between adjacent turns.

Different strategies to reduce the size of the system in the detailed modeling of machine windings for fast front transient studies have also been presented in this chapter. It has been shown that the results from these reduction strategies are equivalent and do not introduce any loss of accuracy when compared to the results considering the complete winding. It has also been demonstrated that the simulation time when using any of these strategies is greatly reduced.

In addition, the feeder cable connecting the excitation source to the winding was included considering a frequency domain distributed parameter model whose parameters are obtained from short and open circuit test measurements. After adding the different lengths of cable to the machine winding model, the results show that the rise time of the source and length of cable have an important effect on the transient overvoltage produced at different turns of the coil, as well as in the potential difference between adjacent turns.

CHAPTER IV

OPTIMIZED DIELECTRIC DESIGN OF FORM-WOUND STATOR COILS FROM ROTATING MACHINES

4.1 Introduction

Insulation breakdown of power components is a severe condition that often results in significant costs due to repairs, replacements, or outages. Even if breakdown does not occur, the deterioration of insulation systems directly impacts the component ageing process. Electrical machines are highly prone to insulation issues related to the dielectric stresses present on the windings while in operation [60].

In this dissertation, a new method to optimize the insulation design of machine windings fed by frequency converters is proposed and tested. The proposed modifications of current winding designs can potentially increase the operating life of motors without the introduction of additional and/or high-performance insulating materials. The method described here relies on the frequency domain model described in Chapter III to predict the transient response of the winding, the finite element method for the determination of the model's parameters and the computation of electric field distribution in the stator region, and several optimization algorithms to identify and evaluate modifications in the winding design resulting in a minimization of dielectric stress.

4.2 Insulation Design

There are different stresses (thermal, electrical, ambient, mechanical) that affect the deterioration process in the insulation design of machine coils. Thermal stress comes from eddy currents, stray load losses in copper conductor, windage, etc. Electrical insulating materials are thermally classified in classes A, B, F, and H based on maximum permissible temperature [60]. Electrical stress depends on the thickness of the insulation. Ambient stress refers to some factors related to the environment surrounding the machine such as high humidity, aggressive chemicals, dirt, etc. Finally, mechanical stress comes from the high rotational speeds effects such as stresses in bearings, rotor, and high centrifugal force [60]–[64].

One of most common types of failure in large industrial motors is inter-turn insulation failure, which can be due to the incidence in service of higher dielectric stresses than those which the insulation was designed to withstand [16], [21]. Insulation design of electromagnetic devices such as transformers and machines has been a topic of great interest over the last decades. The aim in motor design is to make highly efficient and low cost motors having given characteristics [37]–[39], [58]–[60].

In this dissertation optimization tools are used to find the optimal permittivity and thickness of the stator insulation system of form-wound rotating machines to minimize the dielectric stresses.

4.3 Optimization Procedure

This section describes the insulation design optimization procedure followed in this dissertation. The main steps are as follows:

- Step 1 – Parameter computation: The winding's electrical parameters (inductance matrix, capacitance matrix and losses) of the original geometry (before optimization) are obtained using COMSOL, as described in Chapter III.

- Step 2 – Computation of transient voltages: The parameters from the previous step and the model also described in in Chapter III are applied to simulate the transient response of the winding when excited by a fast front waveform.

- Step 3 – Computation of the potential differences between turns: These are obtained from the transient overvoltage obtained in the previous step. The time of maximum potential difference is then used to extract the potentials to be used in the design optimization.

- Step 4 – Optimization of the insulation design: The purpose of this step is to find the parameters that result in the minimum overall dielectric stresses. The optimization variables that are used to find the optimal objective function is the insulation layers' geometry (width and height), and the relative permittivity of each layer.

- Step 5 – Recalculation considering the optimized geometry: Electrical parameters from the optimized geometry are computed and then used as inputs in the winding model to obtain its transient response.

4.4 Optimization in Insulation Design

The objective function (to be minimized) is the maximum electric field (E) in the machine coils. As shown in Figure 4-1, the number of independent variables depends on the number of insulation layers (ℓ) and the relative permittivity (ε) in each layer. The independent variables are based on the geometrical components of each layer width (W_n) and height (H_n). The boundaries of width and height in each layer have to be specified in the corresponding optimization algorithm, as well as the range of relative permittivity, which is defined in this work as 1 to 5 to cover common values used in machine winding design. The dimensions and disposition of the slot (W, H) and the conductors (w, h) are kept constant for all conductors.

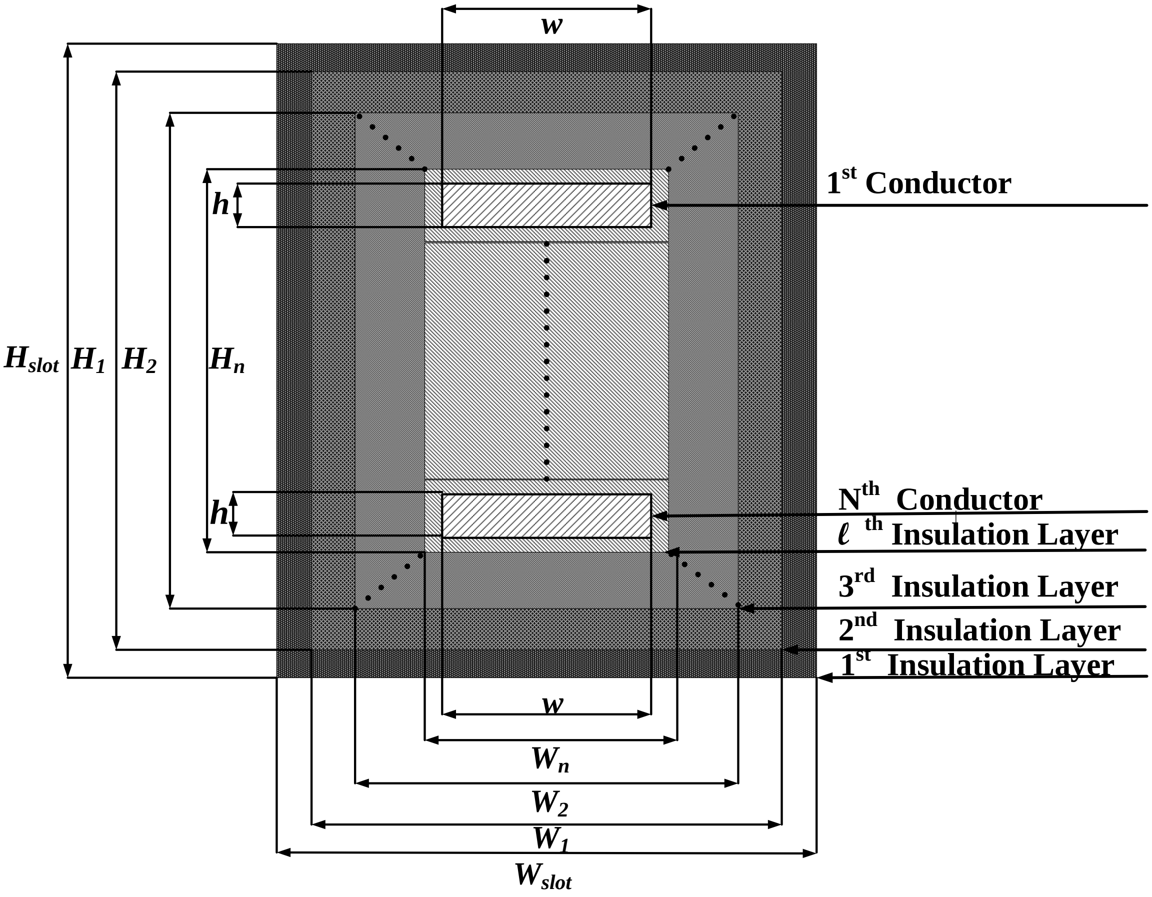

Figure 4-1: Design optimization of machine winding coil

The three main components of this design optimization problem are the objective function (E), the design (independent) variables of each layer (W, H, ε), and the constraints. These components are defined as follows:

1- Design variables (W, H, ε)

$$W = \left(W_{1\,,}\, \dots, W_n\ \right) \tag{4.1}$$

$$H = \left(H_{1\,,}\, \dots, H_n\right) \tag{4.2}$$

$$\varepsilon = \left(\varepsilon_{1\,,}\, \dots, \varepsilon_n\right) \tag{4.3}$$

2- Objective function (E)

$$E = f(W, H, \varepsilon) \tag{4.4}$$

3- Constraints

a. Width

$$\begin{gathered} \underline{W_2} \leq W_1 \leq \overline{W_{max}} \\ \underline{W_3} \leq W_2 \leq \overline{W_1} \\ \vdots \\ \underline{W_{min}} \leq W_n \leq \overline{W_{n-1}} \end{gathered} \tag{4.5}$$

b. Height

$$\begin{gathered} \underline{H_2} \leq H_1 \leq \overline{H_{max}} \\ \underline{H_3} \leq H_2 \leq \overline{H_1} \\ \vdots \\ \underline{H_{min}} \leq H_n \leq \overline{H_{n-1}} \end{gathered} \tag{4.6}$$

c. Relative permittivity

$$\begin{gathered} \underline{1} \leq \varepsilon_1 \leq \overline{5} \\ \underline{1} \leq \varepsilon_2 \leq \overline{5} \\ \vdots \\ \underline{1} \leq \varepsilon_n \leq \overline{5} \end{gathered} \tag{4.7}$$

where $\underline{W_2}$, $\underline{W_3}$, $\underline{W_{min}}$, $\underline{H_2}$, $\underline{H_3}$, and $\underline{H_{min}}$ are the lower limits of the corresponding independent variables. $\overline{W_1}$, $\overline{W_{n-1}}$, $\overline{W_{max}}$, $\overline{H_1}$, $\overline{H_{n-1}}$, and $\overline{H_{max}}$ are the upper limits of the corresponding independent variables . $W_{min.}$ is the width of conductor ($\boldsymbol{w}$). $H_{min.}$ is the summation of height (h) for all conductors in machine coil with the distance between them. $W_{max.}$ is the width of slot. $H_{max.}$ is the height of slot. ε_1, ε_2, and ε_n are the relative permittivities for each insulation layer. All the solutions of the objective function under the constraints define the feasible region of the geometry.

4.5 Optimization Example

Figure 4-2 shows an illustrative geometry to describe the design optimization of the machine winding. This geometry has three conductors with three insulation layers. The main geometrical parameters of this configuration are summarized in Table 4-1.

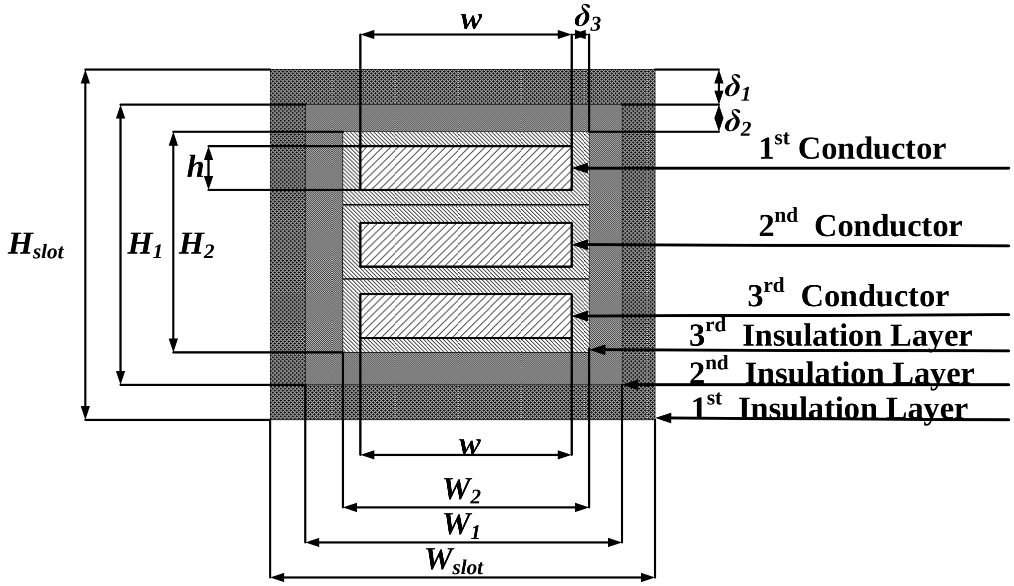

Figure 4-2: Design optimization for example geometry

Table 4-1: Parameters of example geometry

Parameter	Value
Conductor width (w)	3.04 mm
Conductor height (h)	1.59 mm
Thickness of interturn insulation (δ_3)	0.11 mm
Thickness of main insulation (δ_2)	0.96 mm
Thickness of ground wall insulation (δ_1)	0.33 mm
Relative permittivity of the interturn insulation (ε_3)	2.5
Relative permittivity of the main insulation (ε_2)	2
Relative permittivity of the ground wall insulation (ε_1)	4
Slot width (W_{slot})	5.84 mm
Slot Height (H_{slot})	8.01 mm

The main geometrical information for the design optimization is as follows:

1- Width (w = 3.04 mm) and height (h = 1.59mm) of each conductor.
2- Width ($W_1 = 5.18\ mm$) and height ($H_{1,} = 7.35\ mm$) of first insulation layer.
3- Width ($W_2 = 3.26\ mm$) and height ($H_2 = 5.43\ mm$) of second insulation layer.
4- Width ($W_{slot} = 5.84\ mm$) and height ($H_{slot} = 8.01\ mm$) of slot.
5- Maximum width ($W_{max} = W_{slot}$) and maximum height ($H_{max} = H_{slot}$) corresponding to the width and height of the slot.
6- Minimum width ($W_{min} = w$) and minimum height ($H_{min} = 5.21mm$) determined by the conductors' arrangement.
7- Relative permittivity of each insulation layer ($\varepsilon_1 = 4, \varepsilon_2 = 2, and\ \varepsilon_3 = 2.5$).

The design optimization of this geometry has three variables; the objective function (*E*), the design (independent) variables of each layer (*W*, *H*, *ε*), and the constraints. These components are defined as follows:

1- Design variables (*W*, *H*, *ε*)

$$W = \left(W_{1,}W_{2,}\right) \tag{4.8}$$

$$H = (H_{1,}H_2) \tag{4.9}$$

$$\varepsilon = \left(\varepsilon_{1,}\varepsilon_2, \varepsilon_3\right) \tag{4.10}$$

2- Objective function (*E*)

$$E = f(W_, H, \varepsilon) \tag{4.11}$$

3- Constraints

   a. Width

$$\underline{W_2} \leq W_1 \leq \overline{W_{max}} \tag{4.12}$$

$$\underline{W_{min}} \le W_2 \le \overline{W_1} \tag{4.13}$$

b. Height

$$\underline{H_2} \le H_1 \le \overline{H_{max}} \tag{4.14}$$

$$\underline{H_{min}} \le H_2 \le \overline{H_1} \tag{4.15}$$

c. Relative permittivity

$$\begin{gathered} \underline{1} \le \varepsilon_1 \le \overline{5} \\ \underline{1} \le \varepsilon_2 \le \overline{5} \\ \underline{1} \le \varepsilon_3 \le \overline{5} \end{gathered} \tag{4.16}$$

4.6 Optimization Algorithms

The optimization algorithms from the optimization module of COMSOL and the optimization algorithms functions from the MATLAB optimization toolbox interfaced with COMSOL are applied to obtain an optimum insulation design. The algorithms chosen from the COMSOL's optimization module are

1- Nelder–Mead (NM)

The Nelder-Mead simplex algorithm is one of most popular derivative-free methods [65]. This method is used to find the minimum objective function $f(x)$ of parameters $x = [x^{(1)} \quad x^{(2)} \dots x^{(n)}]$.

$$\min f(x) \tag{4.17}$$

Nelder-Mead minimizes $f(x)$ by comparing the function value at (n+1) vertices with the highest value of another points. The vertices of the simplex at each iteration are ordered according to the objective function values:

$$f(x_1) \leq f(x_2) \leq f(x_3) \dots\dots.. \leq f(x_{n+1}) \quad (4.18)$$

In order to converge on the smallest value of $f(x_1)$, the Nelder-Mead algorithm specifies a sequence of steps for iteratively updating the worst design in the simplex $f(x_{n+1})$. At each iteration, the Nelder-Mead algorithm has several steps: sort, reflection, expansion, outside contraction, inside contraction, and shrink [66]–[68]. This method is very robust and can deal with local solutions, indeterminacies, and discontinuities in the function being evaluated.

2- Bound Optimization by Quadratic Approximation algorithm (BOBYQA)

BOBYQA is an optimization algorithm that looks for the least value of an objective function $f(x)$. The objective function can be defined by another subroutine that return the value $f(x)$ for any x that works with the constrains. In general, BOBYQA is an iterative algorithm that is used to find the minimum of a function $f(x)$ subject to bound constraints of the optimization variables. f is specified to return the value $f(x)$ for any feasible x. A quadratic approximation that satisfies the interpolation points is chosen and adjusted automatically at each iteration. In this algorithm, no first derivatives of f are required explicitly [69].

3- Coordinate search algorithm (CS)

Direct-search methods are derivative-free methods that sample the objective function at a finite number of points at each iteration and decide which actions to take next solely based on those function values. One of these directional direct-search methods is called coordinate or compass search. The coordinate search algorithm has two steps: (1) poll step which poll points and start evaluate the objective function until the polling is successful when one of polling points is better than current iteration in terms of value of objective function, and (2) parameter update if the iteration is successful [65].

The algorithms chosen from the MATLAB optimization toolbox are

4- Fmincon (FMC)

This function can be used with constrained nonlinear multivariable functions. Fmincon is based on constrained nonlinear optimization or nonlinear programming models. This function has as a major limitation the possibility of converging to a local minimum. Besides, the objective and constraint functions and their first derivatives have to be continuous [22], [23].

5- Fminsearchband (FMSB)

This algorithm finds the minimum of a scalar function of several variables, starting at an initial estimate. This is generally referred to as unconstrained nonlinear optimization. Lower and upper bound constraints are applied by means of a transformations of the variables [22], [23].

6- Particle swarm optimization (PSO)

In the context of PSO, a swarm can be defined as ‘a population of interacting elements that is able to optimize some global objective through collaborative search of a space’ [70]. The algorithms use a population of search points in the search space. The best position attained in the search space is called experience. In order to find better solutions to the problem of interest, the nature of the interacting elements (particles) move (fly) in an n-dimensional search space. The properties of each particles are: a current position and a velocity. Each particle has a memory of the best location (P_{best}) in the search space and the neighborhood around each particle (g_{best}). The particles are moved from current position at each step of algorithm by applying the velocity vector. The velocity is affected by the location of a particle relative to its P_{best} and g_{best} and the velocity in the previous iteration of the algorithm. Following is the description of PSO algorithm steps [70], [71]

1. Specify the initialization each particle in the population by selecting values for its location and velocity vectors.
2. Calculate the fitness value of each particle.
3. Determine the location of the particle with the highest fitness.
4. Calculate velocity in each particle according to equation (4.19)
5. Update the location of each particle according to equation (4.21)
6. The steps (2-5) are repeated until the criteria are met.

The velocity vector v_i for the particle i is given by:

$$v_\mathrm{i}(t+1) = \left(w\, v_\mathrm{i}(t)\right) + \left(c_1 R_1 (P_{best} - x_\mathrm{i})\right) + (c_2 R_2 (g_{best} - x_\mathrm{i})) \tag{4.19}$$

where

$$w = w_{max} - \left(\frac{w_{max.} - w_{min.}}{iter_{max}}\right) iter \tag{4.20}$$

P_{best} is the best solution in particle i; g_{best} is the location of best solution; c_1 and c_2 are the weights of P_{best} and g_{best}; x_i is the current location of particle i; R_1 and R_2 are the random numbers; w is the a momentum coefficient; $iter_{max}$ and $iter$ are total number of iteration and the current iteration, respectively; $w_{max.}$ and $w_{min.}$ are upper and lower boundaries of the momentum coefficient, respectively.

Once the velocity is updated, the position is updated according to equation (4.21) and P_{best} is updated according to equation (4.22).

$$x_i(t+1) = x_i(t) + v_i(t+1) \tag{4.21}$$

$$y_i(t+1) = \begin{cases} y_i(t) & \text{If } f(x_i(t)) \leq f(y_i(t)), y_i(t+1) \\ x_i(t) & \text{If } f(x_i(t)) > f(y_i(t)), y_i(t+1) \end{cases} \tag{4.22}$$

4.7 Applications

The optimization method described in the previous sections is applied to two different geometries of a form-wound machine coil. The optimization algorithms described in Section 4.6 are tested and compared for these geometries.

4.7.1 Optimization of Geometries

The objective function (to be minimized) is the maximum electric field in the machine coils. The number of independent variables depends on the number of insulation layers and the relative permittivity of each layer. The boundaries of width and height in each layer have to be specified in the corresponding optimization algorithm, as well as the range of relative permittivity, which is defined as 1 to 5 to cover common values used in the machine winding design. The dimensions and disposition of the slot and the conductors are kept constant. The excitation applied is a step voltage waveform with magnitude of 1750 V and rise time of 25 ns. The computer time for a typical simulation is as follows:

- 109 s for the simulation of the winding response using the model implemented in MATLAB.

- 3 s for the simulation of electric field distribution using COMSOL.

These times were obtained using a computer server with 2 Intel Xeon processors running at 2.40 GHz and 128 GB of RAM. Figure 4-3 shows the electric field distribution in the original 2-layer and 3-layer geometries (before optimization) obtained by means of 2D simulations using COMSOL. The maximum electric field is 3.4143 MV/m for the 2-layer geometry and 3.5576 MV/m for the 3-layer geometry.

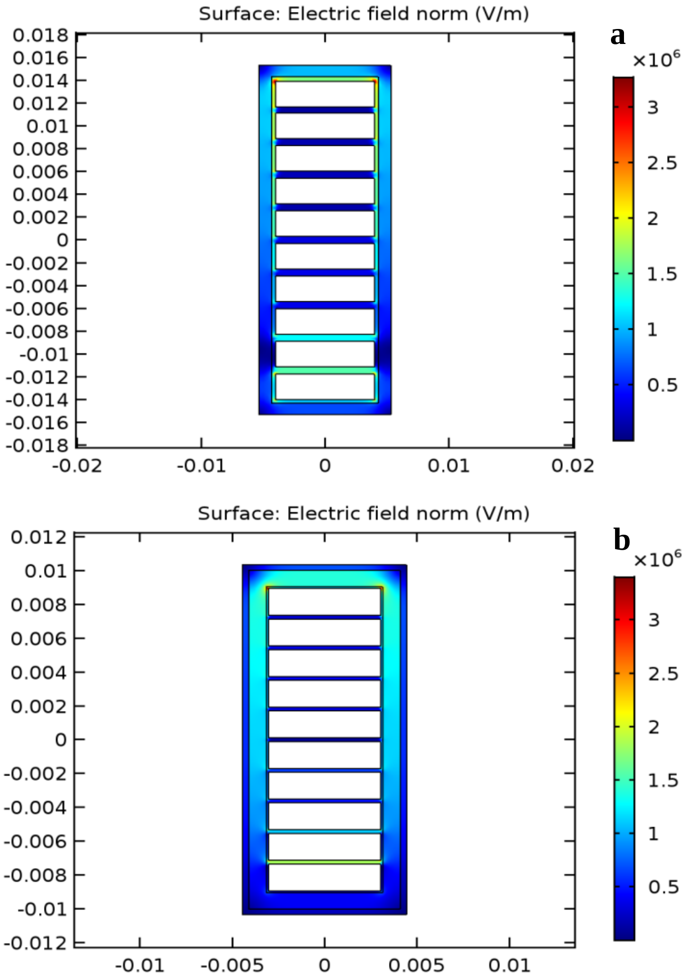

Figure 4-3: Electric field distribution before optimization: (**a**) 2-layer geometry, (**b**) 3-layer geometry

Tables 4-2 and 4-3 show the dimensions and permittivities obtained after applying the optimization algorithms for the 2 and 3-layer geometries. W1, H1 and W2, H2 correspond to the widths and heights including the first and second insulating layers. A, B, C are the permittivities of the first, second and third layer, respectively.

Table 4-2: Optimized parameters for 2-layer geometry

Optimization Algorithms	Geometrical parameters and relative permittivity for 2-layer geometry			
	W1	H1	A	B
	[mm]			
Initial values	8.62	28.6	2.6	4.2
CS	8.62	28.6	4.85	1.41
NM	8.82	29.6	2.63	4.17
BOBYQA	8.62	28.6	2.60	4.20
FMC	9.38	28.1	2.85	1.00
FMSB	8.96	28.7	4.25	1.61
PSO	8.81	29.3	4.18	1.54

Table 4-3: Optimized parameters for 3-layer geometry

Optimization Algorithms	Geometrical parameters and relative permittivity for 3-layer geometry						
	W1	H1	W2	H2	A	B	C
	[mm]						
Initial values	6.3	18.1	8.22	20.00	2.5	2	4
CS	6.30	18.10	8.22	20.02	4.93	1.63	1.00
NM	6.30	18.10	8.91	20.02	2.80	2.00	4.00
BOBYQA	7.48	19.28	7.48	20.67	2.50	2.00	4.00
FMC	7.47	19.18	8.47	20.13	4.98	1.80	1.34
FMSB	6.40	18.26	8.17	20.07	3.03	1.39	3.86
PSO	7.14	19.04	7.86	19.31	4.81	1.71	1.01

Table 4-4: Max. electric field after optimization for 2-layer geometry

Algorithm	Max. (E) before Opt.	Max. (E) after Opt.	Reduction [%]
	[MV/m]		
CS	3.4143	1.8714	45.19
NM		2.9820	12.66
BOBYQA		3.2154	5.83
FMC		1.9274	43.55
FMSB		1.7884	47.62
PSO		1.6888	50.54

Table 4-5: Max. electric field after optimization for 3-layer geometry

Algorithm	Max. (E) before Opt.	Max. (E) after Opt.	Reduction [%]
	[MV/m]		
CS	3.5576	2.2574	36.55
NM		3.1526	11.38
BOBYQA		3.1360	11.85
FMC		2.1709	38.98
FMSB		2.2108	37.86
PSO		2.0159	43.33

Tables 4-4 and 4-5 compare the maximum electric field before and after optimization for the same geometries. According to Tables 4-4 and 4-5, the optimized geometries for both layering configurations can achieve a percentage of reduction of dielectric stress in the order of 43-50%. These tables also show that, for the cases under consideration, particle swarm optimization produced the best results. The optimized geometries obtained with PSO and their electric field distributions are shown in Figure 4-4.

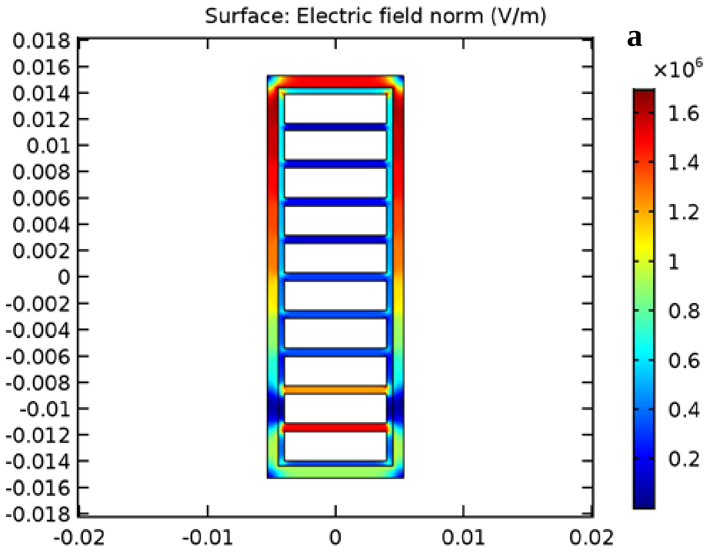

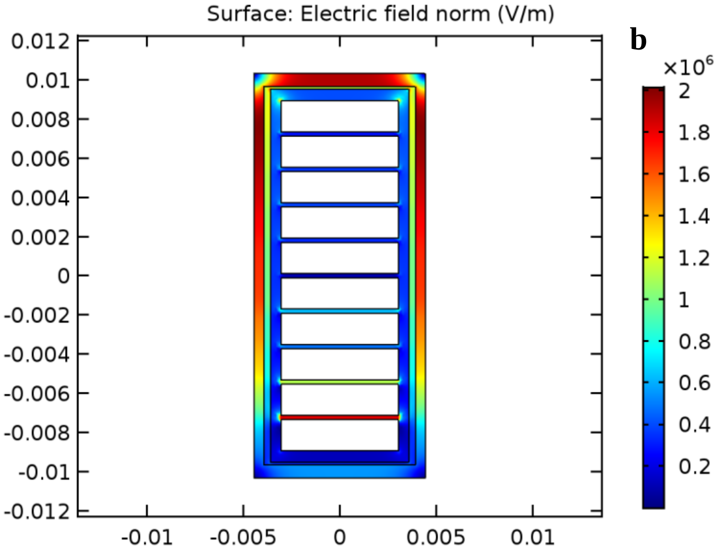

Figure 4-4: Electric field distribution after PSO optimization: (**a**) 2-layer geometry, (**b**) 3-layer geometry

4.7.2 Transient Overvoltages in Optimized Machine Model

The waveforms in Figures 4-5 and 4-6 show the distribution of transient voltages along the 2-layer and 3-layer coils before and after the application of the PSO algorithm. The excitation applied is a step voltage waveform with magnitude of 1750 V and rise times of 25 and 100 ns.

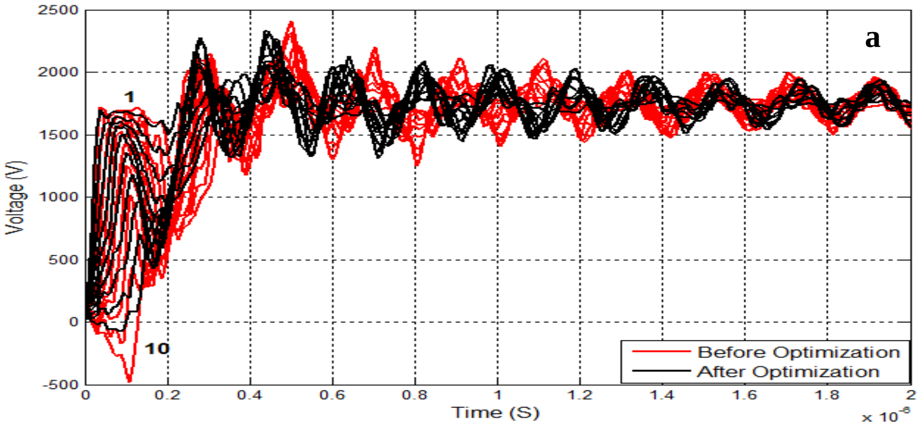

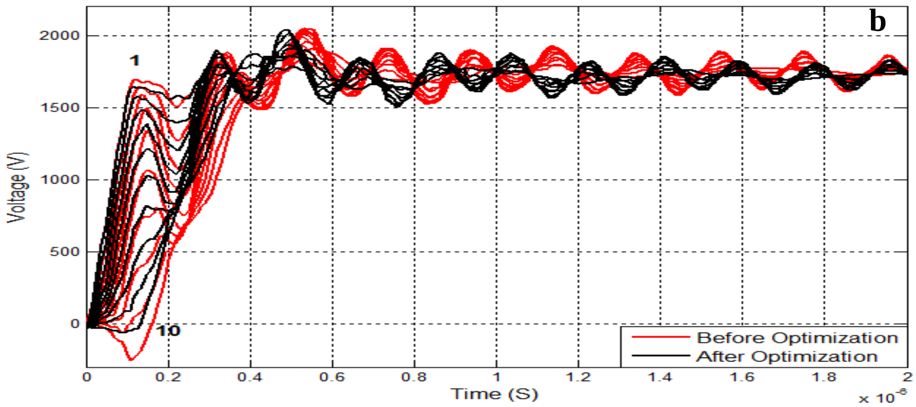

Figure 4-5: Transient voltage along the coil turns before and after PSO optimization in 2-layer geometry: (**a**), 25 ns rise time, (**b**) 100 ns rise time

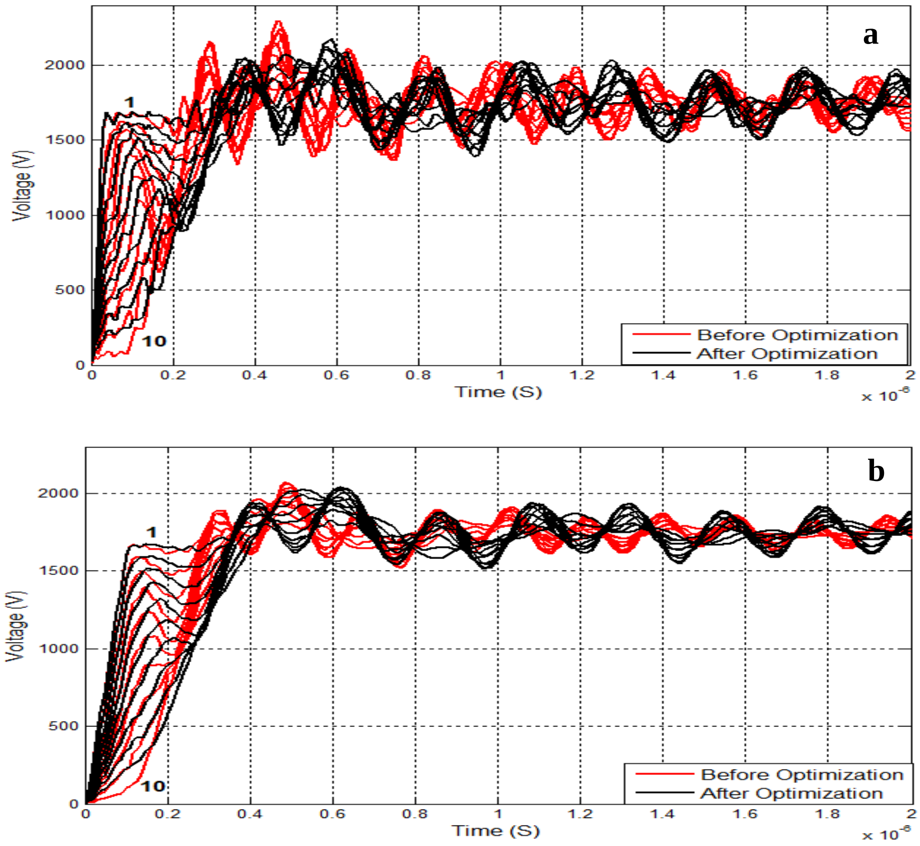

Figure 4-6: Transient voltage along the coil turns before and after PSO optimization in 3-layer geometry: (**a**), 25 ns rise time, (**b**) 100 ns rise time

Tables 4-6 and 4-7 list the maximum transient voltages before and after PSO optimization for the 2 and 3-layer geometries. Although the reduction of transient voltages is discrete, the optimized geometries result in a largely improved transient voltage distribution along the turns, giving rise to a considerable reduction of potential difference between turns, as shown next.

Table 4-6: Max. transient overvoltage for an excitation with rise time of 25 ns

Geometry	Max. overvoltage in 25 ns		
	Before opt. [V]	After opt. [V]	Reduction [%]
2-layer	2414.57	2326.715	3.63
3-layer	2309.36	2176.342	5.76

Table 4-7: Max. transient overvoltage for an excitation with rise time of 100 ns

Geometry	Max. overvoltage in 100 ns		
	Before opt. [V]	After opt. [V]	Reduction [%]
2-layer	2059.09	2035.50	1.14
3-layer	2078.56	2037.96	1.95

4.7.3 Potential Difference Between Turns in Optimized Machine Model

Figures 4-7 and 4-8 show the potential difference for the optimized 2 and 3-layer geometries and rise times under consideration. It can be noticed that the largest potential differences occur in both geometries at the first coil and with 25 ns of rise time.

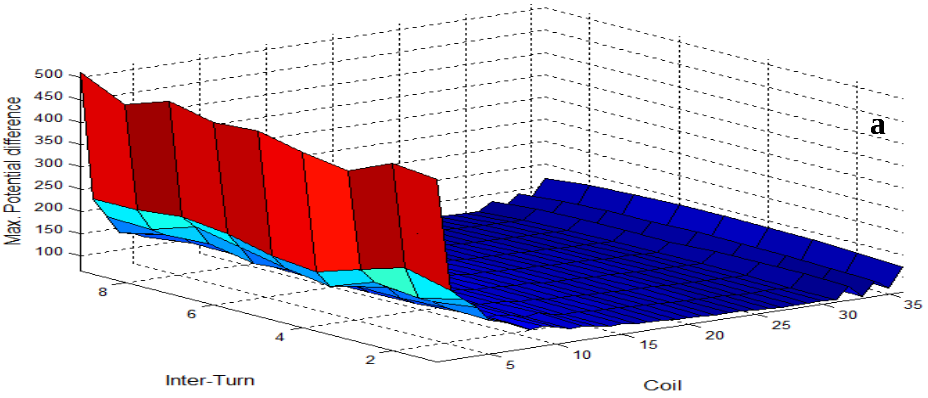

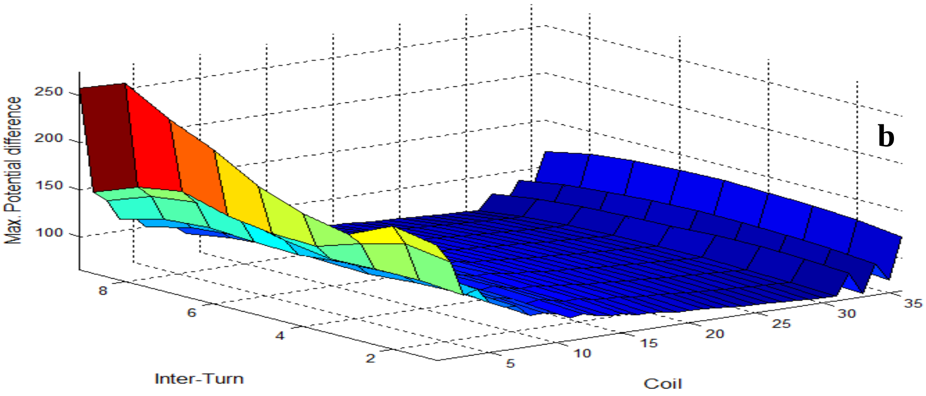

Figure 4-7: Distribution of maximum potential difference along the machine winding after PSO optimization in 2-layer geometry: (**a**) 25 ns rise time, (**b**) 100 ns rise time

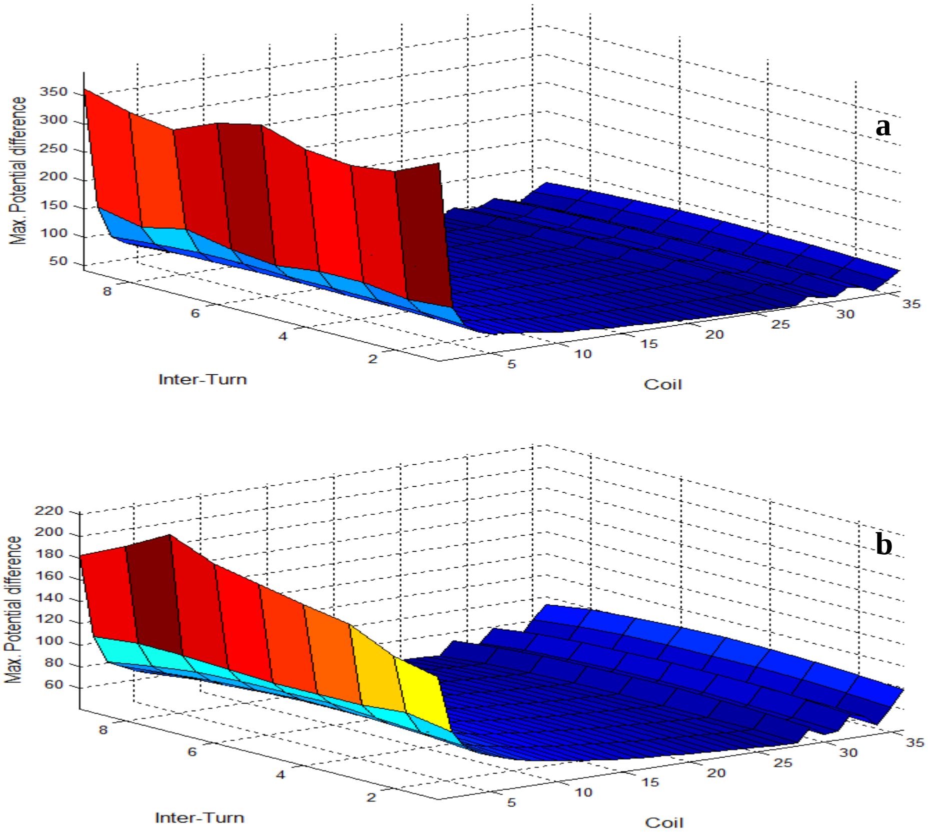

Figure 4-8: Distribution of maximum potential difference along the machine winding after PSO optimization in 3-layer geometry: (**a**) 25 ns rise time, (**b**) 100 ns rise time

Tables 4-8 and 4-9 compare the maximum potential difference before and after PSO optimization for the same geometries with different rise times. It is clear from these tables that the optimized geometries considerably reduce the maximum potential difference between turns.

Table 4-8: Max. potential difference for an excitation with rise time of 25 ns

Geometry	Max. potential difference in 25 ns		
	Before opt. [V]	After opt. [V]	Reduction [%]
2-layer	824.17	512.48	37.82
3-layer	431.67	321.86	25.43

Table 4-9: Max. potential difference for an excitation with rise time of 100 ns

Geometry	Max. potential difference in 100 ns		
	Before opt. [V]	After opt. [V]	Reduction [%]
2-layer	332.12	274.80	17.26
3-layer	233.34	173.81	25.51

4.7.4 Transient Overvoltages in Optimized Machine Model Including Feeder Cable

The waveforms from Figures 4-9 to 4-14 show the distribution of transient voltages along the 2-layer and 3-layer coils before and after the application of the PSO algorithm after adding different length of cable (1, 3, and 5 m). The excitation applied is a step voltage waveform with magnitude of 1750 V and rise times of 25 and 100 ns.

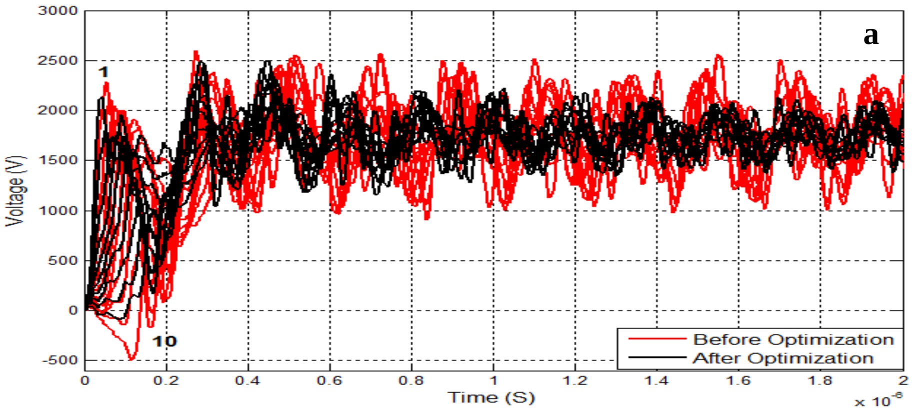

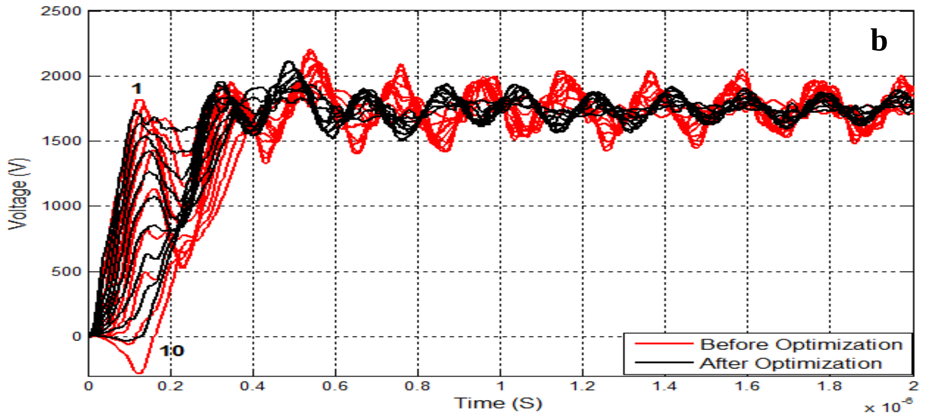

Figure 4-9: Transient voltage along the coil turns before and after PSO optimization in 2-layer geometry with 1-meter cable: (**a**), 25 ns rise time, (**b**) 100 ns rise time

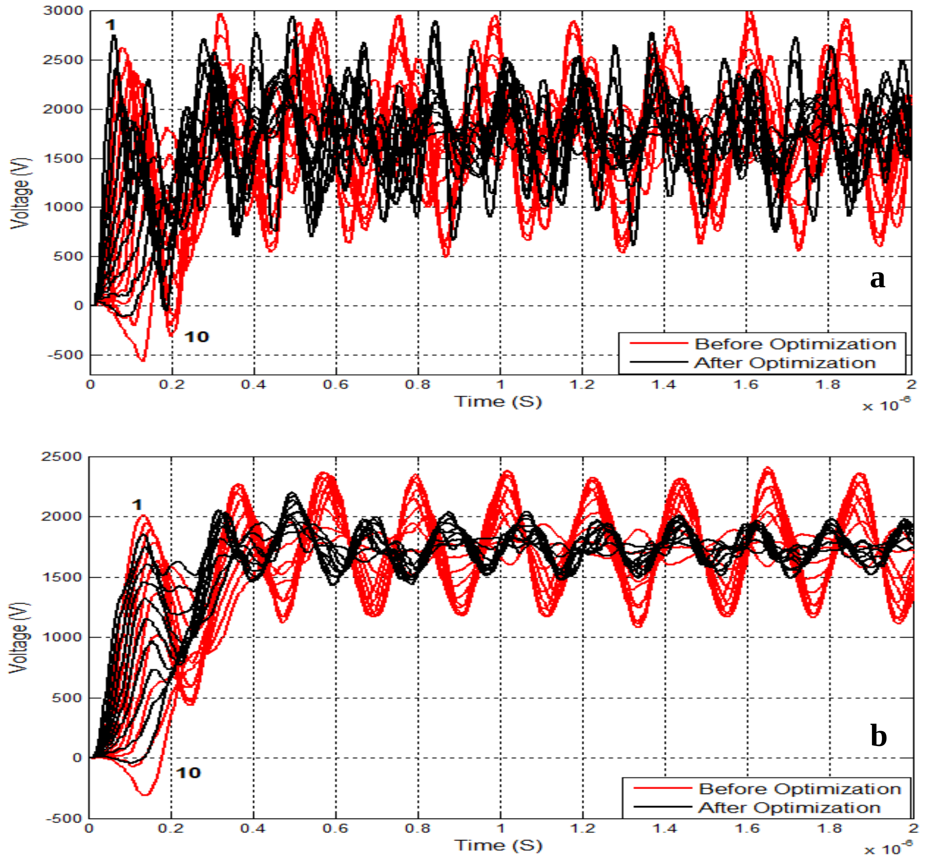

Figure 4-10: Transient voltage along the coil turns before and after PSO optimization in 2-layer geometry with 3-meter cable: (**a**), 25 ns rise time, (**b**) 100 ns rise time

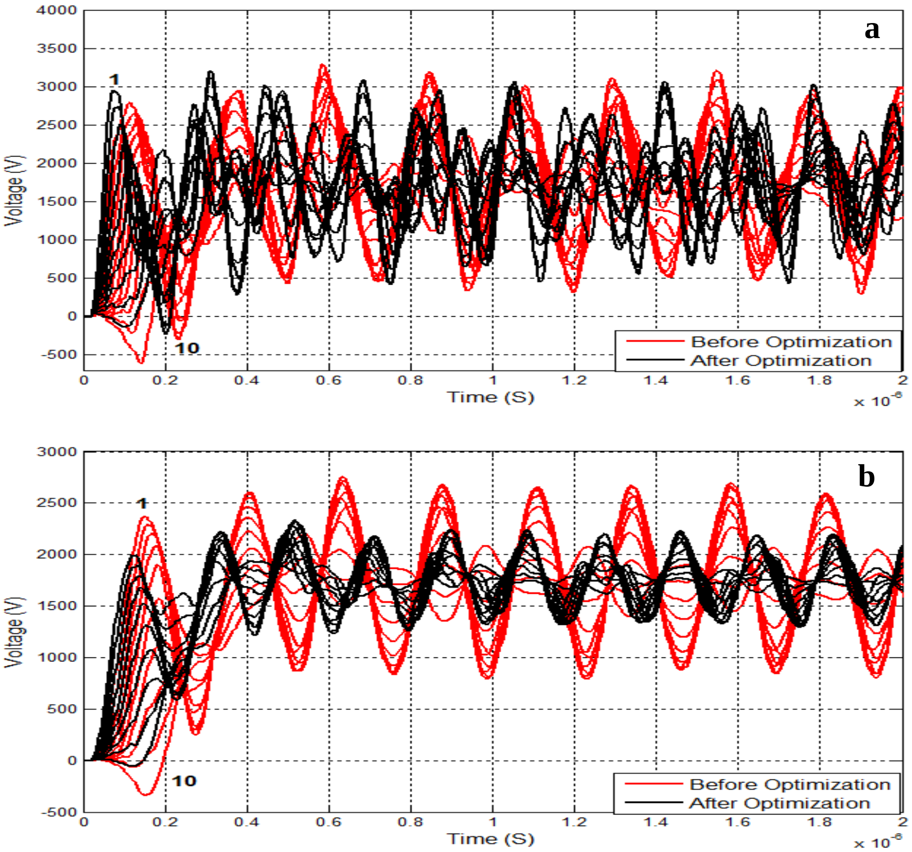

Figure 4-11: Transient voltage along the coil turns before and after PSO optimization in 2-layer geometry with 5-meter cable: (**a**), 25 ns rise time, (**b**) 100 ns rise time

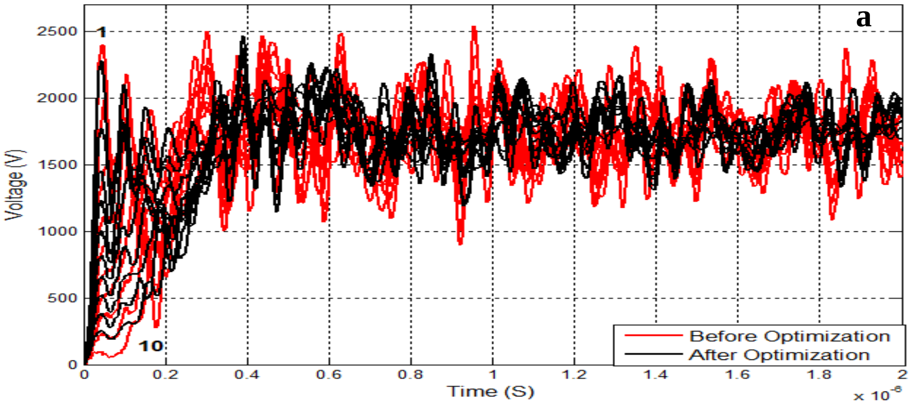

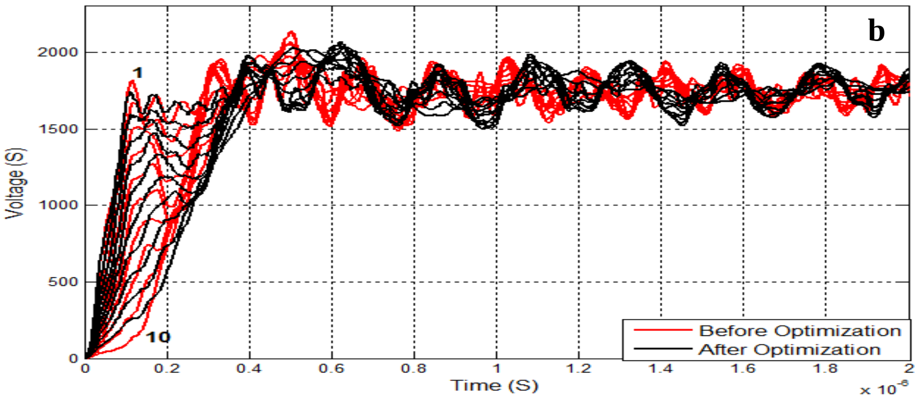

Figure 4-12: Transient voltage along the coil turns before and after PSO optimization in 3-layer geometry with 1-meter cable: (**a**), 25 ns rise time, (**b**) 100 ns rise time

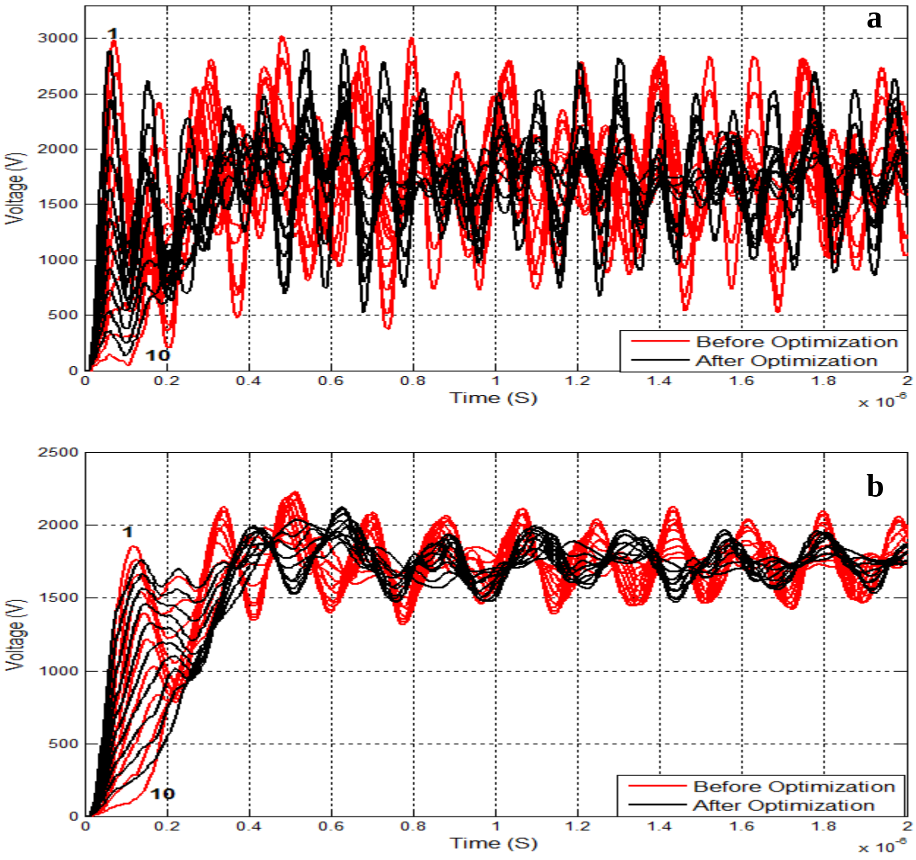

Figure 4-13: Transient voltage along the coil turns before and after PSO optimization in 3-layer geometry with 3-meter cable: (**a**), 25 ns rise time, (**b**) 100 ns rise time

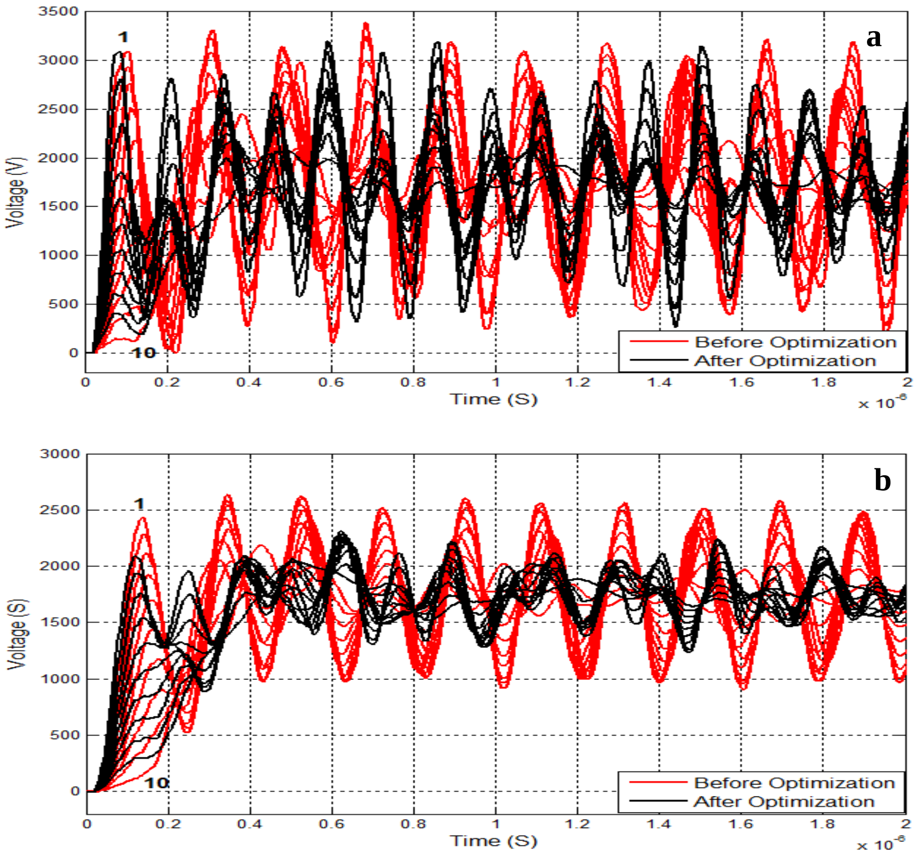

Figure 4-14: Transient voltage along the coil turns before and after PSO optimization in 3-layer geometry with 5-meter cable: (**a**), 25 ns rise time, (**b**) 100 ns rise time

Even though the optimization algorithms find the optimal geometry without considering the effect of feeder cable, the optimal geometry can also reduce the transient overvoltage after adding different lengths of feeder cable, as shown in Figures 4-9 to 4-14.

Table 4-10: Max. transient overvoltage for an excitation with rise time of 25 ns in 2 and 3-layer geometries with different lengths of cable

Geometry	Max. overvoltage, 25 ns			
	Length of cable [M]	Before opt. [V]	After opt. [V]	Reduction [%]
2 -layer	1	2599.56	2501.57	3.7694
	3	3016.06	2953.45	2.0759
	5	3288.22	3190.56	2.9700
3-layer	1	2539.58	2463.83	2.9827
	3	3015.32	2907.79	3.5664
	5	3389.63	3197.34	5.6728

Tables 4-10 and 4-11 list the maximum transient voltages before and after PSO optimization for the 2 and 3-layer geometries with different lengths of cable (1, 3, and 5 m).

Table 4-11: Max. transient overvoltage for an excitation with rise time of 100 ns in 2 and 3-layer geometries with different length of cable

Geometry	Max. overvoltage, 100 ns			
	Length of cable (M)	Before opt. [V]	After opt. [V]	Reduction [%]
2-layer	1	2207.51	2109.57	4.4367
	3	2407.93	2202.50	8.5314
	5	2753.07	2340.98	14.9681
3-layer	1	2140.76	2067.62	3.4165
	3	2230.93	2128.48	4.5920
	5	2633.84	2314.46	12.1259

4.7.5 Potential Difference Between Turns in Optimized Machine Model Including Feeder Cable

Figures 4-15 to 4-20 show the potential difference before optimization with different lengths of cable and rise times under consideration. It can be noticed that the largest potential differences occur in both geometries at the first coil and with 25 ns of rise time.

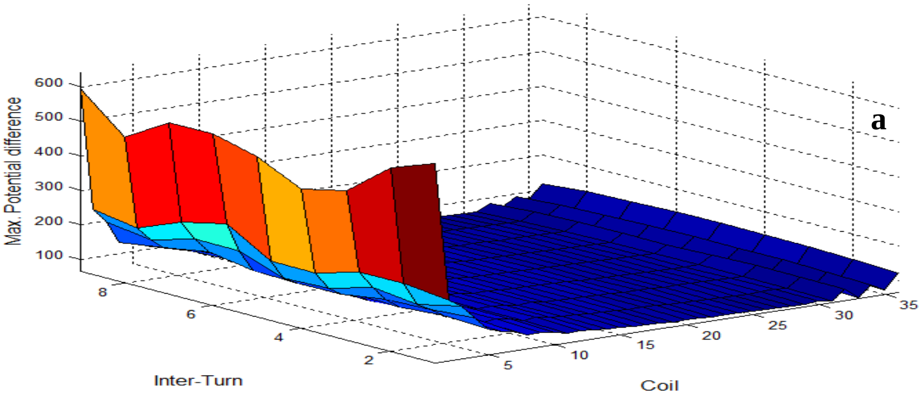

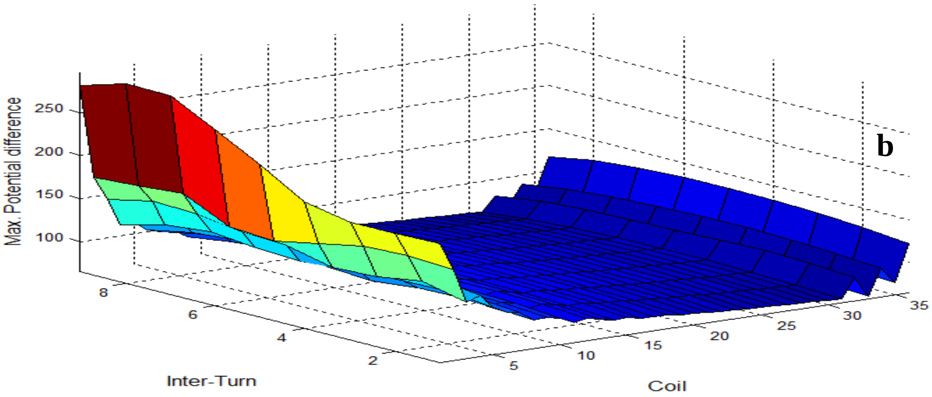

Figure 4-15: Distribution of maximum potential difference along the machine winding after PSO optimization in 2-layer geometry with 1-meter cable: (**a**) 25 ns rise time, (**b**) 100 ns rise time

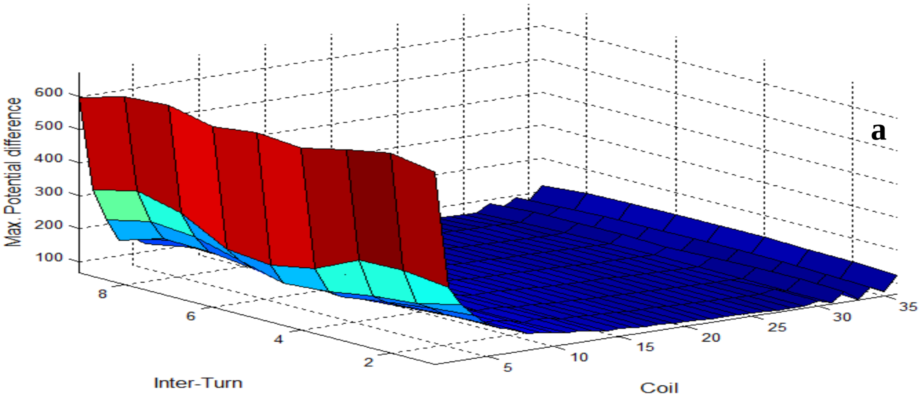

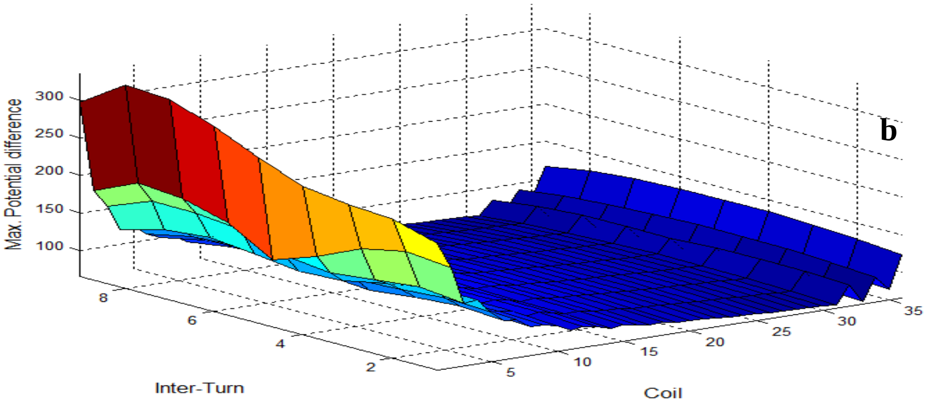

Figure 4-16: Distribution of maximum potential difference along the machine winding after PSO optimization in 2-layer geometry with 3-meter cable: (**a**) 25 ns rise time, (**b**) 100 ns rise time

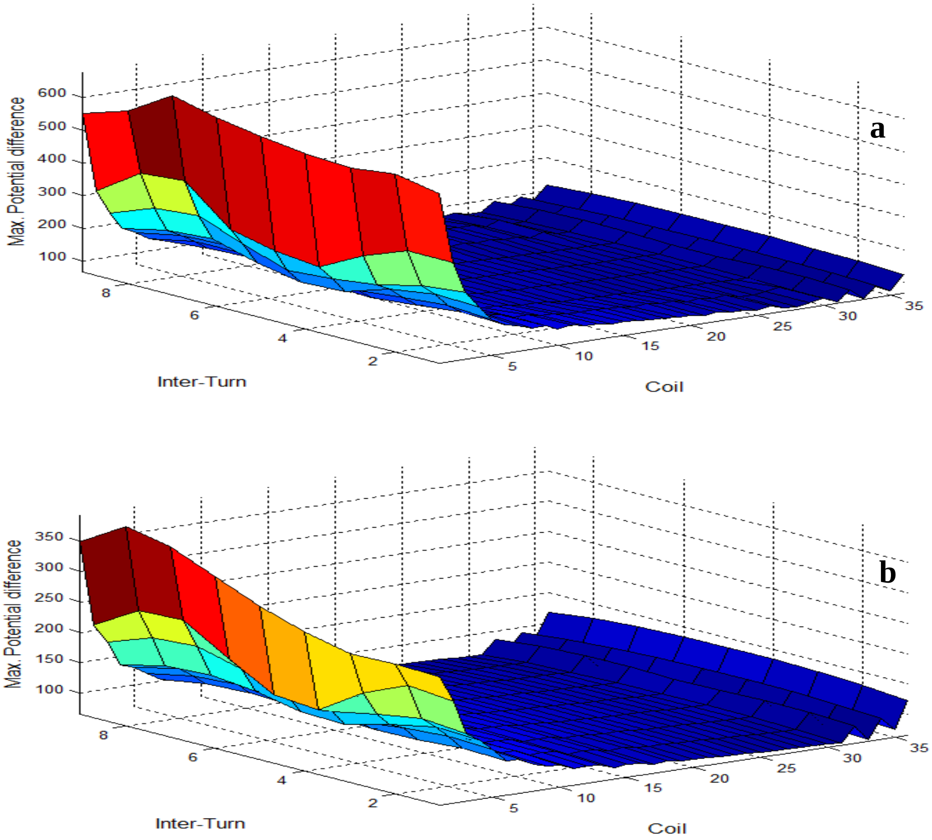

Figure 4-17: Distribution of maximum potential difference along the machine winding after PSO optimization in 2-layer geometry with 5-meter cable: (**a**) 25 ns rise time, (**b**) 100 ns rise time

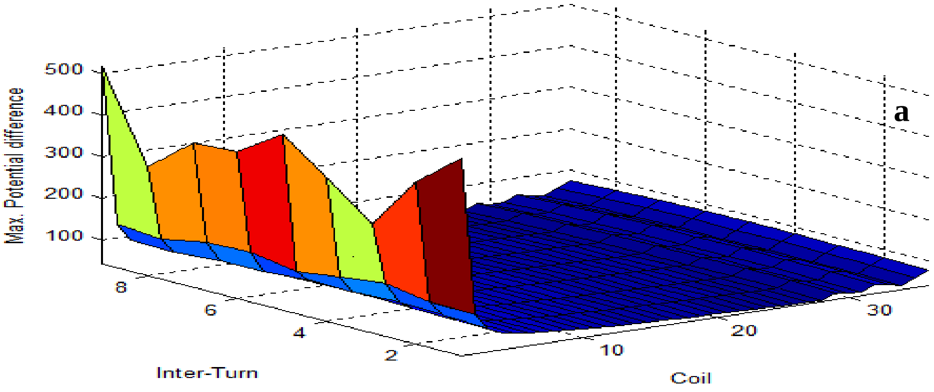

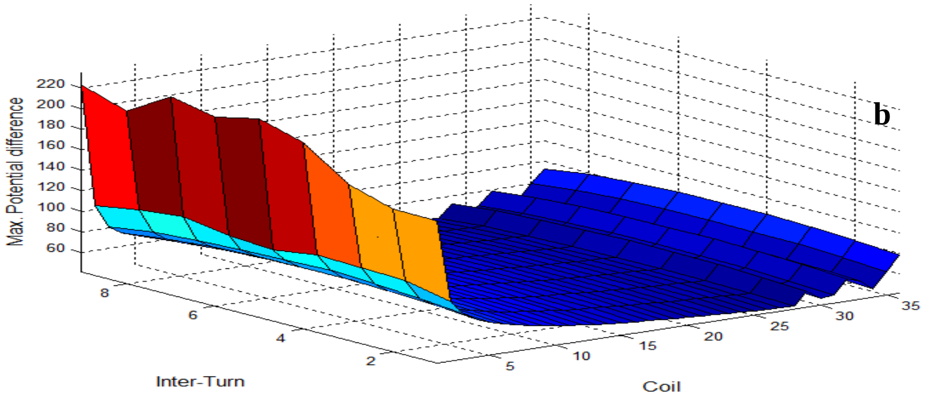

Figure 4-18: Distribution of maximum potential difference along the machine winding after PSO optimization in 3-layer geometry with 1-meter cable: (**a**) 25 ns rise time, (**b**) 100 ns rise time

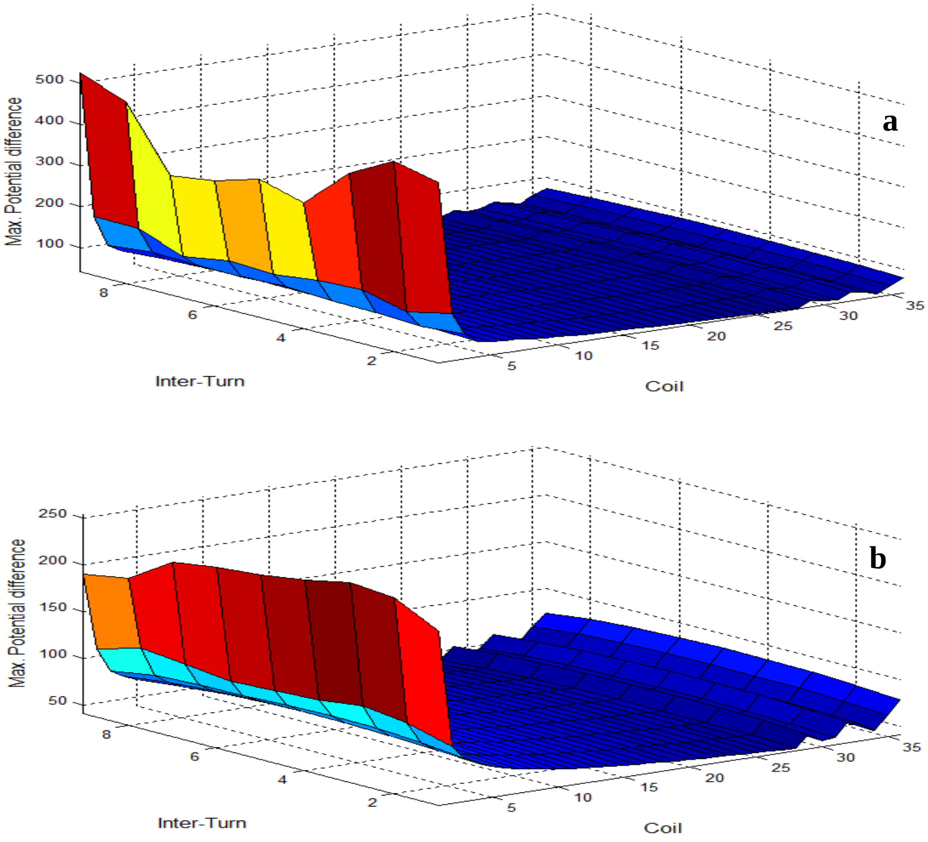

Figure 4-19: Distribution of maximum potential difference along the machine winding after PSO optimization in 3-layer geometry with 3-meter cable: (**a**) 25 ns rise time, (**b**) 100 ns rise time

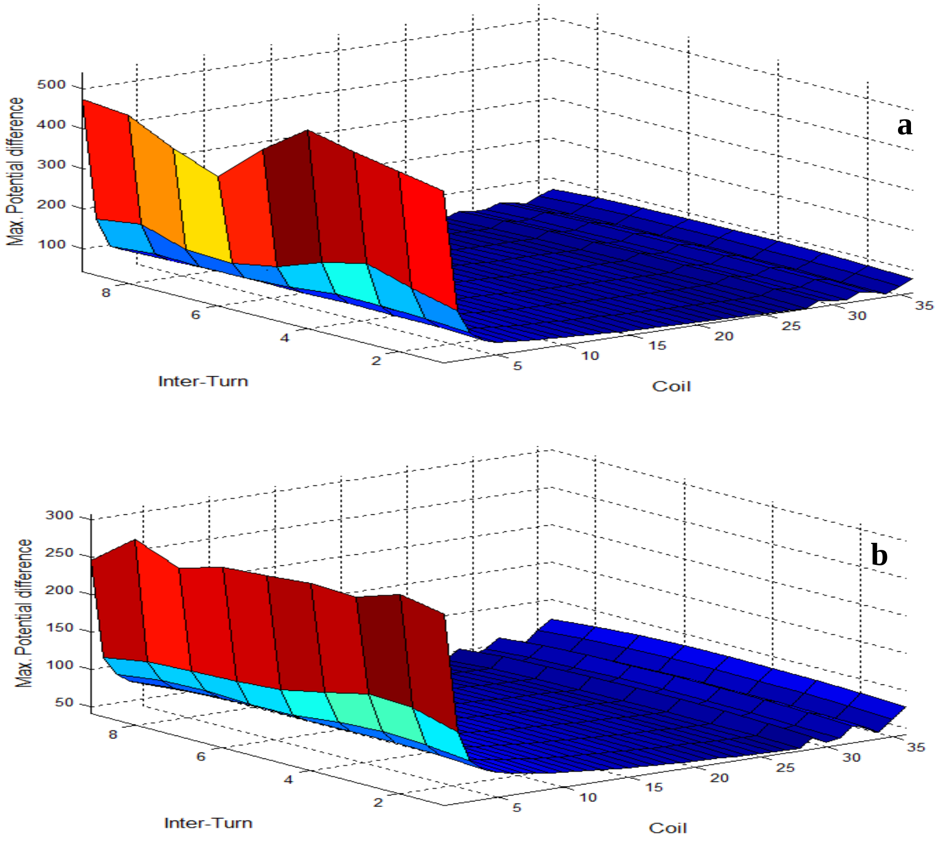

Figure 4-20: Distribution of maximum potential difference along the machine winding after PSO optimization in 3-layer geometry with 5-meter cable: (**a**) 25 ns rise time, (**b**) 100 ns rise time

Tables 4-12 and 4-13 compare the maximum potential difference before and after PSO optimization for the same geometries with different lengths of cable and different rise times.

Table 4-12: Max. potential difference for an excitation with rise time of 25 ns

Geometry	Max. Potential difference, 25 ns			
	Length of cable (M)	before opt. [V]	After opt. [V]	Reduction [%]
2-layer	1	854.222	641.047	24.9555
	3	860.457	672.310	21.8658
	5	868.089	676.193	22.1056
3-layer	1	557.677	501.284	10.4333
	3	596.407	526.062	11.7948
	5	633.488	540.074	14.7459

Table 4-13: Max. potential difference for an excitation with rise time of 100 ns

Geometry	Max. Potential difference, 100 ns			
	Length of cable (M)	before opt. [V]	After opt. [V]	Reduction [%]
2-layer	1	335.991	296.555	11.7373
	3	440.527	335.498	23.8417
	5	483.304	391.862	18.9201
3-layer	1	262.834	234.850	10.6472
	3	280.821	243.612	13.2500
	5	336.588	301.080	10.5496

4.8 Summary

This chapter presented a method to identify improvements in the insulation design of machine winding coils fed by fast front pulses. The proposed method is based on the application of a frequency domain non-uniform multiconductor transmission line approach, in combination with the finite element method and optimization techniques. The results show that modifications in the thicknesses and permittivities of the coil insulation layers, obtained through optimization, produce significant reduction of dielectric stresses due to fast front pulses with different rise times. Particle swarm optimization provided the best results in this work, with dielectric stress reductions of 50% and 43% for the geometries considered. The potential distribution of the optimized geometries is also improved even with different lengths of the feeder cable, giving rise to a considerable reduction of potential difference between turns for the complete machine windings.

CHAPTER V

OPTIMAL PASSIVE FILTER APPLIED TO INVERTER-CABLE-MACHINE SETUP

5.1 Introduction

Adjustable speed drives (ASD) based on pulse width modulation (PWM) provide excellent speed control of AC motors, but they also produce undesirable transient overvoltages in the motor windings [28], [30], [32], [72]. In many industrial applications, a feeder cable is commonly used to connect PWM inverter with the motor [9], [13]. These cables increase the dielectric stress and the overvoltages in the machine winding. The magnitude of these overvoltages depends on the rise time of the PWM pulses and on the characteristic impedance and length of the cable [14], [15]. Passive filters can be used to reduce the effects of transient overvoltages in machine windings [28]–[31]. However, an effective filter requires the correct definition of parameters for the corresponding circuit. The use of an optimized filter to decrease the effect of transient overvoltage in machine windings including the effect of the feeder cable is analyzed in this dissertation. Optimization algorithms are used to select the optimal parameter values of the filter based on its transient response characteristics which are the rise time, the settling time, peak time and the overshoot of the output voltage. The modeling approach of filters described in this chapter is validated experimentally in Chapter VI of this dissertation.

5.2 Design of Optimal Tuning Filter

In the design and analysis of any system, it is important to consider its full response. It is well known that the system response has two components: transient response and steady state response. Transient response is the short period of time that begins after the system is excited and ends when the system arrives to a steady state. As shown in Figure 5-1, the second order underdamped transient response has the following characteristics: rise time T_r, peak time T_p , Maximum percentage overshoot M_P, and settling time T_s [73]–[77].

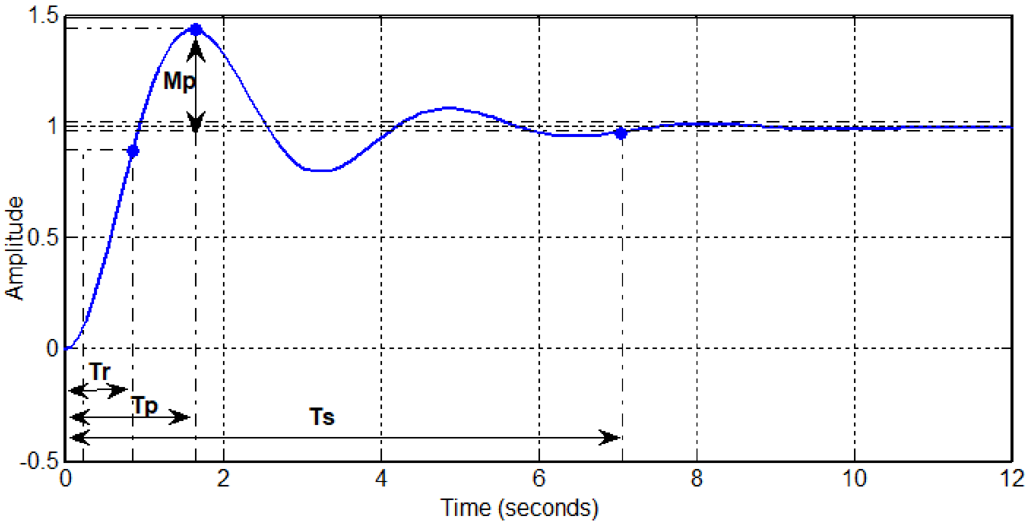

Figure 5-1: Transient response specifications [73]–[77]

In Figure 5-1, rise time T_r is the time required for the response to rise from 10% to 90% of its final value; peak time T_p is the time required for the response to reach its first peak; maximum percentage overshoot M_P, is the maximum percentage peak value of the response curve measured from the steady-state value of the response; and settling time T_s is the time required for the response curve to reach and stay within 2% or 5% of the final value peak of the overshoot.

In the machine winding under analysis, the fast front excitation produces large dielectric stresses related to a highly oscillatory transient response. To overcome these problems, multi objective function optimization algorithms are used to find the optimal parameters of the RLC filter. The objective functions (to be minimized) are the characteristics (T_r, T_p, M_P and T_s) of the transient voltage response of the winding. The number of independent variables depends on the number of electrical components in RLC filter. The boundaries of each element of the RLC filter in the optimization algorithms under consideration is defined according to commercial values of RLC components.

5.3 RLC Filter Circuits

The main objective of the filters analyzed in this dissertation is to reduce the overvoltage in the inverter-cable-motor setup. Passive filters are commonly used to decrease the effect of cable in the machine winding. However, defining their correct arrangements and parameters is a challenging task [42]. Figure 5-2 shows the conventional [14], [31] and proposed passive filters connected between the cable and the machine winding.

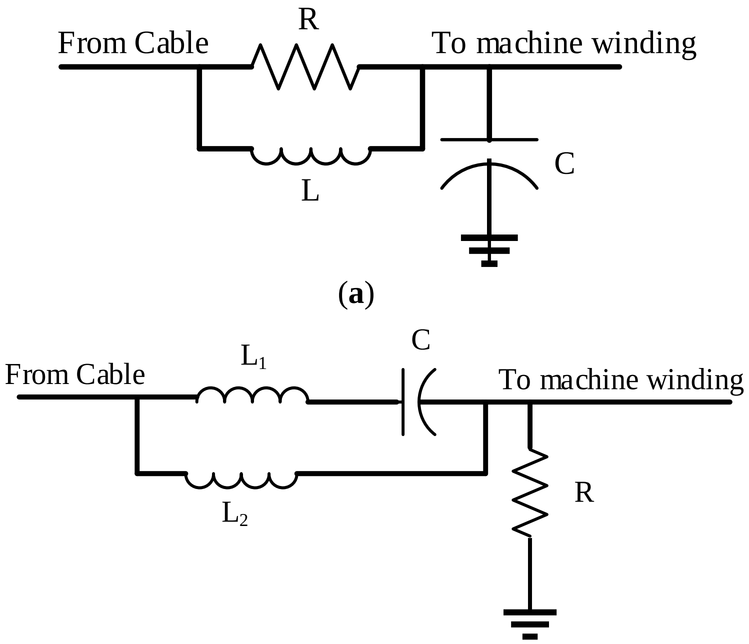

(**a**)

(**b**)

Figure 5-2: RLC filters: (**a**) conventional, (**b**) proposed

In the proposed filter, the series resonant circuit (L_1 - C) defines a band-pass filter and the parallel inductance (L_2) introduces a stop-band resonant frequency. Thus, the series resonant circuit and the parallel inductance are used to reject frequencies below the pass-band [78]. The parallel resistor (R) is added to increase or decrease the bandwidth of output frequencies.

5.4 Design Optimization of Filters

The three main components of this filter design optimization problem are the total objective functions (F_T) to be minimized, the design (independent) variables of filter circuit components (*R*, *L*, *C*), and the constraints of each variable. The number of independent variables depends on the number of components in the specific filter circuit (*n*). These components are defined as follows:

1- Design variables (*R*, *L*, *C*)

$$R = \left(R_{1\,,} \dots, R_n\right) \tag{5.1}$$

$$L = (L_{1\,,} \dots, L_n) \tag{5.2}$$

$$C = \left(C_{1\,,} \dots, C_n\right) \tag{5.3}$$

2- Objective function (F_T)

$$F_T = F_1\left(R_{,}L, C\right), F_2\left(R_{,}L, C\right), F_3\left(R_{,}L, C\right), F_4\left(R_{,}L, C\right) \tag{5.4}$$

where

$$T_r = F_1\left(R_{,}L, C\right) \tag{5.5}$$

$$T_p = F_2\left(R_{,}L, C\right) \tag{5.6}$$

$$M_P = F_3\left(R_{,}L, C\right) \tag{5.7}$$

$$T_s = F_4\left(R_{,}L, C\right) \tag{5.8}$$

3- Constraints

$$\underline{R_{min.}} \leq R \leq \overline{R_{max.}} \tag{5.9}$$

$$\underline{L_{min.}} \leq L \leq \overline{L_{max.}} \tag{5.10}$$

$$\underline{C_{min.}} \leq C \leq \overline{C_{max.}} \tag{5.11}$$

where $\underline{R_{min.}}$, $\overline{R_{max.}}$, $\underline{L_{min}}$, $\overline{L_{max.}}$, $\underline{C_{min.}}$ and $\overline{C_{max.}}$ are the lower and upper limits of the corresponding independent variables based on commercial values of RLC components. The objective functions represent the characteristic components of the output voltage response (T_r, T_p, M_P and T_s).

5.5 Multi-objective Optimization Algorithms

The multi-objective optimization problem is normally used to find the optimal values of a vector of objective functions [79]. Generally, multi-objective optimization algorithms are used to find the optimal design variables $x = (x_1 \quad x_2 \quad \cdots \quad x_n)^T$ that minimize the objective functions $f_{(x)} = (f_{(x_1)} \quad f_{(x_2)} \quad \cdots \quad f_{(x_n)})^T$ over the feasible reign of design variables space x [80]. Several methods have been developed for solving this type of problem. In this dissertation, different multi-objective functions from MATLAB are used to find the optimal parameters of the proposed RLC filter [81].

A. Goal attainment optimization algorithm

This is one of the basic parametric and goal programing methods. In this method, design goals $F^* = (F_1^* \quad F_2^* \quad \ldots \quad F_n^*)^T$ are set for the objective functions $f_{(x)} = (f_{(x_1)} \quad f_{(x_2)} \quad \cdots \quad f_{(x_n)})^T$. The problem formulation allows the objectives to be under or over achievement of the goals. The relative degree of the goals is controlled by the weighting coefficients $w = (w_1 \quad w_2 \quad \cdots \quad w_n)^T$. The weighting parameters are selected to be near the goal values [82]. This method is used to minimize the scalar quantity γ at the design vector x subjected to

$$f_i(x) - w_i \gamma \leq f_i^* \qquad (i = 1, \dots \dots, n) \tag{5.12}$$

where the f_i^* is the objective defined by the user [83].

B. Minimax optimization algorithm

Generally, this algorithm is used to solve a problem that requires minimizing the worst-case of a set of independent variables. Considering the objective function $f(x, \omega)$ used to find a vector x of variables that minimize the objective function over $\omega \in \mathcal{S}$, the quantity of interest depends on the real value parameter ω that belongs to the set $\mathcal{S}$. A minimize problem related to $f(x, \omega)$ can be stated as

$$\underset{x}{minimize} \quad \underset{\omega \in \mathcal{S}}{\max} \quad f(x, \omega) \tag{5.13}$$

The minimax optimization problem involves minimizing the objective function based on the summation of elemental error functions:

$$e(x) = [e_1(x) \quad e_2(x) \quad \dots \dots \quad e_n(x)] \tag{5.14}$$

This method is used to find the vector of design variables which minimizes the multi-objective function over a feasible design region [80], [84], [85].

5.6 Application Example

The method proposed to find the optimal tuning of parameters of passive filters is applied to two different geometrical winding configurations in the inverter-cable-motor setup. Two multi-objective optimization algorithms based on the proposed method are applied in the conventional and proposed filter circuits.

5.6.1 RLC Filter Applied to Original (Non-optimized) Geometries

In this section the RLC filter is applied to the original 2 and 3-layer geometries including different lengths of feeder cable (1, 3, and 5 m). Tables 5-1 and 5-2 show the optimized parameters for the conventional and proposed RLC filters connected to the excitation-cable-motor setup.

Table 5-1: Parameters for conventional filter in original geometries

Geometry	Optimization algorithms	R (ohm)	C (uF)	L (uH)
2-layer	Minimax	4.5	0.05	100
	Goal A.	2	0.2	10
3-layer	Minimax	1.54	0.39	1000
	Goal A.	1.7	0.34	3000

Table 5-2: Parameters for proposed filter in original geometries

Geometry	Optimization algorithms	R (ohm)	C (uF)	L_1 (uH)	L_2 (uH)
2-layer	Minimax	1	0.01	0.001	0.03
	Goal A.	1.5	0.1	0.09	0.003
3-layer	Minimax	0.98	154	0.001	0.0013
	Goal A.	1.67	115	110	0.0018

The excitation applied for both geometrical configurations (2 and 3-layer) is a step voltage waveform with magnitude of 1750 V and rise time of 25 ns, and the feeder cable is 1 m long. Figures 5-3 and 5-4 show the transient overvoltages at different turns along the 2-layer and 3-layer coils considering the conventional and proposed filters tuned by means of the optimization algorithms.

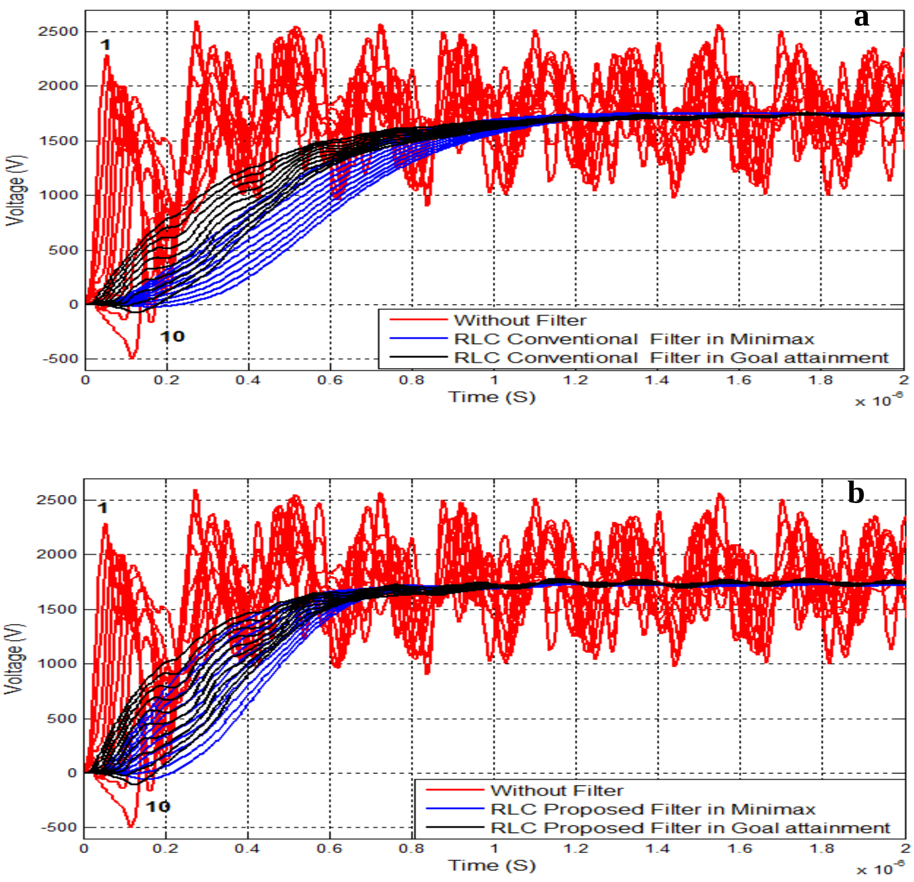

Figure 5-3: Transient overvoltage in 2-layer geometry with cable and filter: (**a**) conventional filter, (**b**) proposed filter

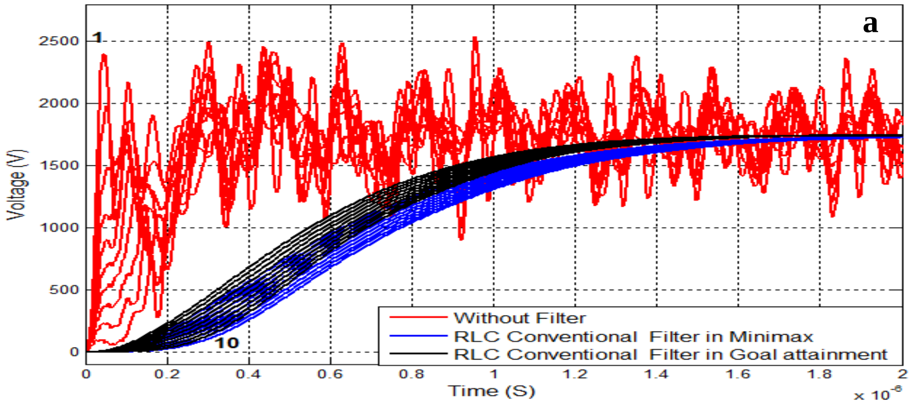

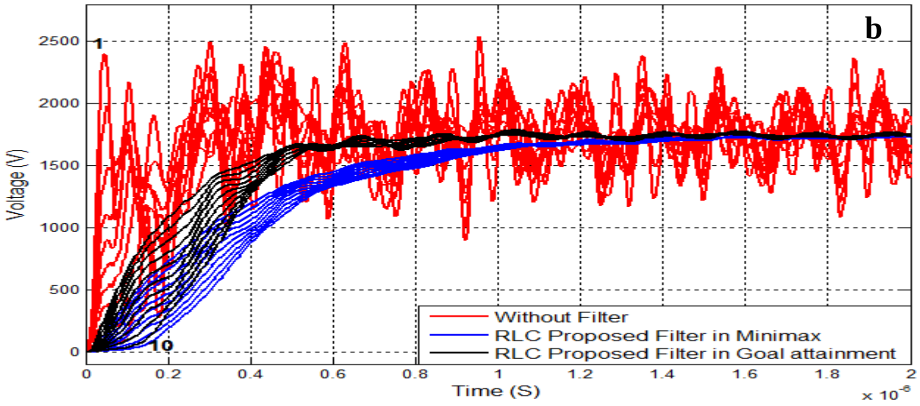

Figure 5-4: Transient overvoltage in 3-layer geometry with cable and filter (**a**) conventional filter, (**b**) proposed filter

Table 5-3 shows the rise times for the transient overvoltage in the 2 and 3-layer geometries after using the filters. As shown in this table the fastest signal appears when using the optimal parameters of the proposed RLC filter obtained with the goal attainment optimization algorithm. However, the output signal in the fastest case still exhibits some delay when compared with the original output signal.

Table 5-3: Rise time in 2 and 3- layer geometries with RLC filters

Geometry	Rise time without filter (ns)	RLC Filter	Optimization algorithms	Rise time with filter (ns)
2 Layer	21.0892	Conventional	Minimax	688.683
			Goal A.	634.329
		Proposed	Minimax	444.751
			Goal A.	409.274
3Layer	20.7999	Conventional	Minimax	977.199
			Goal A.	821.674
		Proposed	Minimax	713.549
			Goal A.	439.995

5.6.2 RLC Filter Applied to Optimized Geometries

In this section the RLC filter is applied to the optimized 2 and 3-layer geometries including different lengths of feeder cable (1, 3, and 5 m).

Tables 5-4 and 5-5 show the parameters of the conventional and optimized RLC filters when applied to the optimized 2 and 3-layer geometries including a 1-meter feeder cable. The parameters of RLC filter are found with the same excitation and rise time considered for the previous case.

Figures 5-5 and 5-6 show the transient overvoltages in both 2 and 3-layer optimized geometries for a step excitation with magnitude of 1750 V and rise times of 25 ns and 100 ns. A feeder cable of 1 m is also included in the simulation.

Table 5-4: Parameters for conventional filter in optimized geometries

Geometry	Optimization algorithms	R filter (ohm)	C filter (uF)	L filter (uH)
2 Layer	Minimax	7.68	0.01	1000
	Goal	21.5	0.0015	30.6
3Layer	Minimax	1.5	0.33	992
	Goal	1.74	0.25	1000

Table 5-5: Parameters for proposed filter in optimized geometries

Geometry	Optimization algorithms	R filter (ohm)	C filter (uF)	L1 filter (uH)	L2 filter (uH)
2 Layer	Minimax	0.953	0.33	0.001	0.0102
	Goal	4.3	2.3	0.047	0.016
3Layer	Minimax	0.5	100	0.001	0.0147
	Goal	6.2	0.001	0.001	0.13

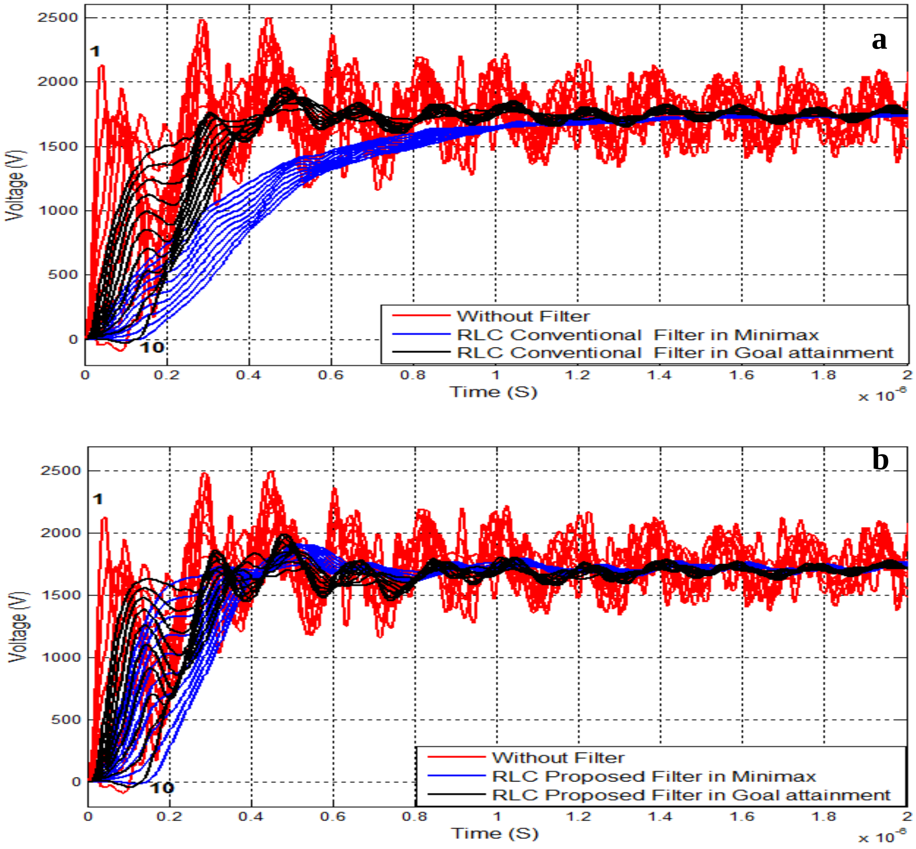

Figure 5-5: Transient overvoltage in 2-layer optimized geometry with cable and filter (**a**) conventional filter, (**b**) proposed filter

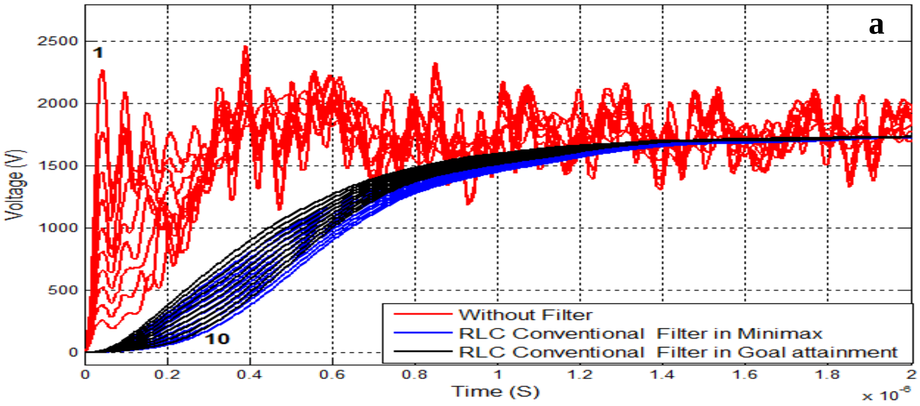

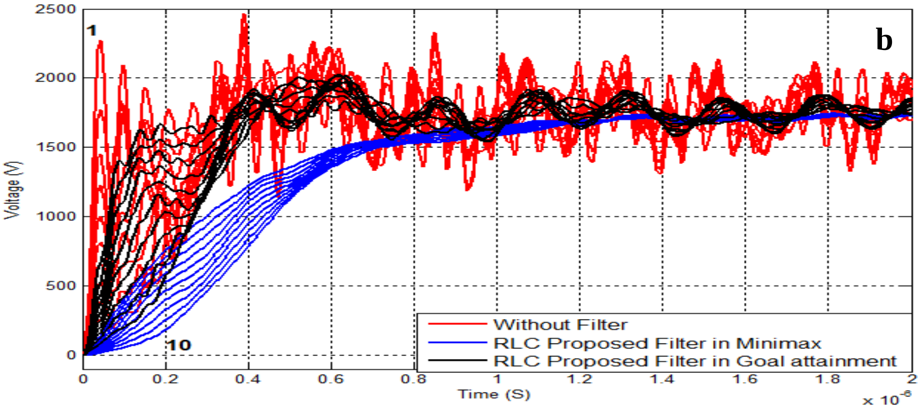

Figure 5-6: Transient overvoltage in 3-layer optimized geometry with cable and filter (**a**) conventional filter, (**b**) proposed filter

Table 5-6 shows the rise times for the transient overvoltage in 2 and 3-layer optimized geometry with 1-meter cable and filter. As shown in Table 5-6 the fastest response produced when using optimal parameters of RLC filter is found by using the goal attainment optimization algorithm in the proposed circuit.

Table 5-6: Rise time in 2 and 3- layer optimized geometries with filter

Geometry	Rise time without filter (ns)	RLC Filter	Optimization algorithms	Rise time with filter (ns)
2 layers	21.0892	Conventional	Minimax	648.450
			Goal	237.903
		Proposed	Minimax	140.433
			Goal	82.7410
3 layers	20.7999	Conventional	Minimax	895.008
			Goal	794.294
		Proposed	Minimax	668.189
			Goal	91.9097

Based on the results listed in Table 5-3 and 5-6, the fastest response occurs when using the optimal parameters in the proposed filter via goal attainment optimization algorithm, combined with the optimized geometry. Figures 5-7 to 5-12 show the distribution of transient voltages along the optimized 2-layer and 3-layer coils with and without the proposed filter and with different lengths of the feeder cable and different rise times of the excitation. In all cases, the filter added corresponds to the proposed filter with optimized parameters via goal attainment.

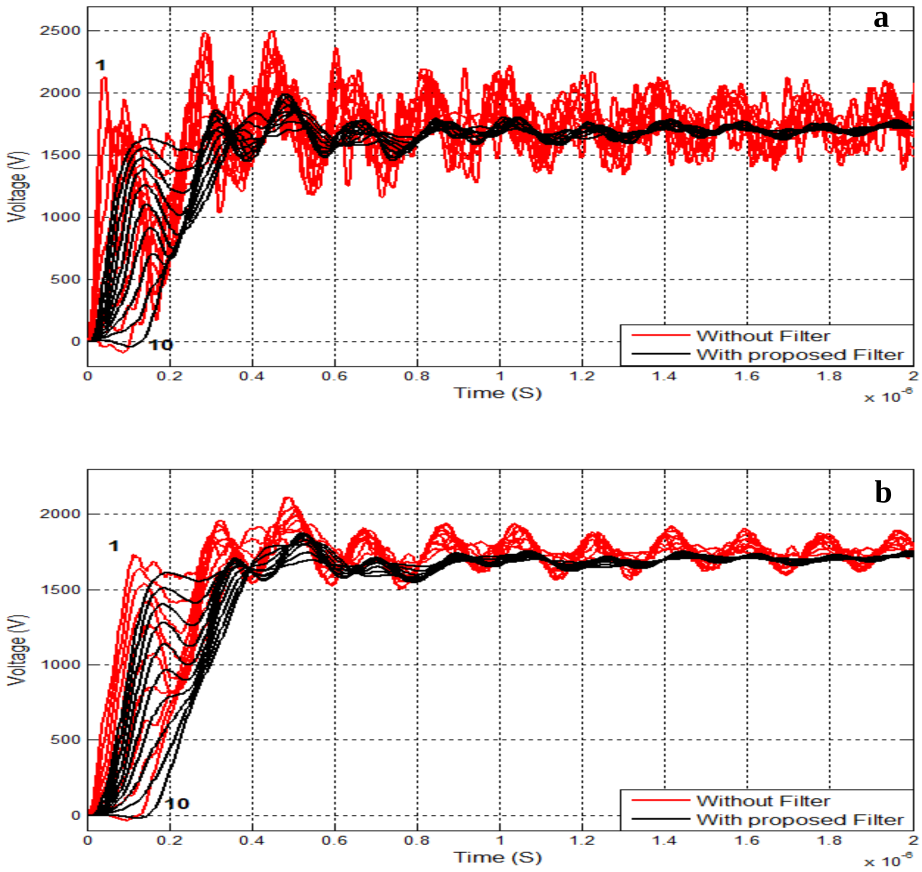

Figure 5-7: Transient voltage along the coil turns in 2-layer optimized geometry with proposed filter and 1-meter cable: (**a**), 25 ns rise time, (**b**) 100 ns rise time

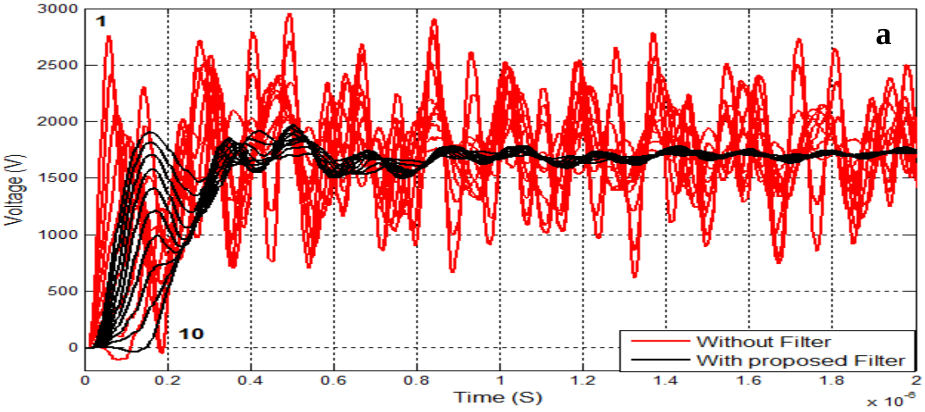

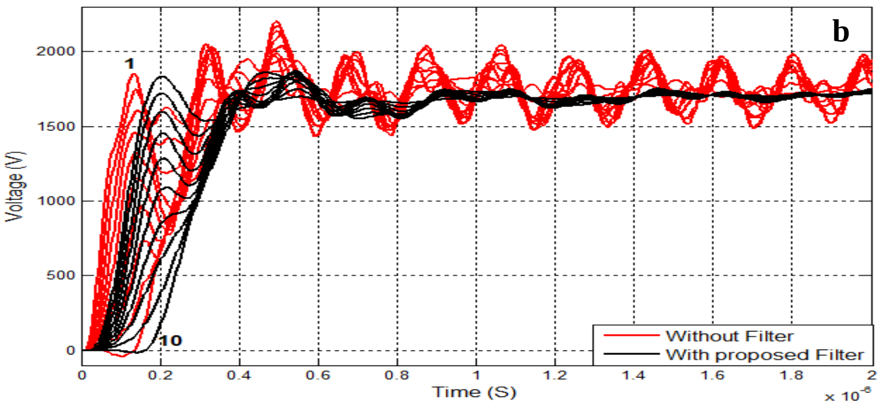

Figure 5-8: Transient voltage along the coil turns in 2-layer optimized geometry with proposed filter and 3-meter cable: (**a**), 25 ns rise time, (**b**) 100 ns rise time

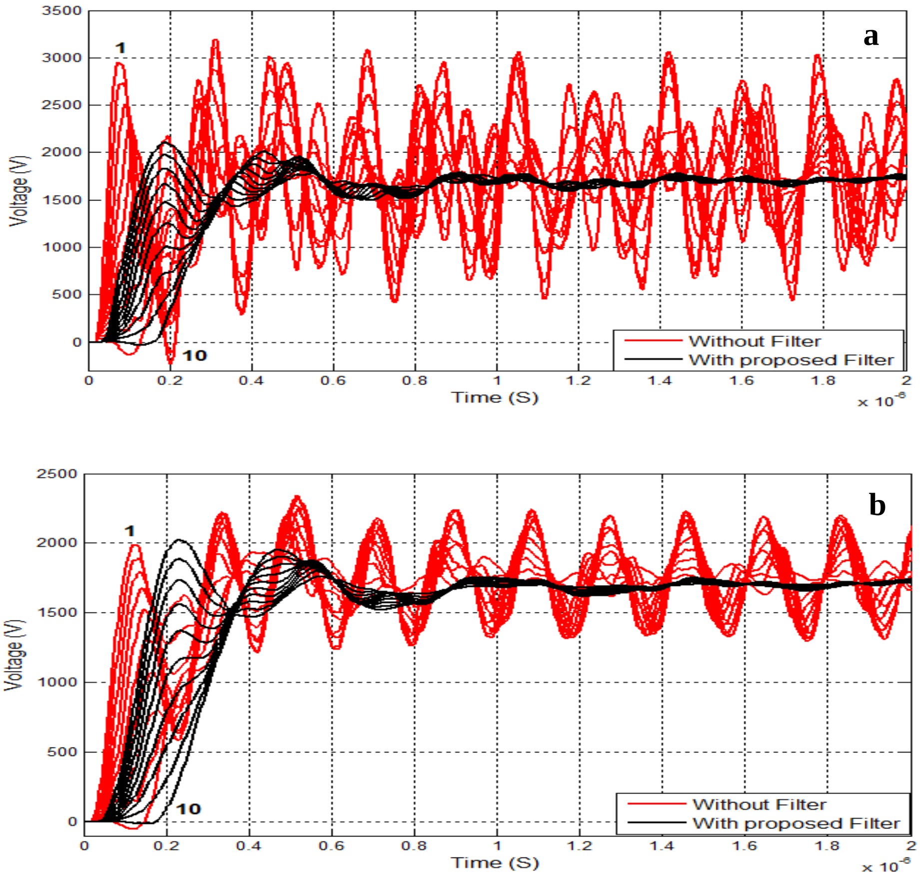

Figure 5-9: Transient voltage along the coil turns in 2-layer optimized geometry with proposed filter and 5-meter cable: (**a**), 25 ns rise time, (**b**) 100 ns rise time

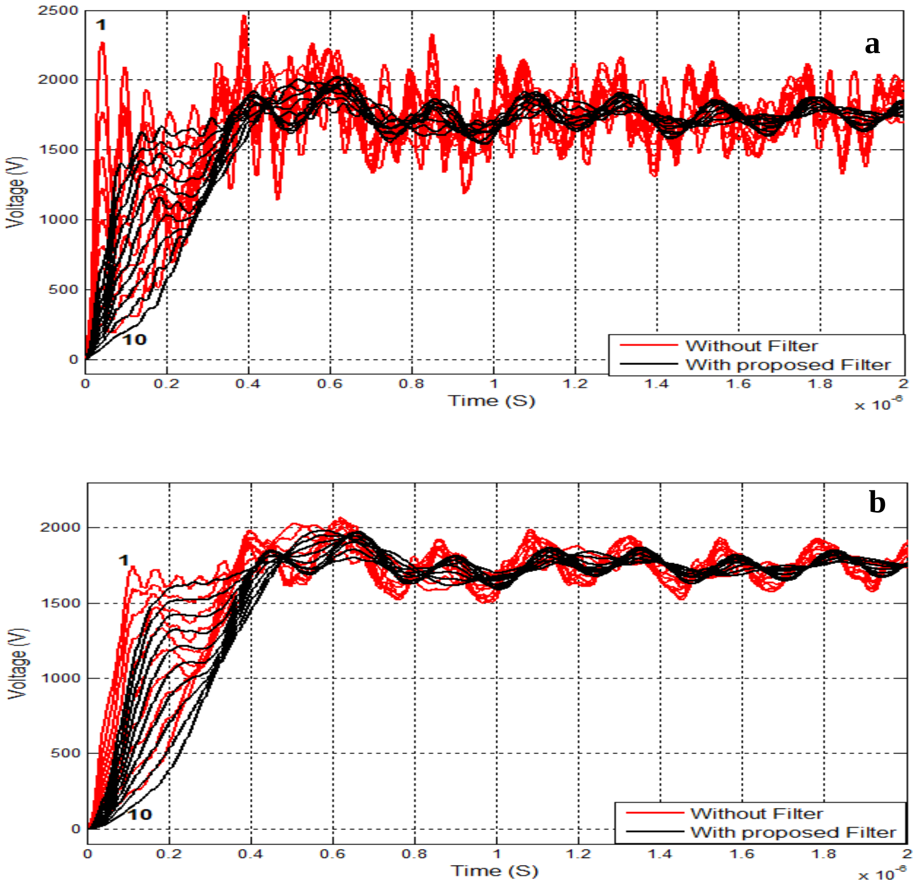

Figure 5-10: Transient voltage along the coil turns in 3-layer optimized geometry with proposed filter and 1-meter cable: (**a**), 25 ns rise time, (**b**) 100 ns rise time

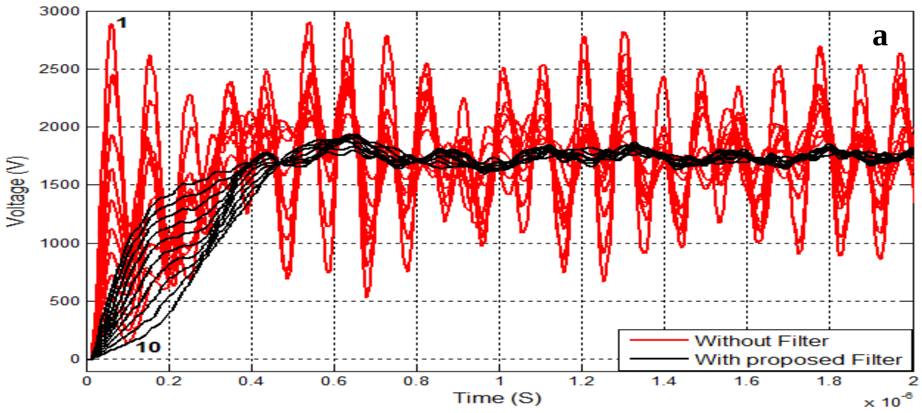

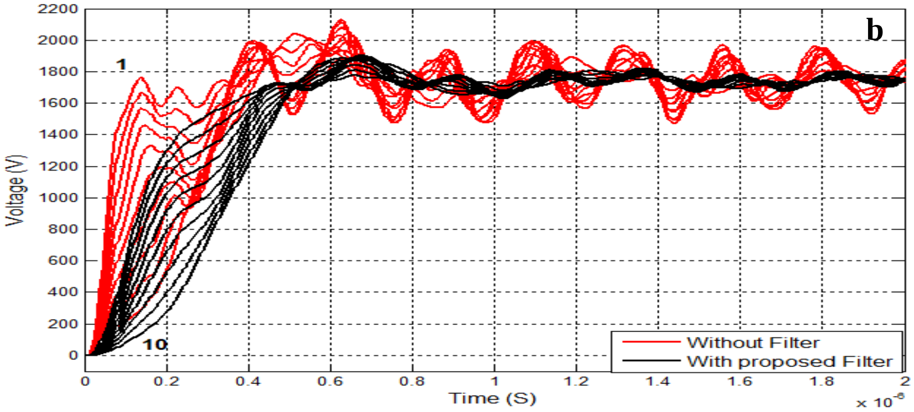

Figure 5-11: Transient voltage along the coil turns in 3-layer optimized geometry with proposed filter and 3-meter cable: (**a**), 25 ns rise time, (**b**) 100 ns rise time

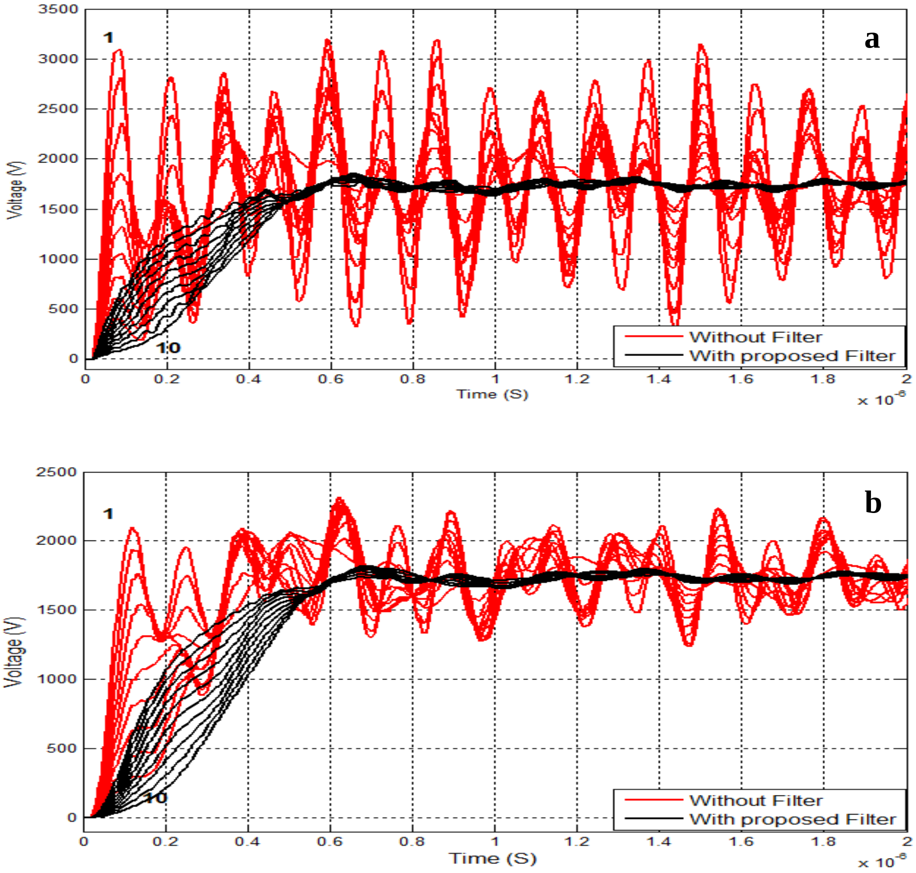

Figure 5-12: Transient voltage along the coil turns in 3-layer optimized geometry with proposed filter and 5-meter cable: (**a**), 25 ns rise time, (**b**) 100 ns rise time

Tables 5-7 and 5-8 list the maximum transient voltages for the optimized 2 and 3-layer geometries with proposed filter, different lengths of feeder cable and different excitation rise times. The optimized parameters of the proposed filter are found via goal attainment.

Table 5-7: Max. transient overvoltage for an excitation with 25 ns rise time in 2 and 3-layer optimized geometries with different lengths of cable and proposed filter

Optimized Geometry	Max. overvoltage, 25 ns rise time			
	Cable length (m)	Before filter [V]	After filter [V]	Reduction [%]
2 layers	1	2501.57	1991.88	20.3748
	3	2953.45	1966.594	33.4138
	5	3190.56	2105.64	34.0038
3 layers	1	2463.83	2021.69	17.9452
	3	2907.79	1933.64	33.5013
	5	3197.34	1848.65	42.1815

Table 5-8: Max. transient overvoltage for an excitation with 100 ns rise time in 2 and 3-layer optimized geometries with different lengths of cable and proposed filter

Optimized Geometry	Max. overvoltage, 100 ns rise time			
	Cable length (m)	Before filter [V]	After filter [V]	Reduction [%]
2 layers	1	2109.57	1870.38	11.3385
	3	2202.50	1868.77	15.1525
	5	2340.98	2022.76	13.5937
3 layers	1	2067.62	1808.92	12.5122
	3	2128.48	1899.93	10.7379
	5	2314.46	1818.69	21.4207

Figures 5-13 to 5-18 show the potential difference in the optimized geometries including the proposed filter and considering different lengths of feeder cable and different rise times of the excitation.

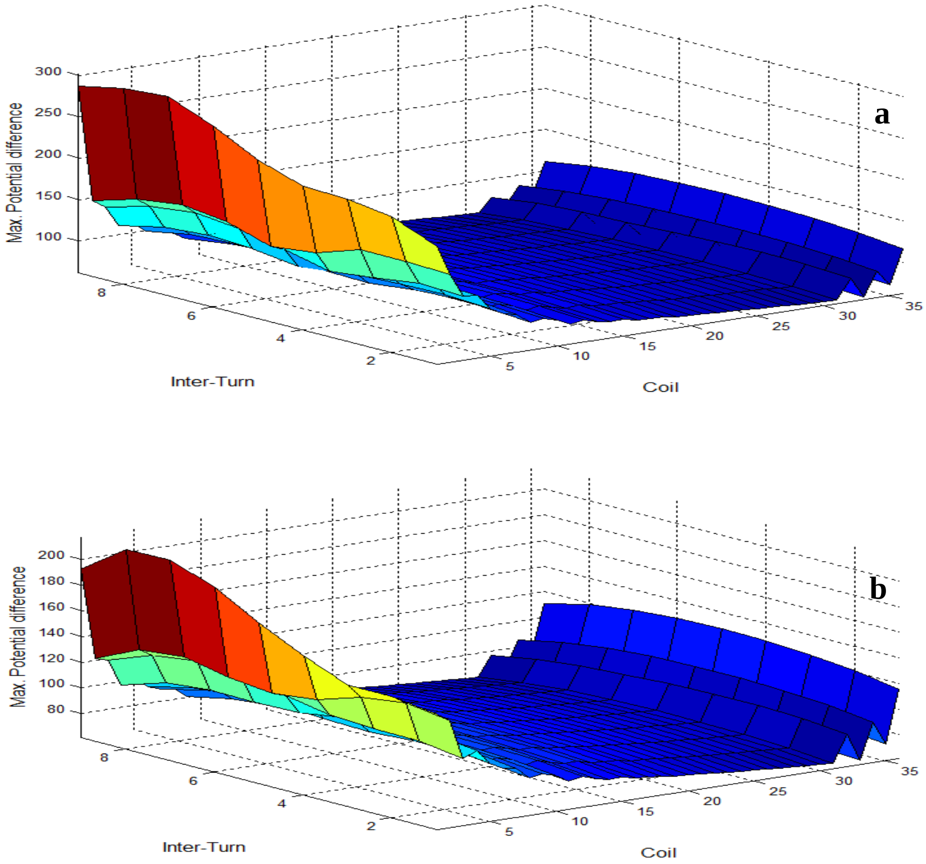

Figure 5-13: Distribution of maximum potential difference along the machine winding in 2-layer optimized geometry with 1-meter cable and proposed filter: (**a**) 25 ns rise time, (**b**) 100 ns rise time

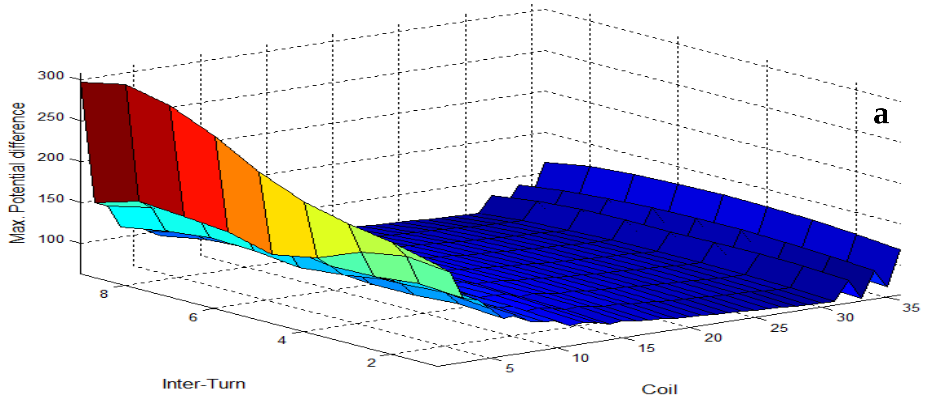

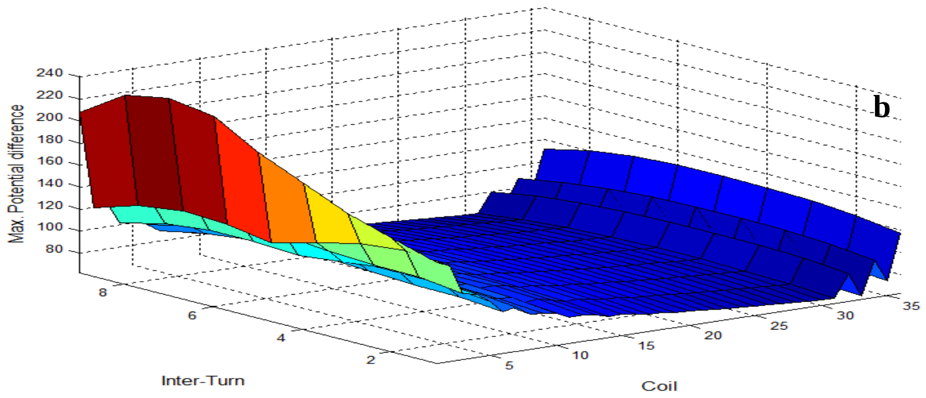

Figure 5-14: Distribution of maximum potential difference along the machine winding in 2-layer optimized geometry with 3-meter cable and proposed filter: (**a**) 25 ns rise time, (**b**) 100 ns rise time

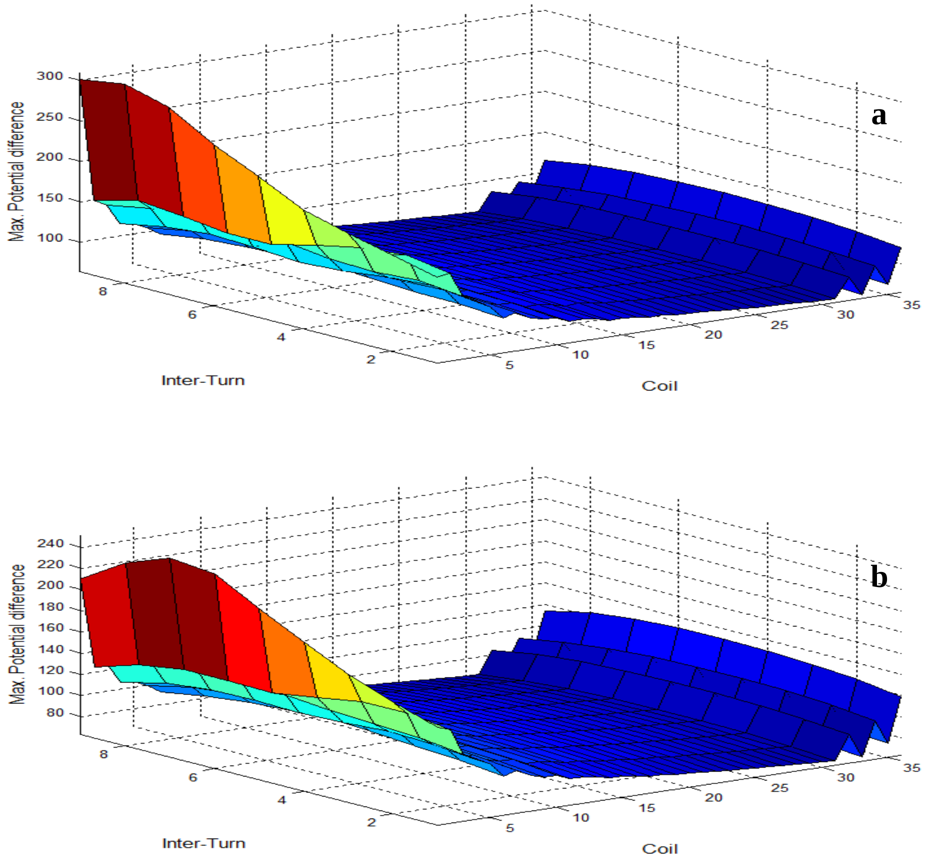

Figure 5-15: Distribution of maximum potential difference along the machine winding in 2-layer optimized geometry with 5-meter cable and proposed filter: (**a**) 25 ns rise time, (**b**) 100 ns rise time

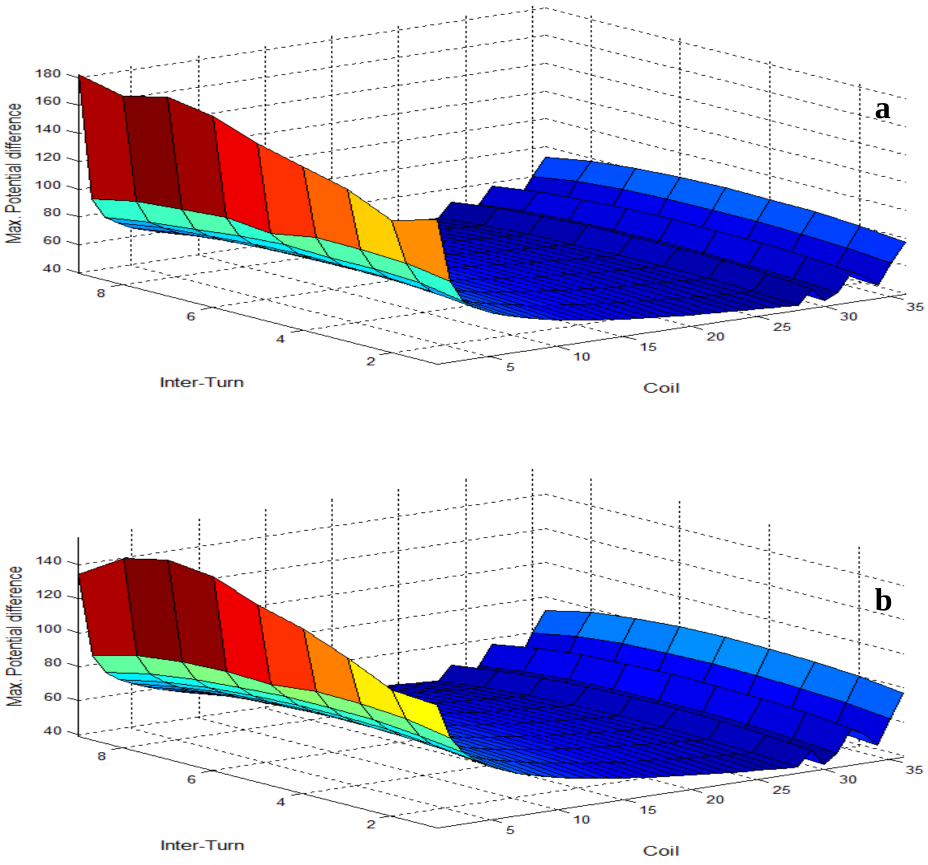

Figure 5-16: Distribution of maximum potential difference along the machine winding in 3-layer optimized geometry with 1-meter cable and proposed filter: (**a**) 25 ns rise time, (**b**) 100 ns rise time

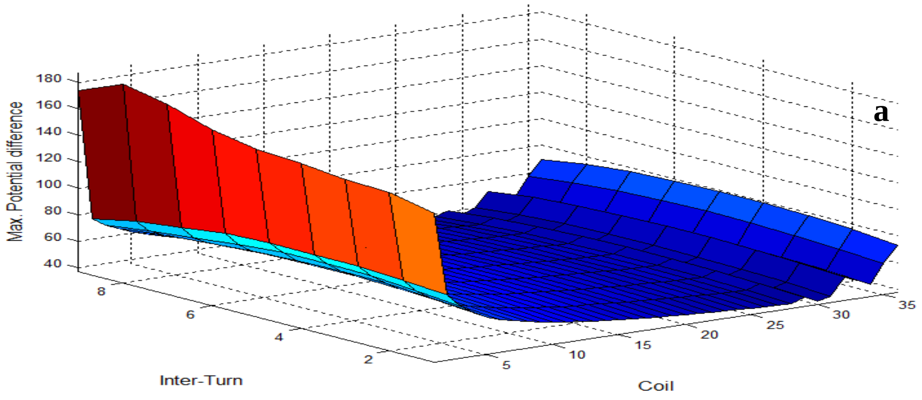

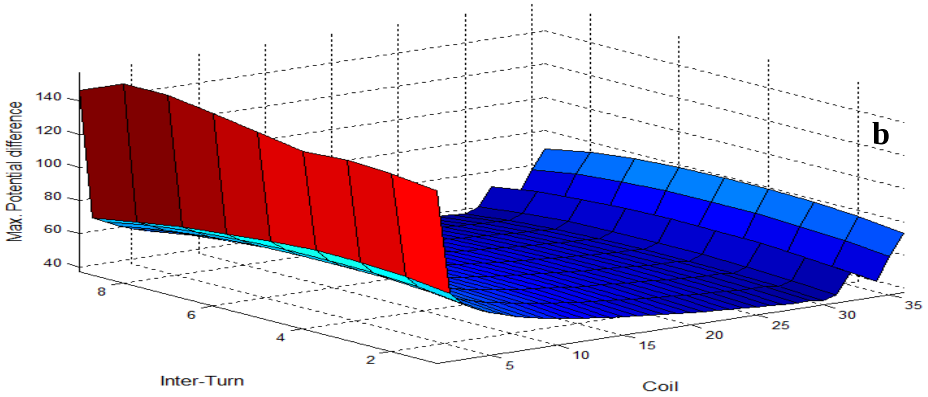

Figure 5-17: Distribution of maximum potential difference along the machine winding in 3-layer optimized geometry with 3-meter cable and proposed filter: (**a**) 25 ns rise time, (**b**) 100 ns rise time

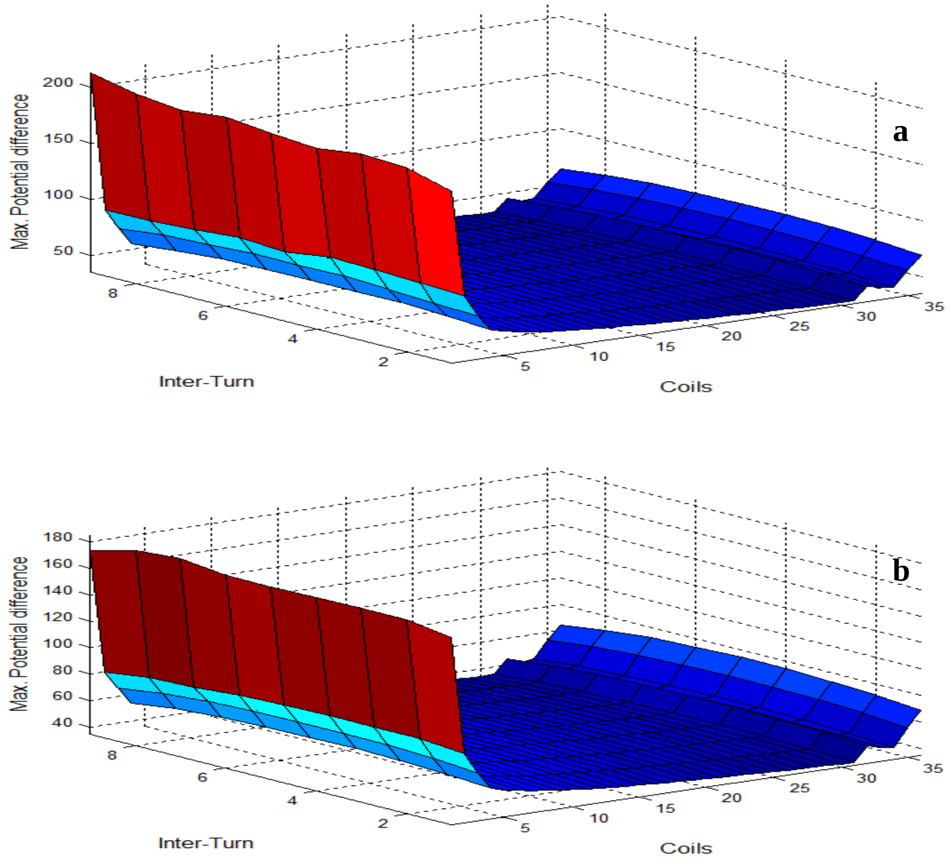

Figure 5-18: Distribution of maximum potential difference along the machine winding in 3-layer optimized geometry with 5-meter cable and proposed filter: (**a**) 25 ns rise time, (**b**) 100 ns rise time

Tables 5-9 and 5-10 compare the maximum potential difference before and after the inclusion of the proposed filter in the optimized geometries with different excitation rise times.

Table 5-9: Max. potential difference for an excitation with rise time of 25 ns in 2 and 3-layer optimized geometries with different lengths of cable and proposed filter

Optimized Geometry	Max. Potential difference, 25 ns rise time			
	Cable length (m)	Before filter [V]	After filter [V]	Reduction [%]
2-layer	1	641.047	301.743	52.9296
	3	672.310	308.509	54.1121
	5	676.193	309.270	54.2630
3-layer	1	501.284	182.328	63.6458
	3	526.062	187.204	64.4139
	5	540.074	212.405	60.6712

Table 5-10: Max. potential difference for an excitation with rise time of 100 ns in 2 and 3-layer optimized geometries with different lengths of cable and proposed filter

Optimized Geometry	Max. Potential difference, 100 ns rise time			
	Cable length (m)	Before filter [V]	After filter [V]	Reduction [%]
2-layer	1	296.555	217.436	26.6791
	3	335.498	241.156	28.1199
	5	391.862	251.222	35.8901
3-layer	1	234.850	155.916	33.6103
	3	243.612	157.299	35.4305
	5	301.080	184.642	38.6734

5.7 Summary

This chapter analyzed the use of filters for the reduction of transient overvoltages in an inverter-cable-motor setup. The proposed method to find the optimal parameters of the filter is based on minimizing the rise time, the settling time, the peak time, and the overshoot of the corresponding output voltage. Two different multi-objective optimization algorithms are used to find the optimal parameters of RLC filters. The optimized RLC filters (conventional and proposed) are applied to the original and optimized machine winding geometries. The results show that the proposed filter with optimized geometry can eliminate the transient overvoltages better and faster than the conventional filter. In addition, the goal attainment algorithm is a better alternative than the minimax algorithm to obtain the optimal parameters of the proposed filter. Finally, the proposed filter with optimized geometry results in a substantial reduction not only of the transient overvoltages in the coil, but also of the potential differences between adjacent turns.

CHAPTER VI

EXPERIMENTAL VALIDATION

6.1 Introduction

The first coil of machine windings usually presents higher transient overvoltages and dielectric stresses than the remaining coils when a fast front excitation is applied [12]. Therefore, for the purpose of simplification of the transient study, a line-end coil is commonly used to validate the computer model while the remaining coils are approximated by a lumped parameter (usually a resistor) [43]–[45], [59], [86]–[89] . In this chapter, the computer winding model described in Chapter III is validated by means of measurements on a line-end coil. Also, the effect of adding the feeder cable is studied experimentally. Finally, the inclusion of RLC filters (conventional and proposed) is studied and validated using the same experimental coil.

6.2 Modeling of Machine Winding

A schematic representation of the system under study is shown in Figure 6-1.

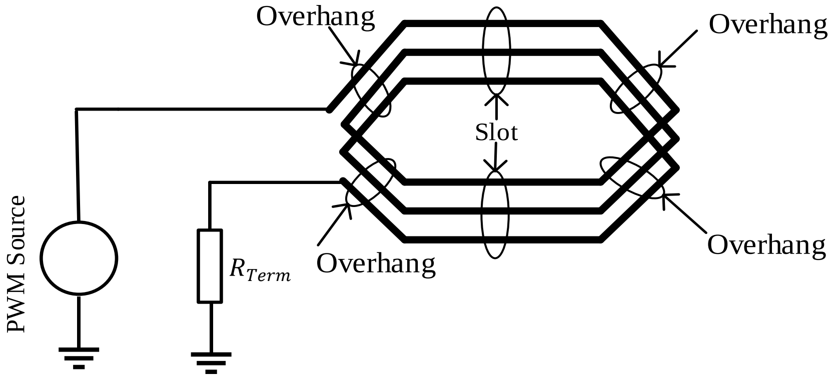

Figure 6-1: Schematic model of a form wound stator coil (3 turns are considered for the purpose of illustration)

A PWM-type excitation is connected to the machine winding coil from a form-wound machine. The typical coil of a machines winding has two regions: slot and overhang, as shown in Figure 6-1. A constant lumped resistance R_{Term} is used to represent the rest of winding after the first coil.

6.2.1 Geometrical Configuration

A schematic cross-section of the coil considered in this study is shown in Figure 6-2. The main parameters of the stator coil are summarized in Table 6-1.

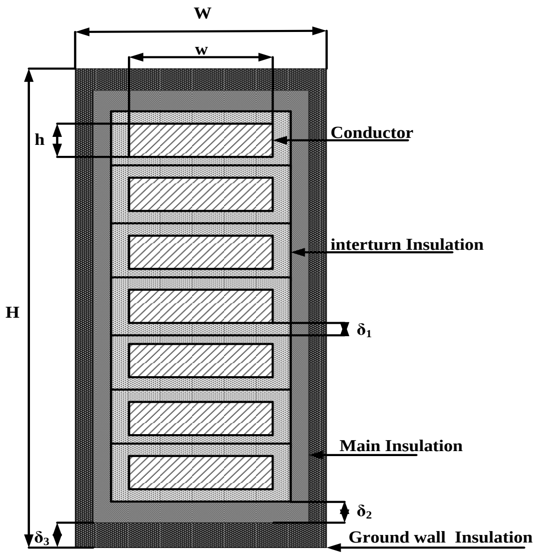

Figure 6-2: Cross-section of the coil with 3 insulation layers

Table 6-1: Main coil parameters for the experimental 3-layer geometry

Parameter	Value
Turns per stator coil	7
Length of overhang region	0.33 m
Conductor width (w)	5.35 mm
Conductor height (h)	2.85 mm
Resistivity of stator bar conductor	1.7×10-8 Ω·m
Thickness of interturn insulation (δ_1)	0.2 mm
Thickness of main insulation (δ_2)	1.41 mm
Thickness of ground wall insulation (δ_3)	0.36 mm

Table 6-1—Continued

Relative permittivity of the interturn insulation	2.5
Relative permittivity of the main insulation	2
Relative permittivity of the ground wall insulation	2.8
Slot width (W)	8.9 mm
Slot Height (H)	24.2 mm
Slot length	0.45 m

6.2.2 Experimental Setup of Machine Winding Model

Figure 6-3 shows a picture of the experimental setup. Besides the form-wound coil under test, it includes a waveform generator, an oscilloscope, and a 100 Ω load connected at the end of the coil. Steel plates were included to emulate the electromagnetic field distribution in the slot region [90]–[93]. The experimental setup is placed in a laboratory facility free of electromagnetic interference.

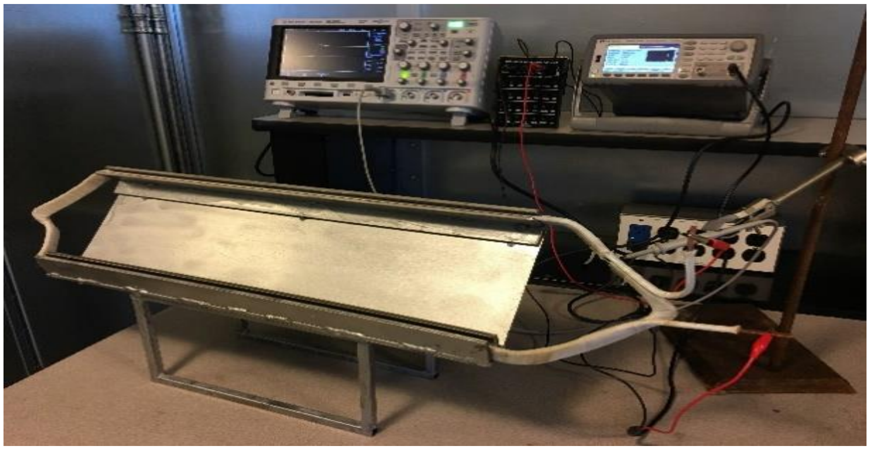

Figure 6-3: Experimental setup for machine winding validation

6.2.3 Computation of Electrical Parameters

A single coil is considered as the basic element for the calculation of machine parameters. As mentioned before, each coil can be divided in two sections: overhang and slot. The capacitance, inductance, and losses matrices in both coil regions are calculated using the FEM-based software

COMSOL Multiphysics. In the slot region, the slot walls behave as magnetic insulation for the high frequencies related to the fast-transient response of the coil. In the overhang region, these walls are replaced by an open boundary condition. The capacitance matrix **C** is calculated using the forced voltage method in the electrostatics module of COMSOL (Figure 6-4). The inductance matrix **L** is calculated using the magnetic energy method (Figure 6-5). The series losses in the coil (**R**) are computed from the concept of complex penetration depth. The dielectric losses matrix (**G**) is computed using the "electric currents" module in COMSOL.

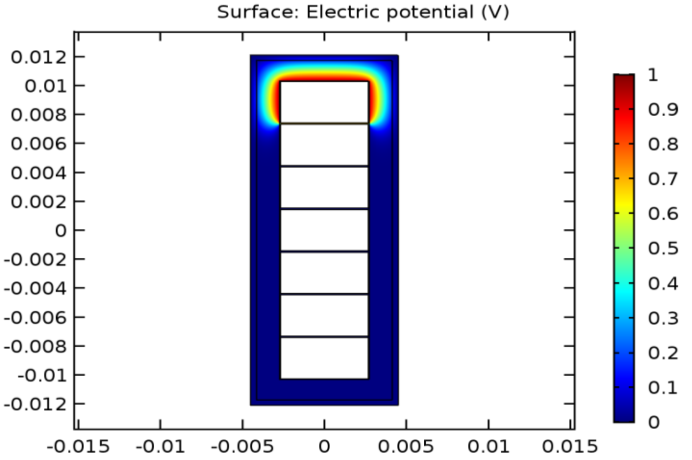

Figure 6-4: Capacitance calculation using forced voltage method in FEM

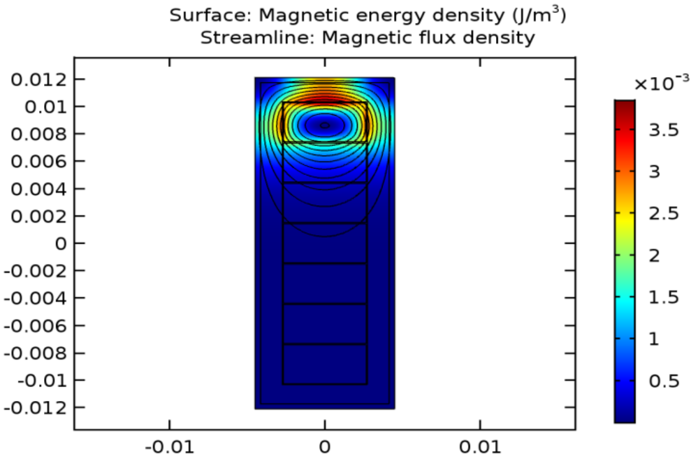

Figure 6-5: Inductance calculation using magnetic energy method in FEM

6.2.4 Experimental Results of Machine Winding

The winding model is validated considering a PWM-type excitation with different rise times between 100 and 500 ns connected to the first turn of the coil. This type of excitation is obtained from the waveform generator emulating the phase to ground voltage from a voltage source inverter. The corresponding waveform is shown in Figure 6-6. Figure 6-7 shows the comparison of the simulated and measured transient voltage at the first winding turn of coil.

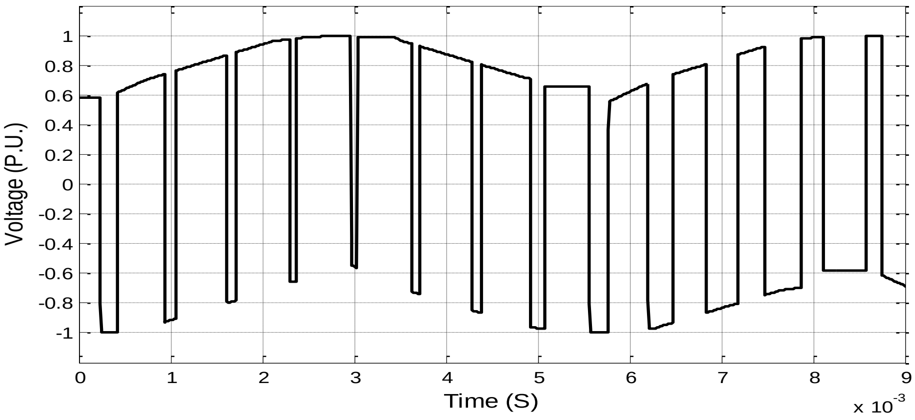

Figure 6-6: Typical PWM-waveform generated by an inverter

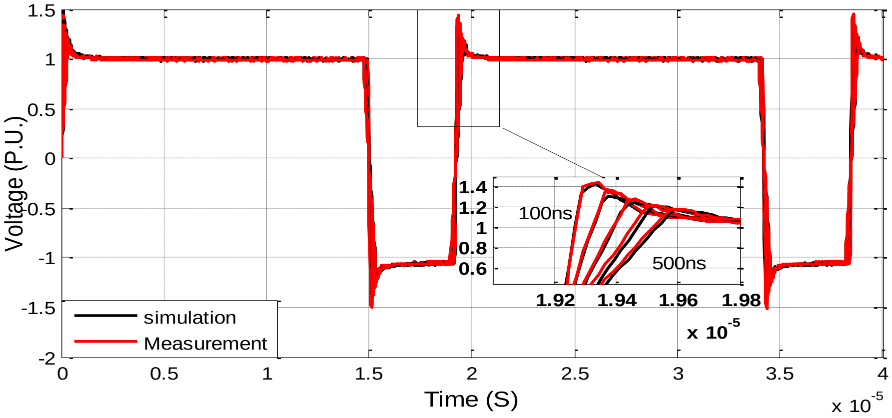

Figure 6-7: Transient overvoltage at the first turn of the coil terminated in 100 Ω load

A second assessment of the winding corresponds to a similar setup, but with an open-ended condition of the coil. This results in noticeable oscillations which are reproduced in a very accurate manner by the winding model, as shown in Figure 6-8, which illustrates the transient response at the far end of the winding.

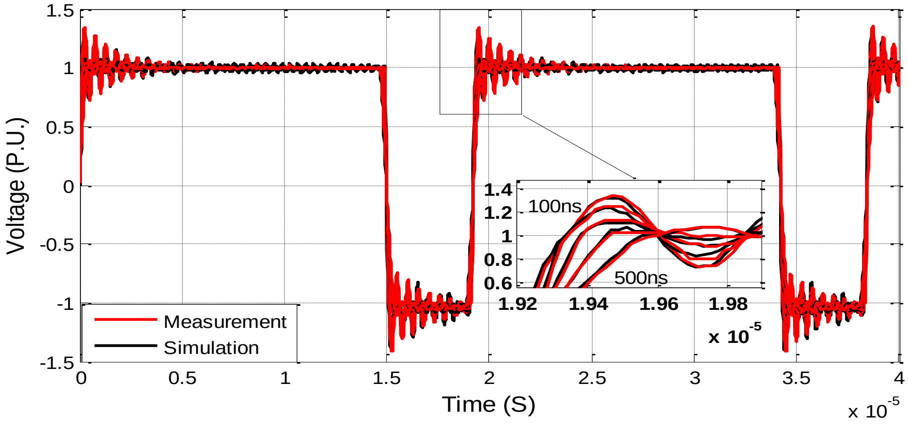

Figure 6-8: Transient overvoltage at the last turn of the coil for open ended case

6.3 Modeling of Machine Winding with Feeder Cable

A schematic representation of the system under study is shown in Figure 6-9. A PWM-type excitation is connected through a single-phase cable to the machine winding coil from a form-wound machine winding.

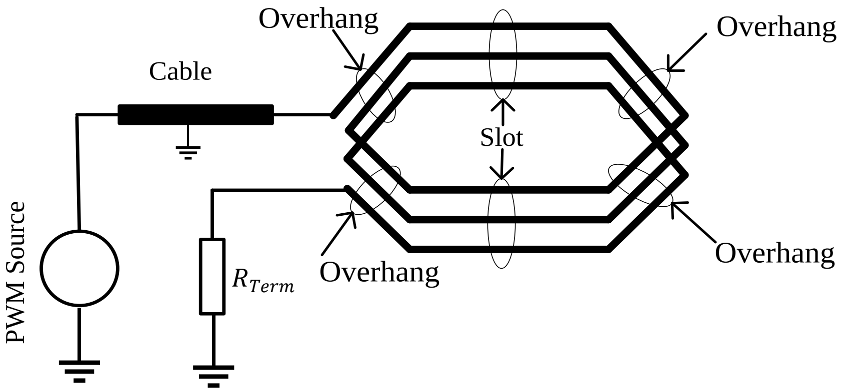

Figure 6-9: Schematic model of a form-wound stator coil (3 turns are considered for the purpose of illustration) with connecting cable

6.3.1 Modeling of Feeder Cable in Frequency Domain Model

Initially, the cable and winding models are assessed separately by means of comparisons with experimental measurements. The cable model is validated by means of the simulation of its step response, considering a unit step with rise time of 100 ns at the sending node and a load of 50 Ω connected at the receiving node. The voltage at the receiving end of the cable and its comparison with the experimental measurement are shown in Figure 6-10 considering a 1 m long unshielded four-wire cable, size 10 AWG.

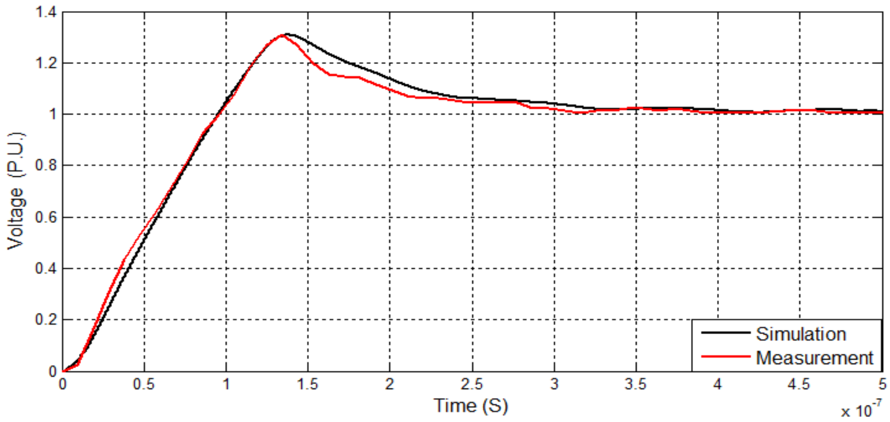

Figure 6-10: Transient voltage at the receiving end of the cable

6.3.2 Experimental Setup of Machine Winding with Feeder Cable

Figure 6-11 shows a picture of the experimental setup. Besides the form-wound coil under test with a 1 m long unshielded four-wire cable, size 10 AWG, it includes a waveform generator, an oscilloscope, and a 100 Ω load connected at the end of the coil. The experimental setup is placed in a laboratory facility free of electromagnetic interference.

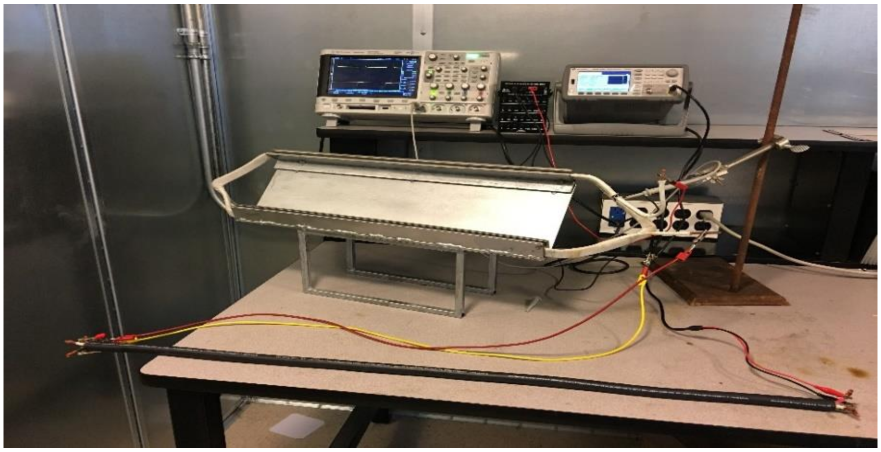

Figure 6-11: Experimental setup for machine winding with feeder cable validation

6.3.3 Experimental Results of Machine Winding with Feeder Cable

The following set of simulations correspond to the response of the coil for different rise times of the PWM-type excitation and for different lengths of the connecting cable. When connecting the inverter to the machine winding coil through a 1-meter cable, the overvoltages are increased, as shown in Figure 6-12. This figure corresponds to a PWM-type excitation with 100 ns of rise time, comparing the results with and without cable.

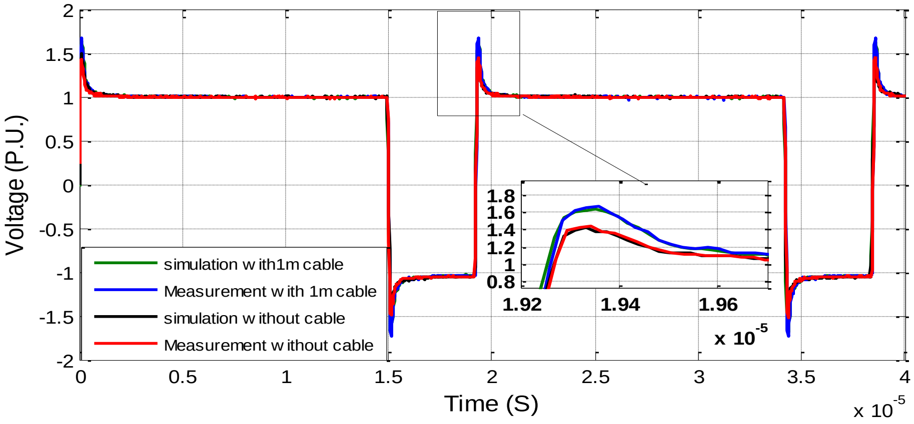

Figure 6-12: Transient overvoltage with and without cable

In addition, Figure 6-13 shows the results for different rises times and 1-meter cable included. These figures also show that, when compared to the experimental results, the simulations corresponding the excitation-cable-machine winding setup produce very accurate results. The effect of the excitation rise time is analyzed in a more general manner in Figure 6-14, which shows the potential difference between turns for different rises times. According to this figure, the potential difference is inversely proportional to the rise time of the excitation.

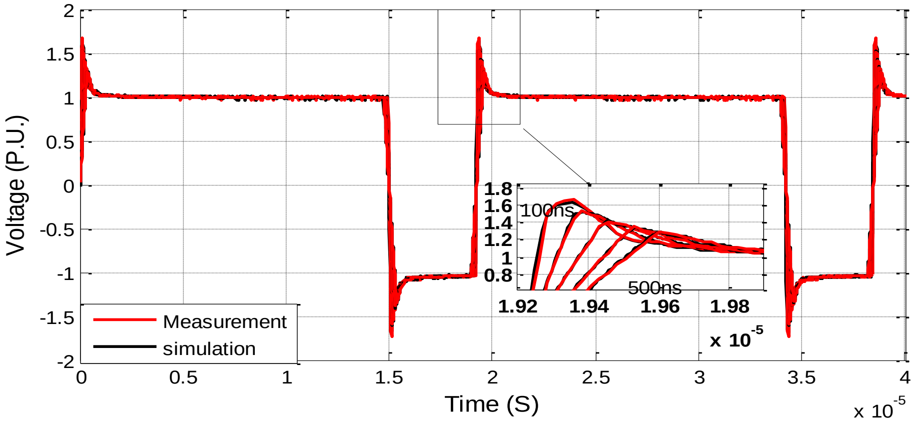

Figure 6-13: Transient overvoltage at the first turn of the coil with cable

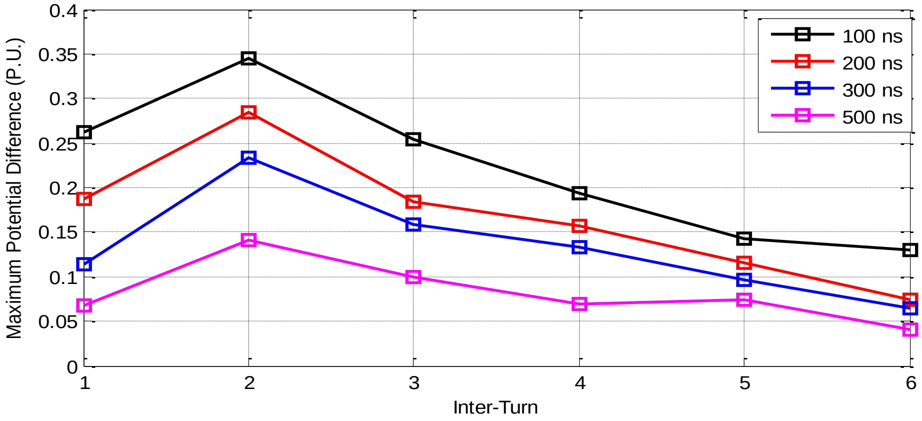

Figure 6-14: Potential difference between turns considering different rise times of the excitation

Finally, the effect of the length of the connection cable is analyzed in Figure 6 15, which illustrates the potential difference between turns for an excitation with 100 ns of rise time connected to the winding by means of cables of different lengths. According to the results, the potential difference is directly proportional to the cable length.

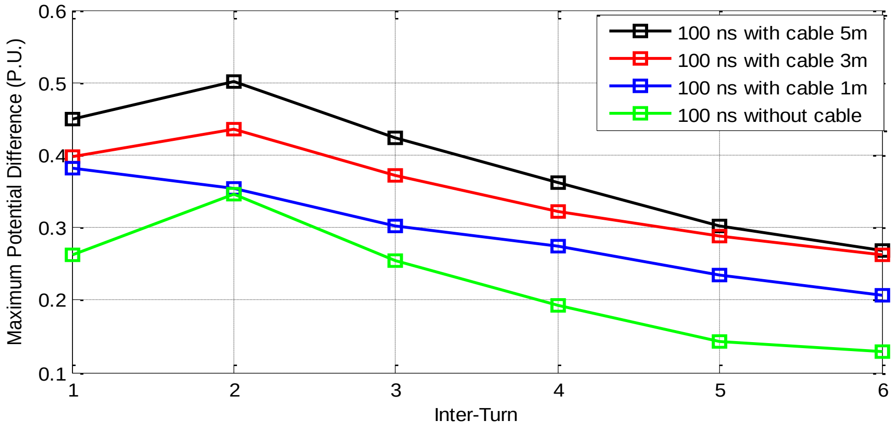

Figure 6-15: Potential difference between turns considering different lengths of connection cable

6.4 Modeling of Machine Winding with Feeder Cable and Filter

A schematic representation of the system under study is shown in Figure 6 16. A PWM-type excitation is connected through a cable and filter to the form-wound machine winding coil.

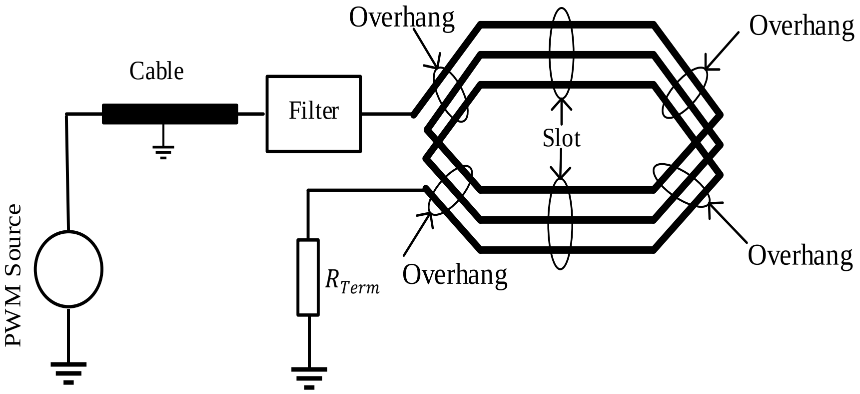

Figure 6-16: Schematic model of a form wound stator coil (3 turns are considered for the purpose of illustration) with feeder cable and filter

6.4.1 Experimental Setup of Machine Winding with Feeder Cable and Filter

Figure 6-17shows a picture of the experimental setup used for validation purposes. Besides the form-wound coil under test, it includes a waveform generator, an oscilloscope, the connection cable, the proposed filter, and a 100 Ω load connected at the end of the coil.

Figure 6-17: Experimental setup for validation of the inverter-cable-coil setup

6.4.2 Inclusion of Filter

Tables 6-2 and 6-3 show the optimal parameters of the conventional and proposed filter obtained from the optimization algorithms. Two filters (conventional and proposed) are physically built using the parameters obtained from these tables and introduced into the experimental setup.

Table 6-2: Parameters for conventional filter

Optimization Algorithm	Parameters of RLC conventional filter		
	R (ohm)	C (uF)	L (uH)
Goal attainment	34	0.012	39
Minimax	2.5	0.22	220

Table 6-3: Parameters for proposed filter

Optimization Algorithm	Parameters of RLC proposed filter			
	R (ohm)	C (uF)	L1 (uH)	L2 (uH)
Goal attainment	64.9	0.01	360	17
Minimax	50	10	125	20

6.4.3 Experimental Results of Machine Winding with Feeder Cable and Filter

Figure 6-18 shows the voltages measured at the first coil turn of the machine winding for 100 ns rise time before and after inclusion of the conventional and proposed filters. It can be noticed that the proposed filter optimized via goal attainment algorithm produces the best results in terms of reducing the transient overvoltages without introducing a substantial overdamp or distorting the voltage waveform. Figure 6-19 shows the transient voltages measured at the first coil turn considering different rise times (100 ns to 500 ns) of the excitation and including the proposed filter with parameters optimized using the goal attainment algorithm. The effectiveness of the proposed filter is evident.

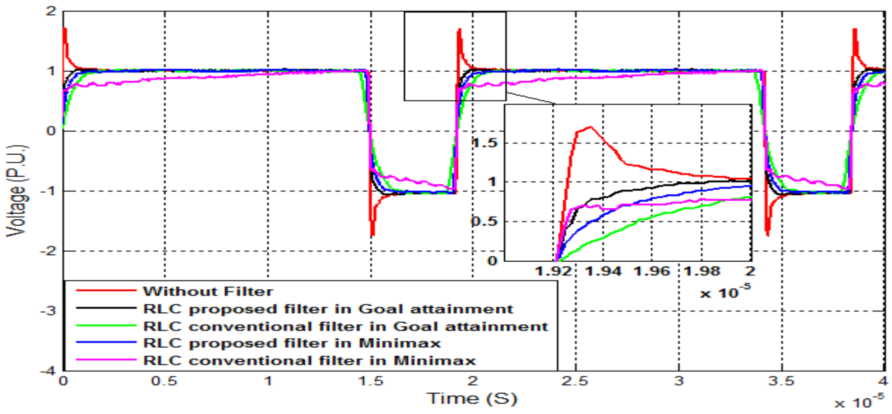

Figure 6-18: Transient overvoltage at the first turn of the coil with cable and different filters

The effects of the length of the connection cable and the proposed filter are analyzed in Figure 6-20, which illustrates the potential difference between turns for an excitation with 100 ns of rise time connected to the winding by means of cables of different lengths. According to these simulation results, the potential difference is directly proportional to the cable length. Figure 6-20 also demonstrates that the proposed filter effectively decreases the potential difference between turns, which is directly related to the dielectric stress between turns. Table 6-4 compares the maximum potential difference before and after using the proposed filter with different lengths of feeder cable.

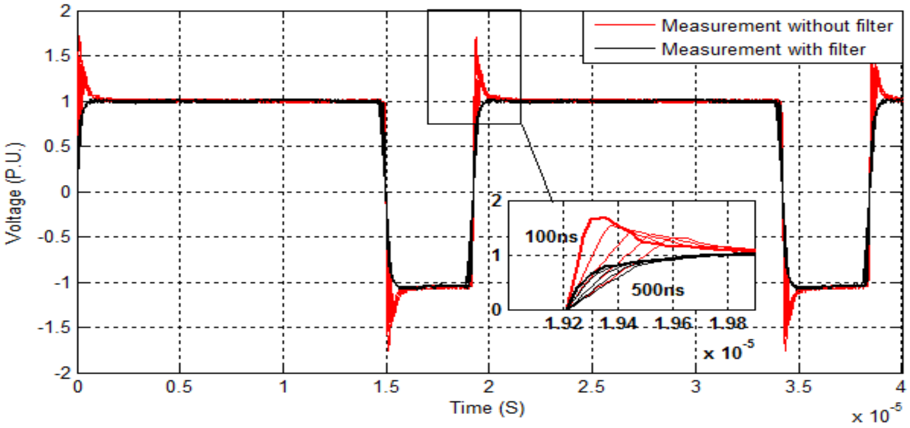

Figure 6-19: Transient overvoltage at the first turn of the coil with proposed filter and cable

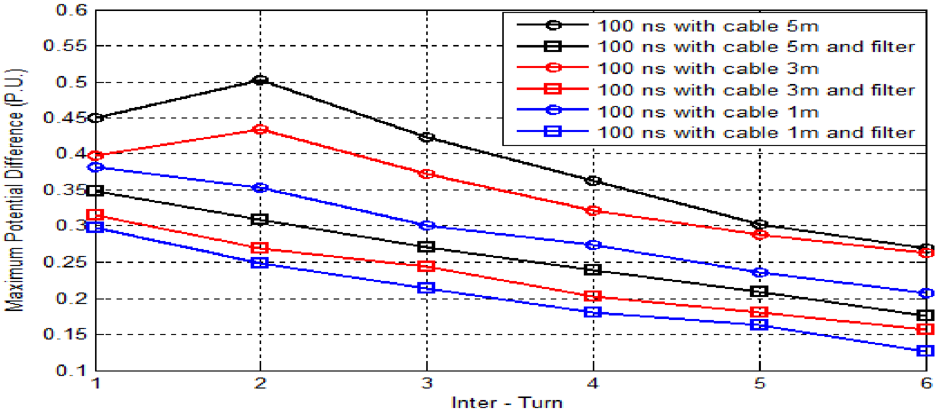

Figure 6-20: Potential difference between turns considering different lengths of connection cable and proposed filter

Table 6-4: Max. potential difference considering different lengths of cable and proposed filter

Max. Potential difference, 100 ns rise time			
Cable length (m)	Before proposed filter [V]	After proposed filter [V]	Reduction [%]
1	0.3821	0.2972	22.219
3	0.4349	0.3153	27.50
5	0.5016	0.3485	30.522

6.5 Summary

This chapter presents the experimental validation of the machine winding model by means of measurements on a form-wound line-end coil from a medium voltage motor. Comparisons between simulation results and experimental measurements in terms of transient voltage response show very good agreement for different rise times of the PWM-type excitation. The feeder cable connecting the inverter to the motor is also included. For the simulations, a frequency domain distributed parameter model of the cable is considered, with electrical parameters obtained from short and open circuit test measurements. Comparisons between simulations and experimental results for the PWM inverter-cable-motor setup showed that the modeling approach provides a very accurate prediction of the fast-transient response of the system in terms of both oscillatory behavior and magnitude. Finally, two different optimization algorithms were used to find the optimal filter parameters of conventional and proposed RLC filters based on minimizing the rise time, the settling time, peak time, and the over shoot of the corresponding output voltage. The results when applying a PWM-type excitation to the coil show that the proposed filter can eliminate the transient overvoltages better and faster than the conventional filter. In addition, the goal attainment algorithm is a better alternative than the minimax algorithm to obtain the optimal parameters the proposed filter. These results were previously obtained via simulations that explained in Chapter V and confirmed in this chapter experimentally.

CHAPTER VII

CONCLUSIONS AND FUTURE WORK

7.1 Conclusions

The main goal of this dissertation is to reduce the transient overvoltages and the dielectric stress of machine windings under fast front excitation. In order to achieve this goal, three main ideas are proposals and introduced. First, a computer model of an inverter-cable-motor setup is presented for the accurate and fast prediction of transient overvoltages and dielectric stress. Second, a method to specify the optimal insulation arrangement to minimize the dielectric stress in machine coils is presented. Finally, an RLC filter and its optimal tuning to reduce transient overvoltages along the machine winding are proposed. The effectiveness of these proposals has been evaluated based on observations of simulated and experimental results. The following points summarize the main contributions and conclusions of this dissertation.

1- A frequency domain non-uniform multiconductor transmission line approach has been used to study the fast-front transient response of a machine winding coil. The parameters of the coil were calculated using the finite element method in nonhomogeneous layers, considering the variation in the distribution of electric and magnetic fields in the slot and overhang regions. These methods showed an accurate predicting of the transient overvoltages produced at different turns of the coil and the potential difference between adjacent turns in different rise time of the source.

2- Three strategies have been proposed to represent the rest of the winding after the first coil as a function of frequency. These strategies can reduce the size of the system and the simulation time of machine windings model for fast front transient studies. It has been shown that the results from these reduction strategies are equivalent and do not introduce any loss of accuracy when compared to the results considering the complete winding.

3- A frequency domain distributed parameter model of the feeder cable has been proposed to study the effect of different lengths of cable on the transient overvoltages and in the interturn insulation of the machine winding.

4- A method was proposed to identify improvements in the insulation design of machine winding coils fed by fast front pulses. This method was based on the application of a frequency domain non-uniform multiconductor transmission line approach, in combination with the finite element method and optimization techniques. The results showed that modifications in the thicknesses and permittivities of the coil insulation layers, obtained through optimization, produce significant reduction of dielectric stresses due to fast front pulses with different rise times. The choice of the optimization technique was critical: particle swarm optimization provided the best results in this work, with dielectric stress reductions of 50 % and 43 % for the geometries considered in this work. The potential distribution of the optimized geometries was also improved, giving rise to a considerable reduction of potential difference between turns for the complete machine windings.

5- A method was proposed to find the optimal parameters of RLC filters for the reduction of transient overvoltages in an inverter-cable-motor setup. Multi-objective optimization algorithms were used to find the optimal RLC filter parameters based on minimizing rise time, peak time, maximum percentage overshoot, and settling time of the corresponding output voltage. Optimal parameter tuning was applied in a proposed RLC filter and compared with a conventional RLC filter. The results showed that optimal proposed filter can eliminate the transient overvoltages better and faster than the optimal conventional filter.

6- The optimal insulation layers with optimal proposed RLC filter showed high performance in terms of decreasing the transient over voltage and the dielectric stress in machine winding with different lengths of the feeder cable.

7.2 Future Work

The present work might be further expanded considering the following topics:

1. Frequency dependent modeling of machine winding including the effect of stator core and other phases.
2. Application of other optimization algorithms in the insulation design of machine coils and tuning of filter.
3. Experimental verification of optimized geometries by means of accelerated aging tests on prototype coils.
4. Analyzing the use of different types of insulation materials in inverter-fed rotating machines.

APPENDIX

PUBLICATIONS

Transactions:

- M. K. Hussain and P. Gomez, "Optimized dielectric design of stator windings from medium voltage induction machines fed by fast front pulses," in *IEEE Transactions on Dielectrics and Electrical Insulation*, vol. 24, no. 2, pp. 837-846, April 2017.

Book Chapter:

- F. P. Espino-Cortes, P. Gómez, M. K. Hussain, "Modeling and simulation of machine windings fed by high-power frequency converters for insulation design" in *Simulation and Modelling of Electrical Insulation Weaknesses in Electrical Equipment* (Edited by R. Albarracin), IntechOpen, London, UK, 2018.

Conference:

- M. K. Hussain and P. Gomez, "Modeling of machine coils under fast front excitation using a non-uniform multiconductor transmission line approach," *2016 North American Power Symposium (NAPS)*, Denver, CO, 2016, pp. 1-6.

- M. K. Hussain and P. Gomez, "Equivalent representation of machine winding in frequency domain model for fast transient studies," *2017 IEEE Power and Energy Conference at Illinois (PECI)*, Champaign, IL, 2017, pp. 1-6.

- M. K. Hussain, P. Gomez, "Modeling and Experimental Analysis of the Transient Overvoltages on Machine Windings Fed by PWM Inverters," *12th International Conference on Power Systems Transients (IPST'17)*, Seoul, South Korea, June 2017.

- M. K. Hussain and P. Gomez, "Optimal filter tuning to minimize the transient overvoltages on machine windings fed by PWM inverters," *2017 North American Power Symposium (NAPS)*, Morgantown, WV, 2017, pp. 1-6.

- G. A. Bilal, J. M. Villanueva-Ramirez, M. K. Hussain and P. Gomez, "Network reduction for frequency domain transient analysis of power components," *2017 IEEE International Conference on Electro Information Technology (EIT)*, Lincoln, NE, 2017, pp. 206-210.

BIBLIOGRAPHY

[1] G. Lupo, C. Petrarca, M. Vitelli and V. Tucci, "Multiconductor transmission line analysis of steep-front surges in machine windings," in *IEEE Transactions on Dielectrics and Electrical Insulation*, vol. 9, no. 3, pp. 467-478, Jun 2002.

[2] C. Petrarca, A. Maffucci, V. Tucci and M. Vitelli, "Analysis of the voltage distribution in a motor stator winding subjected to steep-fronted surge voltages by means of a multiconductor lossy transmission line model," in *IEEE Transactions on Energy Conversion*, vol. 19, no. 1, pp. 7-17, March 2004.

[3] J. L. Guardado, "Computer models for representing electrical machines during switching transients," Ph.D. Dissertation, University of Manchester, 1989.

[4] B. S. Oyegoke, “Transient voltage distribution in stator winding of electrical machine fed from a frequency converter,” Ph.D. Dissertation, Helsinki University of Technology, 2000.

[5] A. Krings, G. Paulsson, F. Sahlén and B. Holmgren, "Experimental investigation of the voltage distribution in form wound windings of large AC machines due to fast transients," *2016 XXII International Conference on Electrical Machines (ICEM),* Lausanne, 2016, pp. 1700-1706.

[6] C. Petrarca, G. Lupo, V. Tucci and M. Vitelli, "MTL model and FEM package for the evaluation of steep-front surges distribution in machine windings," *2001 Annual Report Conference on Electrical Insulation and Dielectric Phenomena (Cat. No.01CH37225)*, Kitchener, Ont., 2001, pp. 685-688.

[7] B. Basavaraja and D. V. S. S. S. Sarma, "Modelling, Simulation and Experimental Analysis of Transient Terminal Overvoltage in PWM-Inverter fed Induction Motors," *2007 IEEE Power Engineering Society General Meeting*, Tampa, FL, 2007, pp. 1-8.

[8] T. G. Arora, M. V. Aware and D. R. Tutakne, "Effect of pulse width modulated voltage on induction motor insulation," *2012 7th IEEE Conference on Industrial Electronics and Applications (ICIEA),* Singapore, 2012, pp. 2044-2048.

[9] C. J. Melhorn and L. Tang, "Transient effects of PWM drives on induction motors," in *IEEE Transactions on Industry Applications*, vol. 33, no. 4, pp. 1065-1072, Jul/Aug 1997.

[10] H. De Paula, M. L. R. Chaves, D. A. Andrade, J. L. Domingos and M. A. A. Freitas, "A new strategy for differential overvoltages and common-mode currents determination in PWM induction motor drives," *IEEE International Conference on Electric Machines and Drives, 2005.*, San Antonio, TX, 2005, pp. 1075-1081.

[11] V. Venegas, R. Escarela, R. Mota, E. Melgoza and J. L. Guardado, "Calculation of electrical parameters for transient overvoltage studies on electrical machines," *Electric Machines and Drives Conference*, 2003. IEMDC'03. IEEE International, 2003, pp. 1978-1982 vol.3.

[12] J. L. Guardado and K. J. Cornick, "A computer model for calculating steep-fronted surge distribution in machine windings," in *IEEE Transactions on Energy Conversion*, vol. 4, no. 1, pp. 95-101, Mar 1989.

[13] A. von Jouanne, P. Enjeti and W. Gray, "The effect of long motor leads on PWM inverter fed AC motor drive systems," *Applied Power Electronics Conference and Exposition, 1995. APEC '95. Conference Proceedings 1995., Tenth Annual*, Dallas, TX, 1995, pp. 592-597 vol.2.

[14] A. F. Moreira, T. A. Lipo, G. Venkataramanan and S. Bernet, "High-frequency modeling for cable and induction motor overvoltage studies in long cable drives," in *IEEE Transactions on Industry Applications*, vol. 38, no. 5, pp. 1297-1306, Sep/Oct 2002.

[15] L. Wang, C. Ngai-Man Ho, F. Canales and J. Jatskevich, "High-Frequency Modeling of the Long-Cable-Fed Induction Motor Drive System Using TLM Approach for Predicting Overvoltage Transients," in *IEEE Transactions on Power Electronics*, vol. 25, no. 10, pp. 2653-2664, Oct. 2010.

[16] M. S. Moonesan, S. Jayaram, E. Cherney, R. Omranipour and S. U. Haq, "Analysis of times-to-failure of various turn insulations of form-wound coils under PWM voltage waveform," *2013 IEEE Electrical Insulation Conference (EIC)*, Ottawa, ON, 2013, pp. 187-190.

[17] J. L. Guardado, K. J. Cornicki, V. Venegas, J. L. Naredo and E. Melgoza, "A three-phase model for surge distribution studies in electrical machines," in *IEEE Transactions on Energy Conversion*, vol. 12, no. 1, pp. 24-31, Mar 1997.

[18] M. T. Wright, S. J. Yang and K. McLeay, "General theory of fast-fronted interturn voltage distribution in electrical machine windings," in *IEE Proceedings B - Electric Power Applications*, vol. 130, no. 4, pp. 245-256, July 1983.

[19] M. T. Wright, S. J. Yang and K. McLeay, "The influence of coil and surge parameters on transient interturn voltage distribution in stator windings," in *IEE Proceedings B - Electric Power Applications*, vol. 130, no. 4, pp. 257-264, July 1983.

[20] P. G. McLaren and H. Oraee, "Multiconductor transmission-line model for the line-end coil of large AC machines," in *IEE Proceedings B - Electric Power Applications*, vol. 132, no. 3, pp. 149-156, May 1985.

[21] P. Nussbaumer, A. Mitteregger and T. M. Wolbank, "Online detection of insulation degradation in inverter fed drive systems based on high frequency current sampling," *IECON 2011 - 37th Annual Conference of the IEEE Industrial Electronics Society*, Melbourne, VIC, 2011, pp. 1954-1959.

[22] D. C. Domínguez, F. P. Espino-Cortés and P. Gomez, "Optimization of electric field grading systems in non-ceramic insulators," 2*011 Electrical Insulation Conference (EIC).*, Annapolis, MD, 2011, pp. 231-234.

[23] D. Cruz Dominguez, F. P. Espino-Cortes and P. Gomez, "Optimized design of electric field grading systems in 115 kV non-ceramic insulators," in *IEEE Transactions on Dielectrics and Electrical Insulation*, vol. 20, no. 1, pp. 63-70, February 2013.

[24] W. Sima, F. P. Espino-Cortes, E. A. Cherney and S. H. Jayaram, "Optimization of corona ring design for long-rod insulators using FEM based computational analysis," *Conference Record of the 2004 IEEE International Symposium on Electrical Insulation*, 2004, pp. 480-483.

[25] W. S. Chen, H. T. Yang and H. Y. Huang, "Contour Optimization of Suspension Insulators Using Dynamically Adjustable Genetic Algorithms," in *IEEE Transactions on Power Delivery*, vol. 25, no. 3, pp. 1220-1228, July 2010.

[26] S. Zhang, Z. Peng and P. Liu, "Inner insulation structure optimization of UHV RIP oil-SF6 bushing using electro-thermal simulation and advanced equal margin design method," in *IEEE Transactions on Dielectrics and Electrical Insulation*, vol. 21, no. 4, pp. 1768-1777, August 2014.

[27] D. Ivanov, V. Ostreiko, and D. Yaroshenko, “On optimization of the insulation of high-voltage coaxial bushing,” *Russ. Electr. Eng.*, vol. 87, no. 4, pp. 228–230, Apr. 2016.

[28] A. von Jouanne, D. A. Rendusara, P. N. Enjeti and J. W. Gray, "Filtering techniques to minimize the effect of long motor leads on PWM inverter-fed AC motor drive systems," in *IEEE Transactions on Industry Applications*, vol. 32, no. 4, pp. 919-926, Jul/Aug 1996.

[29] D. Rendusara and P. Enjeti, "New inverter output filter configuration reduces common mode and differential mode dv/dt at the motor terminals in PWM drive systems," *PESC97. Record 28th Annual IEEE Power Electronics Specialists Conference. Formerly Power Conditioning Specialists Conference 1970-71. Power Processing and Electronic Specialists Conference 1972, St. Louis, MO, 1997*, pp. 1269-1275 vol.2.

[30] D. A. Rendusara and P. N. Enjeti, "An improved inverter output filter configuration reduces common and differential modes dv/dt at the motor terminals in PWM drive systems," in *IEEE Transactions on Power Electronics*, vol. 13, no. 6, pp. 1135-1143, Nov 1998.

[31] A. F. Moreira, P. M. Santos, T. A. Lipo and G. Venkataramanan, "Filter networks for long cable drives and their influence on motor voltage distribution and common-mode currents," in *IEEE Transactions on Industrial Electronics*, vol. 52, no. 2, pp. 515-522, April 2005.

[32] C. Q. Su, Electromagnetic Transients in Transformer and Rotating Machine Windings, 1st ed., IGI Global: Hersey, PA, 2013.

[33] J. A. Martinez-Velasco, *Power System Transients: Parameter Determination*, 1st ed. Boca Raton: CRC Press, 2009.

[34] J. L. Guardado and K. J. Cornick, "Calculation of machine winding electrical parameters at high frequencies for switching transient studies," in *IEEE Transactions on Energy Conversion*, vol. 11, no. 1, pp. 33-40, Mar 1996.

[35] B. S. Oyegoke, "A comparative analysis of methods for calculating the transient voltage distribution within the stator winding of an electric machine subjected to steep-fronted surge," *1997 Eighth International Conference on Electrical Machines and Drives (Conf. Publ. No. 444)*, Cambridge, 1997, pp. 294-298.

[36] A. H. Mabrek and K. E. Hemsas, "Transient operation modeling of induction machine using standstill frequency response test," *2015 4th International Conference on Electrical Engineering (ICEE)*, Boumerdes, 2015, pp. 1-6.

[37] J. L. Guardado and K. J. Cornick, "The effect of coil parameters on the distribution of steep-fronted surges in machine windings," in *IEEE Transactions on Energy Conversion*, vol. 7, no. 3, pp. 552-559, Sep 1992.

[38] S. Palko and T. Jokinen, "Optimisation of squirrel cage induction motors using finite element method and genetic algorithms," *1997 Eighth International Conference on Electrical Machines and Drives (Conf. Publ. No. 444)*, Cambridge, 1997, pp. 21-25.

[39] M. R. Feyzi and H. V. Kalankesh, "Optimization of induction motor design by using the finite element method," *Canadian Conference on Electrical and Computer Engineering 2001. Conference Proceedings (Cat. No.01TH8555)*, Toronto, Ont., 2001, pp. 845-850 vol.2.

[40] M. R. Feyzi, H. V. Kalankesh and M. B. B. Sharifian, "A comparative study of three optimization methods in FEM design of induction motors," *The 4th International Power Electronics and Motion Control Conference, 2004. IPEMC 2004.*, Xi'an, 2004, pp. 305-309 Vol.1.

[41] F. Castelli-Dezza, M. M. Maglio, G. Marchegiani, D. F. Ortega and D. Rosati, "Reduction of motor overvoltage fed by PWM AC drives using a universal model," *The XIX International Conference on Electrical Machines - ICEM 2010*, Rome, 2010, pp. 1-6.

[42] B. Anirudh Acharya and V. John, "Design of output dv/dt filter for motor drives," *2010 5th International Conference on Industrial and Information Systems*, Mangalore, 2010, pp. 562-567.

[43] B. K. Gupta, D. K. Sharma and D. C. Bacvarov, "Measured Propagation of Surges in the Winding of a Large A-C Motor," in *IEEE Power Engineering Review*, vol. PER-6, no. 3, pp. 39-40, March 1986.

[44] P. G. McLaren and M. H. Abdel-Rahman, "Steep fronted surges applied to large AC motors-effect of surge capacitor value and lead length," in *IEEE Transactions on Power Delivery*, vol. 3, no. 3, pp. 990-997, Jul 1988.

[45] B. Banakara and D. V. S. S. S. Sarma, "Non-uniform voltage distribution in stator winding of PWM fed induction motor," *TENCON 2008 - 2008 IEEE Region 10 Conference*, Hyderabad, 2008, pp. 1-6.

[46] P. Gomez, P. Moreno and J. L. Naredo, "Frequency-domain transient analysis of nonuniform lines with incident field excitation," in *IEEE Transactions on Power Delivery*, vol. 20, no. 3, pp. 2273-2280, July 2005.

[47] P. Moreno, P. Gomez, M. Davila and J. L. Naredo, "A Uniform Line Model for Non-Uniform Single-Phase Lines with Frequency Dependent Electrical Parameters," *2006 IEEE/PES Transmission & Distribution Conference and Exposition: Latin America*, Caracas, 2006, pp. 1-6.

[48] C. Paul, *Analysis of Multiconductor Transmission Lines*, 2nd ed. Wiley-IEEE Press, 2007.

[49] P. Gomez, “Non Uniform Transmission Line Modeling for Electromagnetic Transient Analysis,” Ph.D. Dissertation, CINVESTAV del I.P.N., Guadalajara, 2005.

[50] F. P. Espino-cortes, P. Gomez and J. D. Betanzos Ramirez, "Modeling of heat generated on stress grading coatings of motors fed by multilevel drives," in *IEEE Transactions on Dielectrics and Electrical Insulation*, vol. 18, no. 4, pp. 1328-1333, August 2011.

[51] P. Gomez and J. C. Escamilla, “Frequency domain modeling of nonuniform multiconductor lines excited by indirect lightning,” *Int. J. Electr. Power Energy Syst.*, vol. 45, no. 1, pp. 420–426, Feb. 2013.

[52] R. Nuricumbo-Guillén, P. Gomez and F. P. Espino-Cortés, "Computation of transient voltage profiles along transmission lines by successive application of the numerical Laplace transform," *2013 North American Power Symposium (NAPS)*, Manhattan, KS, 2013, pp. 1-6.

[53] P. Gomez and F. A. Uribe, “The numerical Laplace transform: An accurate technique for analyzing electromagnetic transients on power system devices,” *Int. J. Electr. Power Energy Syst.*, vol. 31, no. 2, pp. 116–123, 2009.

[54] J. R. Shackleton, “Introduction to COMSOL Multiphysics 5.2,” *Econ. Aff.*, vol. 37, no. 1, p. 1, Feb. 2017.

[55] P. Gomez and F. de León, "Accurate and Efficient Computation of the Inductance Matrix of Transformer Windings for the Simulation of Very Fast Transients," in *IEEE Transactions on Power Delivery*, vol. 26, no. 3, pp. 1423-1431, July 2011.

[56] Z. Luna López, P. Gomez, F. P. Espino-Cortés and R. Peña-Rivero, "Modeling of Transformer Windings for Fast Transient Studies: Experimental Validation and Performance Comparison," in *IEEE Transactions on Power Delivery*, vol. 32, no. 4, pp. 1852-1860, Aug. 2017.

[57] Chakrabarti and Abhijit, *Power System Dynamics and Simulation*. Delhi: PHI Learning Pvt., 2013.

[58] H. Oraee and P. G. McLaren, "Surge Voltage Distribution in Line-End Coils of Induction Motors," in *IEEE Power Engineering Review*, vol. PER-5, no. 7, pp. 51-52, July 1985.

[59] P. G. McLaren and M. H. Abdel-Rahman, "Modeling of large AC motor coils for steep-fronted surge studies," in *IEEE Transactions on Industry Applications,* vol. 24, no. 3, pp. 422-426, May/Jun 1988.

[60] G. C. Stone, I. Culbert, E. A. Boulter, And H. Dhirani, *Electrical Insulation for Rotating Machines: Design, Evaluation, Aging, Testing, and Repair*, 2nd ed. John Wiley & Sons, 2014.

[61] T. Munih and D. Miljavec, "A method for accelerated ageing of electric machine insulation," *Proceedings of the 16th International Conference on Mechatronics - Mechatronika 2014*, Brno, 2014, pp. 65-70.

[62] M. Junaid Akhtar, R. K. Behera and S. K. Parida, "Optimized rotor slot shape for squirrel cage induction motor in electric propulsion application," *2014 IEEE 6th India International Conference on Power Electronics (IICPE),* Kurukshetra, 2014, pp. 1-5.

[63] S. Williamson and C. I. McClay, "Optimization of the geometry of closed rotor slots for cage induction motors," in *IEEE Transactions on Industry Applications*, vol. 32, no. 3, pp. 560-568, May/Jun 1996.

[64] K. Idir, Liuchen Chang and Heping Dai, "Improved neural network model for induction motor design," in *IEEE Transactions on Magnetics*, vol. 34, no. 5, pp. 2948-2951, Sep 1998.

[65] L. N. V. Andrew R. Conn Katya Scheinberg, *Introduction to derivative-free optimization*. Society for Industrial and Applied Mathematics/Mathematical Programming Society SIAM/MPS, 2009.

[66] F. Gao and L. Han, “Implementing the Nelder-Mead simplex algorithm with adaptive parameters,” *Comput. Optim. Appl.*, vol. 51, no. 1, pp. 259–277, Jan. 2012.

[67] H. P. Gavin, The Nelder-Mead Algorithm in Two Dimensions, Course Notes, *Department of Civil and Environmental Engineering- Duke University*, USA, 2016.

[68] K. Klein and J. Neira, “Nelder-Mead Simplex Optimization Routine for Large-Scale Problems: A Distributed Memory Implementation,” *Comput. Econ.*, vol. 43, no. 4, pp. 447–461, Apr. 2014.

[69] M. J. Powell, The BOBYQA algorithm for bound constrained optimization without derivatives, *Department of Applied Mathematics and Theoretical Physics, Cambridge University*. DAMTP 2009/NA06, 2009.

[70] N. Nedjah and L. M. Mourelle, Swarm Intelligent Systems, 1st ed., *Springer-Verlag, Netherlands*, 2006.

[71] K. E. Parsopoulos, M. N. Vrahatis, Particle Swarm Optimization and Intelligence: Advances and Applications, 1st ed., IGI Global: Hersey, PA, 2010.

[72] M. T. Tsai, J. H. Liu and T. J. Cheng, "A novel method for suppression of high voltage gradient transient effects in voltage-fed PWM inverter," *2002 IEEE 33rd Annual IEEE Power Electronics Specialists Conference. Proceedings (Cat. No.02CH37289)*, 2002, pp. 1537-1542 vol.3.

[73] D. Xue, D. P. Atherton, and Y. Chen, *Linear feedback control*. Philadelphia, PA: SIAM, 2007.

[74] E. Umez-Eronini, *System dynamics and control*. Pacific Grove, CA: PWS Publ, 1999.

[75] K. Ogata, *Modern control engineering*, 5. ed., Internat. ed. Boston: Pearson, 2010.

[76] C. L. Phillips and J. Parr, *Feedback control systems*, 5. ed., Internat. ed. Boston; Munich : Pearson, 2011.

[77] N. Nise, *Control Systems Engineering*, 6th ed. New York, NY: John Wiley & Sons, Inc., 2000.

[78] R. L. Boylestad, *Introductory circuit analysis*, 11. ed. Upper Saddle River, NJ: Pearson Prentice Hall, 2007.

[79] A. Abraham, L. Jain, and R. Goldberg, *Evolutionary Multiobjective Optimization Theoretical Advances and Applications*. Springer-Verlag London Limited 2005.

[80] C. H. Tseng and T. W. Lu, “Minimax multiobjective optimization in structural design,” *Int. J. Numer. Methods Eng.*, vol. 30, no. 6, pp. 1213–1228, 1990.

[81] S. S. Rao, *Engineering optimization;Theory and Practice*. Wiley, Hoboken 2009.

[82] F. W. Gembicki, “Performance and Sensitivity Optimization: A Vector-Index Approach,” Ph.D. Dissertation, Case Western Reserve University ,1974.

[83] H. R. Imani, A. Mohamed, H. Shareef, and M. Eslami, “Multi-objective optimization based approaches for active power filter design - A comparison,” *Przeglad Elektrotechniczny*, vol. 89, no. 6, pp. 98–103, 2013.

[84] A. Antoniou and W.-S. Lu, *Practical Optimization ;Algorithms and Engineering Applications*. Boston, MA: Springer US, 2007.

[85] F. Giannessi, V. F. Demianov, and F. H. Clarke, Eds., *Nonsmooth optimization and related topics*. New York: Plenum Press, 1989.

[86] P. G. McLaren and H. Oraee, "Multiconductor transmission-line model for the line-end coil of large AC machines," in *IEE Proceedings B - Electric Power Applications*, vol. 132, no. 3, pp. 149-156, May 1985.

[87] W. W. L. Keerthipala and P. G. McLaren, "The effects of laminations on steep fronted surge propagation in large AC motor coils," in *IEEE Transactions on Energy Conversion*, vol. 5, no. 1, pp. 84-90, Mar 1990.

[88] W. W. L. Keerthipala and P. G. McLaren, "A multiconductor transmission line model for surge propagation studies in large a.c. machine windings," *Proceedings of the 33rd Midwest Symposium on Circuits and Systems*, Calgary, Alta., 1990, pp. 629-632 vol.2.

[89] W. W. L. Keerthipala and P. G. McLaren, "Modeling of effects of laminations on steep fronted surge propagation in large AC motor coils," in *IEEE Transactions on Industry Applications*, vol. 27, no. 4, pp. 640-644, Jul/Aug 1991.

[90] S. Ul Haq, M. K. W. Stranges and B. Wood, "A Proposed Method for Establishing Partial Discharge Acceptance Limits on API 541 and 546 Sacrificial Test Coils," in *IEEE Transactions on Industry Applications*, vol. 53, no. 1, pp. 718-722, Jan.-Feb. 2017.

[91] S. U. Haq and R. Omranipour, "Accelerated life testing of high voltage stator coils with enhanced PET-mica insulation system," *2011 Electrical Insulation Conference (EIC).*, Annapolis, MD, 2011, pp. 479-482.

[92] S. Ul Haq, R. Omranipour and L. Teran, "Surge withstand capability of electrically and thermo-mechanically aged turn insulation of medium voltage form-wound AC stator coils," *2014 IEEE Electrical Insulation Conference (EIC)*, Philadelphia, PA, 2014, pp. 78-81.

[93] R. Omranipour and S. U. Haq, "Effect of electrical and thermo-mechanical stresses on the surge capability of MV form-wound AC stator coils," *2013 IEEE Electrical Insulation Conference (EIC)*, Ottawa, ON, 2013, pp. 183-186.